CHALMERS
UNIVERSITY OF TECHNOLOGY

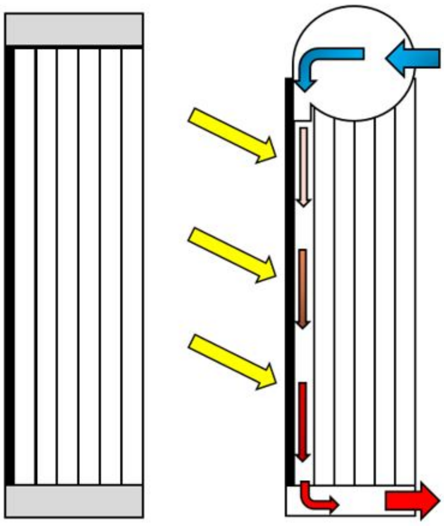

Assessment and optimization of energy smart window curtains

A pilot study to evaluate the energy performance and a parametric study to optimize the design of the newly developed Climate Curtains

Master's thesis in Master Program Structural engineering and building technology

ALI KARIM

Department of Architecture and Civil Engineering
CHALMERS UNIVERSITY OF TECHNOLOGY
Master's thesis ACEX30-18-84
Gothenburg, Sweden 2018

Master's thesis 2018

Assessment and optimization of energy smart window curtains

A pilot study to evaluate the energy performance and a parametric study to optimize the design of the newly developed Climate Curtains

ALI KARIM

Department of Architecture and Civil Engineering
Division of Building Technology
Building Physics Group
Chalmers University of Technology
Gothenburg, Sweden 2018

Assessment and optimization of energy smart window curtains
A pilot study to evaluate the energy performance and a parametric study to optimize the design of the newly developed Climate Curtains

ALI KARIM

Supervisor: Professor Carl-Eric Hagentoft, Department of Architecture and Civil Engineering
Examiner: Professor Carl-Eric Hagentoft, Department of Architecture and Civil Engineering

Department of Architecture and Civil Engineering
Division of Building Technology
Building Physics Group
Chalmers University of Technology
SE-412 96 Gothenburg
Telephone +46 31 772 1000

Cover: An illustration of two different designs of Climate Curtain.

Department of Architecture and Civil Engineering
Gothenburg, Sweden 2018

Assessment and optimization of energy smart window curtains
A pilot study to evaluate the energy performance and a parametric study to optimize the design of the newly developed Climate Curtains

Master's thesis in Master Program Structural engineering and building technology

ALI KARIM
Department of Architecture and Civil Engineering
Division of Building Technology
Building Physics Group
Chalmers University of Technology

Abstract

According to the Swedish Energy Agency, buildings account for 40 % of Sweden's demand for energy. Windows are often the weak spots of the building envelope concerning the energy performance, and for heated buildings, a tremendous amount of energy is lost through the windows. Lately, many new types of windows with improved thermal properties have been developed and have been used in new buildings. However, there are still a large number of old buildings all around the world and in Sweden, where windows with high U-value are used. Additionally, many buildings such as schools, offices and recreational homes are, on average, used actively for only a fraction of a year.
Climate Curtain is a new energy smart window curtain, with the aim to reduce the heat losses through windows. By covering windows with Climate Curtain, for instance when the buildings are not occupied, the energy performance can be improved and become more economical and sustainable.

The project aims to evaluate the energy performance of the curtains by in-situ measurements and simulations. In this project, 2 different designs of Climate Curtain have been studied. Curtain design (A) has the aim to increase the overall thermal resistance of window constructions and by that decrease the heat losses through windows. Curtain design (B) has an additional solar collector function which is aimed to capture some part of solar radiation striking the window and warm up the indoor temperature by small fans inside the curtain. The project investigates also the possibilities to optimize the design of the curtains regarding emissivity of the material and air velocity of the fans used in design (B). During the 27 days measurement campaign, interior and exterior temperatures, intensity of solar radiation and energy consumption in each test hut are continuously measured. The interior temperatures are kept constant using radiators.

Results from the pilot study show that the total U-value of windows can be improved by using the curtains. For the case studied in this project, using the curtain design (A) improved the U-value of the window by approximately 50 %. For Curtain design (A) a surface to surface resistance of 0.65 $\frac{\mathrm{m^2 \cdot K}}{\mathrm{W}}$ and for design (B) a resistance of 0.38 $\frac{\mathrm{m^2 \cdot K}}{\mathrm{W}}$ is estimated. The solar collector function of design (B) has the ability to capture some part of solar radiation striking the window. It is also shown that the solar collector function is more profitable for windows with lower height. However, the efficiency of this function is always less than the case with just a window where solar radiation reaches the interior parts directly.

The parameter study performed, shows a rather week relation between the efficiency of the solar collector function and the air velocity of the fans. Regarding the material used in the curtain, it is shown that the efficiency of the curtain can be further improved by using low emissivity material. Decreasing the emissivity of the material from 0.9 to 0.5 can theoretically improve the thermal properties of the curtain by almost 55 %.

Based on the studies made in the project and the comparison between the 2 designs of the Climate Curtain, it is concluded that the optimal option is to have the curtain design (A) and pull the curtain up whenever the solar intensity increases above a certain value. It should also be mentioned that the results and conclusions of this report are very much case dependent and are based on the limited studies performed. In order to fully capture the properties and the long-term behaviour of the curtains, additional studies are required.

Keywords: energy efficiency, heat transfer, solar radiation, window, curtain, blower door, emissivity, air flow rate, comsol, simulink.

Utvärdering och optimering av energismarta gardiner
En pilotstudie för att utvärdera energiprestandan och en parametrisk studie för att optimera utformningen av de nyutvecklade Climate Curtains

Examensarbete inom masterprogrammet Konstruktionsteknik och Byggnadsteknologi
ALI KARIM
Institutionen för arkitektur och samhällsbyggnadsteknik
Avdelningen for Byggnadsteknologi
Byggnadsfysik
Chalmers Tekniska Högskola

Sammanfattning

Enligt Energimyndigheten står byggnader för 40 % av Sveriges energiåtgång. Fönstren är oftast de svagaste länkarna i byggnadensklimatskal, gällande energiprestanda, och i uppvärmda byggnader går enorma mängder energi förlorad genom fönstren. På senare tid har flera nya typer av fönster med förbättrade termiska egenskaper utvecklats och har använts i nya byggnader. Det finns dock fortfarande ett stort antal gamla byggnader runt om i världen och i Sverige, där fönster med höga U-värden används. Dessutom används många byggnader så som skolor, kontor och fritidshem, i genomsnitt enbart en bråkdel av ett år. Climate Curtain är en ny energismart fönstergardin, med syfte att minska värmeförlusterna genom fönstren. Genom att täcka fönstren med Climate Curtain, till exempel när byggnader står tomma, kan energiprestandan på fönstren förbättras och på så sätt bidra till ett mer ekonomiskt och hållbart samhälle.

Projektet syftar till att utvärdera gardinernas energiprestanda genom in-situ mätningar samt simuleringar. I detta projekt har två olika typer av Climate Curtain studerats. Gardin typ (A) som bidrar till att öka fönstrets värmemotstånd och därigenom minska värmeförlusterna genom fönstren. Gardin typ (B) har däremot en extra solfångarfunktion som fångar en del av solstrålningen på fönstret och värmer då upp inomhustemperaturen. Uppvärmningen sker med hjälp av små fläktar inuti gardinen. Projektet undersöker också möjligheterna att optimera designen på gardinerna, med avseende på materialens emissivitet och lufthastigheten på fläktarna som används i gardin typ (B). Under 27-dagars lång mätningsperiod mäts inre och yttre temperaturer, solintensitet och energiförbrukning i varje testhus kontinuerligt. Inomhustemperaturer hålls konstanta med hjälp av ett element i varje testhus.

Resultat från studien visar att U-värdet på fönster kan förbättras genom att använda gardinerna. För det fall som studeras i detta projekt, förbättrade fönstrets U-värde med cirka 50 %, tack vare det extra motståndet som Climate Curtain bidrar med. För gardin typ (A), en yta till yta värmemotstånd på 0,65 $\frac{\mathrm{m^2 \cdot K}}{\mathrm{W}}$ och för typ (B), ett motstånd på 0,38 $\frac{\mathrm{m^2 \cdot K}}{\mathrm{W}}$ är beräknad. Solfångarfunktionen i typ (B) har förmågan att fånga en del av solstrålning som träffar fönstret. Det visas även att solfångarfunktionen är mer lönsam för fönster med lägre höjd. Effektiviteten av denna funktion är något mindre än fallet med bara ett fönster där solstrålningen når direkt till de inre ytorna via strålning.

Vidare visar parameterstudien en relativt svag relation mellan effektiviteten hos solfångarfunktionen och fläktarnas lufthastighet. När det gäller materialet som används i gardinen visas att gardinens effektivitet kan förbättras ytterligare genom användning av lågemissivitetsmaterial. En minskning på emissiviteten hos materialet från 0,9 till 0,5 kan teoretiskt förbättra gardinens termiska egenskaper med cirka 55 %.

Baserat på de studier som gjordes i projektet och jämförelsen mellan de två typerna av Climate Curtain, dras slutsatsen att det optimala alternativet är att ha gardin typ (A) och vid behov ställa upp denna om solintensiteten ökar över ett visst värde. Slutligen bör det också nämnas att resultaten och slutsatserna i denna rapport är starkt kopplade till de specifika fallen och baseras således på de begränsade studierna som har utförts. För att fullt utforska gardinernas egenskaper och långsiktiga effekt krävs ytterligare studier.

Nyckelord: energieffektivitet, värmetransport, solstrålning, fönster, gardin, blower door, emissivitet, luftflöde, comsol, simulink

Acknowledgements

This report is a master thesis of 30 credits, in the program Structural Engineering and Building Technology. The project has been carried out at the division of Building Technology, in collaboration with the company Climate Curtains AB, and under the supervision of professor Carl-Eric Hagentoft.

I would like to express my deepest gratitude to professor Carl-Eric Hagentoft for his useful knowledge and constant feedback and support throughout the project. Many thanks to Peter Hertz, Ulf Östemar and Olle Stenberg at Climate Curtains AB for their support and help with the practical issues of the project.

I would like to thank Marek Machowski for providing laboratory equipments, Tommie Månsson for his good advice about measuring instruments, Fredrik Domhagen for our interesting discussions and a special thank to Raheb Mirzanamadi for his limitless support during the project. I would like to thank all my teachers and colleagues at the division of building technology for their support and assistance during the project.

I would also like to express my appreciation to associate professor Paula Wahlgren for her knowledge and support during my years at Chalmers. She has been one of the reasons why I become interested in Building Physics. Finally, thanks to my family and friends for their support and encouragement.

Gothenburg June 2018
Ali Karim

Contents

List of Figures

List of Tables

Nomenclature

Roman upper case letters

A	Area [m^2]
C	Volumetric heat capacity [$\frac{J}{kg \cdot K}$]
I_{sol}	Solar radiation intensity [W/m^2]
K	Thermal conductance [$\frac{W}{K}$]
Q	Heat flow [W]
R	Thermal resistance [$\frac{m^2 \cdot K}{W}$]
R_a	Air flow rate [$\frac{m^3}{s}$]
RH	Relative humidity [%]
T	Temperature [$°C, K$]
U	U-value [$\frac{W}{m^2 \cdot K}$]
V	Volume [m^3]

Roman lower case letters

a	Thermal diffusivity [m^2/s]
c	Specific heat capacity [J/kgK]
g	g-value [$-$]
l_c	Characteristic length [m]
n	Air change rate [$\frac{1}{h}, \frac{1}{s}$]
q_c	Convective heat flow rate [W/m^2]
t	Time

Greek upper case letters

$\triangle P$	Pressure difference
$\triangle T$	Temperature difference [$°C, K$]

Greek lower case letters

α	Absorptance [-]
α_c	Heat transfer coefficient for convection [$\frac{W}{m^2 \cdot K}$]
α_r	Heat transfer coefficient for long wave radiation [$\frac{W}{m^2 \cdot K}$]
α_{sol}	Absorptivity of material [-]
ϵ	Emissivity [-]
λ	Thermal conductivity [$\frac{W}{m \cdot K}$]
ψ	thermal transmittance [$\frac{W}{m \cdot K}$]
ρ	Density[kg/m^3]
ρ	Reflectance [-]
ρ_a	Density of air [$\frac{kg}{m^3}$]
σ	Stefan-Boltzmann constant [W/m^2K^4]
τ	Transmittance [-]
$\tau_{window.diffuse}$	Window transmittance for diffuse radiation[-]

$\tau_{\text{window.direct}}$ Window transmittance for direct radiation[-]
φ Angel between the incident solar rays and the normal component of surfaces
c_{pa} Specific heat capacity of air $[\frac{J}{kg \cdot K}]$
c_p Specific heat capacity $[\frac{J}{kg \cdot K}]$

1
Introduction

Climate Curtain is a new type of energy smart window curtain. The purpose of this curtain is to cover windows and to increase the thermal resistance of the windows. Climate Curtain consists of several layers of textile and the corresponding air gaps in between. The high insulation properties of the curtain is due to several layers of stagnant air.
In many of already existing buildings, windows with high U-value are used. In these buildings, replacing the windows by new and low U-value windows can reduce the energy consumption. However, as the rest of the building envelope is, in most of the cases, also in a bad condition, changing the windows without improving the thermal properties of the rest of the building envelope is not an option. This means that in most of the cases, it has to be a proper and in general expensive retrofitting of the whole building.
Climate curtain can be a much cheaper solution for such buildings and windows with relatively bad U-values. By covering windows with this curtain, the U-value of windows can be improved without replacing the windows by new and expensive ones.
The curtains are partially tested with promising results at the testing institute RISE in Borås, Sweden. As a continuation to this, a pilot test under more realistic conditions is made in this project to evaluate the thermal performance of the curtain, before marketing the product.

1.1 Aim

The purpose of this thesis is to evaluate the energy performance of the window curtains, Climate Curtains, in term of thermal resistance. Additionally, possibilities for optimization of the design, considering material and air velocity of the fans will be investigated.
The following questions are to be answered:

- What is the thermal resistance of the curtains estimated by in-situ measurements?
- What is the impact of the solar collector function, on the energy performance of the curtain?
- What is the optimal design of the curtain regarding the air velocity created by fans?
- How much is the energy performance of the curtain improved if low emissivity material are used in the design of the curtain?

1.2 Methodology

The project is initiated with a literature study to better understand the theory, to find proper measuring instruments and also how to perform the experiments in accordance with standards. Before the main measurement campaign, a prestudy is done to roughly estimate the minimum extension of the measurements. After the construction of the test huts, a blower door test is made to evaluate the air permeability of the huts. Additionally,

a calibration campaign of 14 days is performed to ensure that the conditions in all 3 test huts are the same. A measurement campaign is finally conducted between the 27th of Mars and 22th of April.
A parameter study is made to evaluate the possibilities to optimize the performance of the curtains. In this study, emissivity of the material and air velocity of the fans are considered.
A model in Simulink is designed to simulate different case studies to evaluate the performance of the curtains. Figure 1.1 shows the work flow of the project.

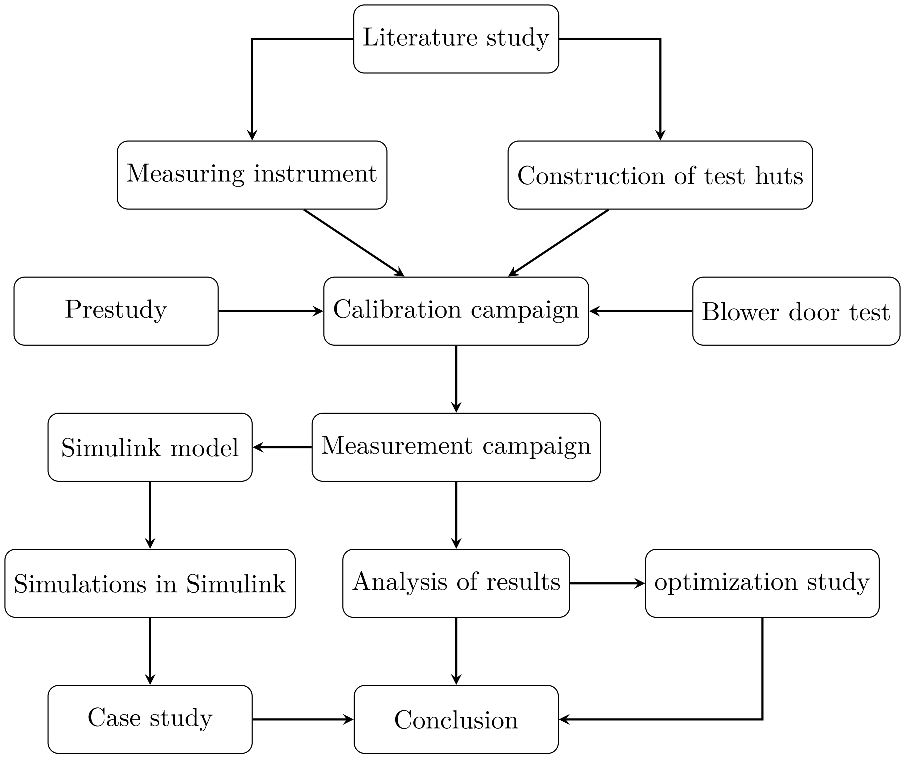

Figure 1.1: Flowchart showing the work flow for the project.

1.3 Limitations

This report evaluates only the energy performance of the curtains and other aspects such as moisture performance, environmental and economical aspects are not included. The measurements are performed during a period of 27 days and the conclusions are based on this study only. The long term effects on the performance of the curtains are not considered.

2
Theory

In this chapter the fundamental theories of physical phenomena used in the report, important to have knowledge about, are briefly described.

2.1 Heat transfer mechanisms

Energy (heat) is continuously transported from the parts with higher temperatures to the parts with lower temperatures (Petersson, 2007). The heat exchange between different materials and building components can be defined by three main heat transfer mechanisms listed below. All these mechanisms have to be considered when studying the thermal conditions of the building envelop.

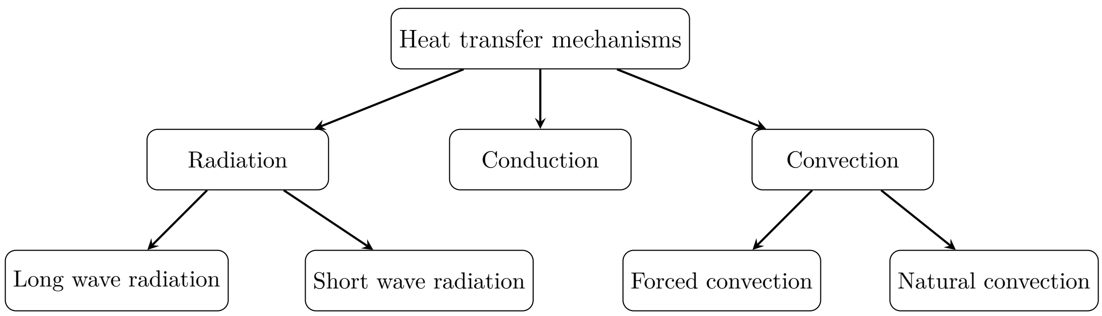

Figure 2.1: Different heat transfer mechanisms through the building envelope.

Conduction

In solid homogeneous material, the vibrations of the molecules result in heat exchange between the molecules (Petersson, 2007). Heat transfer due to conduction ends at absolute zero, (-273) degrees on the Celsius scale, at which the molecules can not move anymore. The driving force for this heat transfer mechanism is temperature differences which means that heat flows from warmer to colder parts through materials.
The transient three dimensional heat flux due to conduction in homogeneous materials can be expressed by the partial differential equation shown in Equation 2.1(Hagentoft, 2001).

$$\begin{aligned} \frac{\partial \mathrm{T}}{\partial \mathrm{t}} &= \mathrm{a} \cdot \nabla^2 \mathrm{T} = \mathrm{a} \cdot \left(\frac{\partial^2 \mathrm{T}}{\partial \mathrm{x}^2} + \frac{\partial^2 \mathrm{T}}{\partial \mathrm{y}^2} + \frac{\partial^2 \mathrm{T}}{\partial \mathrm{z}^2}\right) \\ \mathrm{a} &= \frac{\lambda}{\mathrm{c} \cdot \rho} \end{aligned} \tag{2.1}$$

a	Thermal diffusivity $[m^2/s]$
λ	Thermal conductivity [W/mK]
c	Specific heat capacity [J/kgK]
ρ	Density$[kg/m^3]$
T	Temperature[°C, K]
t	Time[s]

Convection

The heat transfer mechanism where heat is transferred from one part to another part by a main fluid, for instance air, is called convection (Hagentoft, 2001). The driving force for convection is differences in air pressure. Natural convection is due to differences in densities and forced convection is due to for instance the wind or mechanical fans. The convective heat flow can be expressed by Equation 2.2. Figure 2.2 shows how heat can be transferred from a surface to the ambient air by convection.

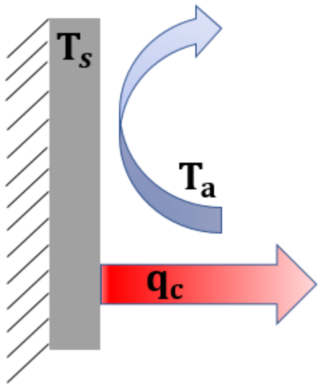

Figure 2.2: Convective heat exchange at a surface via air movements. The driving force is the temperature gradient between the air and the surface.

$$q_c = \alpha_c \cdot (T_s - T_a) \tag{2.2}$$

q_c	Convective heat flow rate $[W/m^2]$
α_c	Convective heat transfer coefficient $[W/m^2K]$
T_s	Surface temperature[°C, K]
T_a	Ambient air temperature[°C, K]

Radiation

Radiation is the propagation of electromagnetic waves (Petersson, 2007). All bodies with a temperature above the absolute zero radiate. The driving force for radiation is temperature differences between surfaces resulting in a net radiation from the warmer to the colder surface.

Unlike conduction and convection, radiation requires no medium (liquid,gas or solid), thus radiation occurs even in vacuum (Massoud, 2005). The thermal radiation that is emitted from a surface with a certain temperature T (in Kelvin) can be expressed by Equation 2.3.

$$Q = \epsilon \cdot \sigma \cdot A \cdot T^4 \tag{2.3}$$

ϵ Emissivity of the surface [-]
σ Stefan-Boltzmann constant [W/m^{2}K^4], $\sigma = 5.67 \cdot 10^{-8}$

The radiation that strikes a surface is just partly absorbed by the surface (Hagentoft, 2001). The remaining radiation energy is reflected and transmitted. The relation between these physical features is shown in Equation 2.4 and Figure 2.3.

$$\alpha + \rho + \tau = 1 \tag{2.4}$$

α Absorptance [-]
ρ Reflectance [-]
τ Transmittance [-]

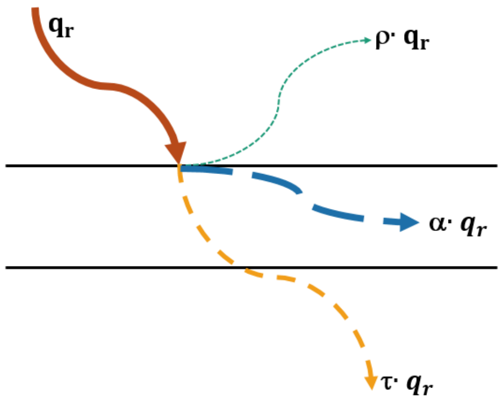

Figure 2.3: Thermal radiation acting on a surface and its division into absorption, reflection and transmission.

Solar radiation

The major part of solar radiation is considered to be a type of short wave electromagnetic radiation (Iqbal, 2012). The impact of the solar radiation that strikes a surface is dependent on the intensity of the radiation, absorptivity of the surface and the angel between the incident solar rays and the normal component of the surface (Petersson, 2007). The amount of solar heat that is absorbed by a surface can be calculated by Equation 2.5:

$$q = \alpha_{sol} \cdot I_0 \cdot \cos\varphi \tag{2.5}$$

α_{sol} Absorptivity of the surface [-]
I_0 Solar radiation intensity [W/m^2]
φ Angel between the incident solar rays and the normal component of the surface.

Night sky radiation

Night sky radiation is the long-wave radiation between the sky and any other surface facing the sky (Petersson, 2007). Due to this phenomenon, heat will be transferred from a warmer surface to the colder sky. The heat losses from the surface can result in a lower surface temperature than the surrounding outdoor air.
During clear and cold nights, surface temperatures can be 10-15 °C lower than the air temperature.

2.2 Heat transfer through a non-ventilated air gap

A non-ventilated air gap is, as the name implies an air gap between to different components that is not ventilated by any mechanical ventilation or wind. This means that, assuming a temperature difference between the inner surfaces of the two components, the heat transfer cross such an air gap will be due to natural convection, conduction and radiation (Hagentoft, 2001), see Figure 2.4. Thus the total amount of heat exchange can be calculated using Equation 2.6.

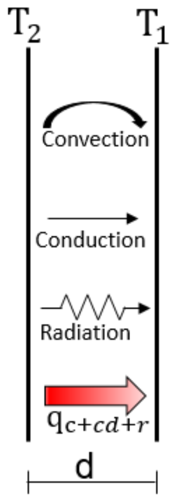

Figure 2.4: Heat flow in a non-ventilated air gap.

$$
\begin{aligned}
q_{\mathrm{c+cd+r}} &= (\alpha_{\mathrm{c+cd}} + \alpha_{\mathrm{r}}) \cdot (\mathrm{T_2} - \mathrm{T_1}) \\
\alpha_{\mathrm{c+cd}} &= \frac{\lambda_{\mathrm{air}}}{\mathrm{d}} + \alpha_{\mathrm{c}}
\end{aligned}
\tag{2.6}
$$

As seen in Equation 2.6, the heat transfer coefficient $\alpha_{\mathrm{c+cd}}$ consists of two terms where the first term accounts for conduction and the second one for convection. According to (Hagentoft, 2001), the width of the air gap determines whether convection or conduction is the dominating heat transfer mechanism. When the gap is very narrow, about 1-2 cm wide, the air is stagnant and thus conduction is dominating. By increasing the width of the gap, the contribution of convection increases as well.

2.3 Air movements through the building envelope

As described in Section 2.1, heat can be transferred via air (convection). Due to that and in order to evaluate the heat performance of the building envelope, it is necessary to

consider air movements through or within the building envelop and also its driving forces (Hagentoft, 2001).
As soon as there is a pressure difference at a certain location, in combination with an open flow path for instance a leakage, an air movement will be created (Straube, 2002). The driving forces for creating pressure differences are listed below:

- Stack effect (bouyancy)
- Wind pressure
- Mechanical ventilation

2.3.1 The stack effect

Stack or buoyancy effect is the air movement generated by temperature differences (Straube, 2002). Due to the temperature difference, the warm air with lower density will move upwards while the colder air sinks. The pressure difference cross the building envelope due to stack effect that generates at a certain height from the neutral pressure plane, NNP, can be calculated by Equation 2.7. Neutral pressure plane is the position where the pressure difference is zero.

$$\triangle \mathrm{P_s} = \mathrm{z} \cdot 3456 \cdot (\frac{1}{\mathrm{T_e}} - \frac{1}{\mathrm{T_i}}) \tag{2.7}$$

z	Height measured from NNP(m)
T_e	Exterior temperature[K]
T_i	Interior temperature[K]

2.3.2 Wind Pressure

For a building exposed to wind flowing from a certain direction, there will typically be a positive pressure on the windward side and a negative pressure on the leeward side and also on the roof, if the roof is flat (Hagentoft, 2001). A negative pressure difference causes a suction of air out from the building.
The pressure difference generated by wind forces acting on a building envelop can be calculated using Equation 2.8.

$$\triangle \mathrm{P_w} = (\mathrm{C_p} - \mathrm{C_{pi}}) \cdot \frac{\rho_\mathrm{a} \mathrm{v}^2}{2} \tag{2.8}$$

C_p	Wind pressure coefficient [-]
C_{pi}	Interior wind pressure coefficient [-]
ρ_a	Density of air $[\frac{kg}{m^3}]$
v	Reference wind speed $[\frac{m}{s}]$

2.3.3 Mechanical ventilation

Depending on type of the ventilation system, it is possible to introduce various types of pressure in a building (Straube, 2002). A supply ventilation system, i.e more supplied air than exhaust air, will cause an over pressure. Accordingly, an extract ventilation system, i.e more exhausted air that supplied air, will create an under pressure.

2.3.4 Air mass balance in a building

In a building, considered entirely as one zone, the air mass change rate corresponds to the difference between the total inlet air flow and outlet air flow, see Equation 2.9 (Roulet, 2012). This means that if there is no inertia in the system, the total amount of air flowing into the building must be the same as the air leaving the building, see Equation 2.9.

$$\begin{gathered}\sum \mathrm{M_{a,in}} = \sum \mathrm{M_{a,out}} \quad \text{if} \quad \frac{\mathrm{dM}}{\mathrm{dt}} = 0 \\ \sum(\rho_{\mathrm{a,in}} \cdot \mathrm{R_{a,in}}) = \sum(\rho_{\mathrm{a,out}} \cdot \mathrm{R_{a,out}})\end{gathered} \tag{2.9}$$

$\frac{\mathrm{dM}}{\mathrm{dt}}$	Change in air mass.
$\mathrm{M_{a,in}}$	Incoming mass flow rate.
$\mathrm{M_{a,out}}$	Outgoing mass flow rate.
$\rho_{\mathrm{a,in}}$	Density of inlet air.
$\rho_{\mathrm{a,out}}$	Density of outlet air.
$\mathrm{R_{a,in}}$	Volumetric flow rate of inlet air.
$\mathrm{R_{a,out}}$	Volumetric flow rate of outlet air.

The volumetric flow rate through an air gap can be expressed in terms of pressure differences, using the power low model (Walker et al., 1998). The flow rate can then be expressed according to Equation 2.10.

$$\mathrm{R_a} = \mathrm{C} \cdot \triangle \mathrm{P^n} \tag{2.10}$$

C	Flow coefficient.
n	Flow exponent.

By Using 2.10 to rewrite 2.9, the air mass balance equation can be expressed as:

$$\sum \rho_{\mathrm{air}} \cdot (\mathrm{C} \cdot \triangle \mathrm{P^n})_{\mathrm{inlet}} = \sum \rho_{\mathrm{air}} \cdot (\mathrm{C} \cdot \triangle \mathrm{P^n})_{\mathrm{outlet}} \tag{2.11}$$

2.3.5 Laminar and turbulent air flow

Depending on the velocity and viscosity of the fluid flowing in an air gap or between two parallel layers, two different types of flow can possibly occur (Batchelor, 2000). These two types are in fluid dynamics defined as laminar flow and turbulent flow. In case of laminar flow, there is no disturbance in the channel and the fluid will flow in parallel lines without being mixed to each other. Laminar flow occurs at low velocities.
On the other hand, in case of high velocity and low viscosity, the fluid is not flowing in parallel lines anymore and turbulent flow will occur, see Figure 2.5.

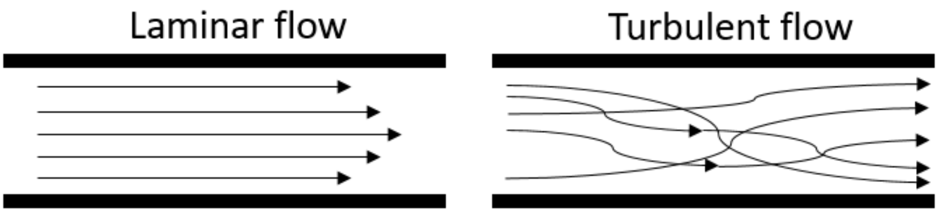

Figure 2.5: Laminar and turbulent air flow.

To predict the flow type, the dimensionless constant Reynolds number (Re) can be used (Hagentoft, 2001). Laminar flow occurs at low Reynolds number and the criterion for having laminar flow is expressed in Equation 2.12.

$$\mathrm{Re} = \frac{\mathrm{v_{mean}} \cdot 2 \cdot \mathrm{b} \cdot \rho_\mathrm{a}}{\mu} < 2000 \qquad (2.12)$$

$\mathrm{v_{mean}}$	Mean air speed $[\frac{\mathrm{m}}{\mathrm{s}}]$
b	Height of the air gap [m]
ρ_a	Air density $[\frac{\mathrm{kg}}{\mathrm{m^3}}]$
μ	Dynamic air velocity $[\frac{\mathrm{N \cdot s}}{\mathrm{m^2}}]$

2.3.6 Air movements through a ventilated air gap

The air transfer through an air gap penetrating a building envelope, is typically of the type laminar flow for the inner of the air gap (Hagentoft, 2001). The total air flow through the air gap can be estimated by knowing the total pressure difference over the gap and the total air flow resistance. For the air flowing into an air gap, there are flow resistances both at the entrance and exit of the gap but also a resistance inside the gap, see Figure 2.6.

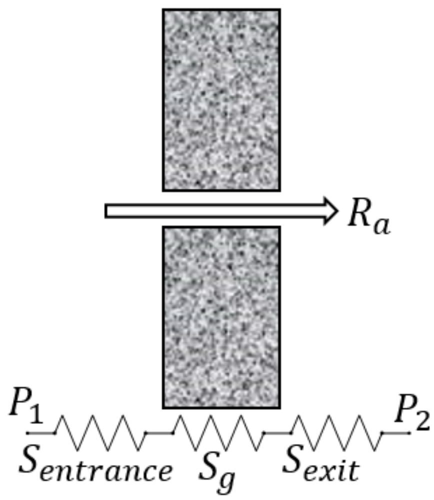

Figure 2.6: An air gap and the corresponding air flow resistance network.

The total air flow through an air gap can be calculated by Equation 2.13. It should be noticed that Equation 2.13 is valid only in case of laminar flow in the air gap, see Chapter 2.3.5.

$$
\begin{aligned}
R_a &= \frac{1}{2 \cdot S'_e} \cdot (\sqrt{S_g^2 + 4 \cdot \triangle P \cdot S'_e} - S_g)) \\
S'_e &= \frac{1.8 \cdot \rho_a}{2 \cdot A^2} \\
S_g &= \frac{12 \cdot \mu \cdot L}{b^2 \cdot A}
\end{aligned}
\tag{2.13}
$$

S'_e	Describes the relation between air flow and the resistances at the entrance and the exit of the air gap $[\frac{Pa}{(m^3/s)^2}]$.
S_g	Inner flow resistance $[\frac{Pa \cdot s}{m^3}]$.
$\triangle P$	Total pressure difference over the air gap [Pa].
ρ_a	Air density $[\frac{kg}{m^3}]$.
A	Area perpendicular to the flow direction $[m^2]$.
L	Length of the air gap parallel to the flow direction [m].
b	Height of the air gap [m].

Considering a ventilated air gap as shown in Figure 2.7, the air temperature at different positions through the air gap can be estimated if the temperature and the flow rate of the inlet air is known (Hagentoft, 2001). The temperature at a position far away from the air inlet, where there is no disturbance in the temperature is here described as T_0 and can be estimated using Equation 2.14.

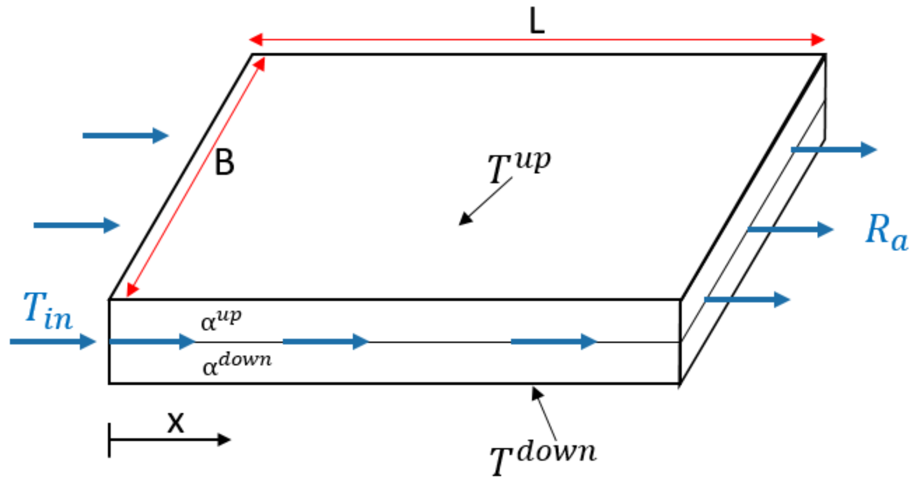

Figure 2.7: A ventilated air gap between two layers, and the corresponding temperatures and heat transfer coefficients.

$$
T_0 = \frac{\alpha_{up} \cdot T_{up} + \alpha_{down} \cdot T_{down}}{\alpha_{down} + \alpha_{down}} \tag{2.14}
$$

α_{up} Upper heat transfer coefficient between the upper temperature and the air in the gap $[W/m^2K]$.
α_{down} Lower heat transfer coefficient between the lower temperature and the air in the gap $[W/m^2K]$.
T_{up} Temperature at the top $[°C, K]$.
T_{down} Temperature at the bottom $[°C, K]$.

Furthermore, the air temperature at any position in the air gap can then be estimated by Equation 2.15.

$$T(x) = T_0 + (T_{in} - T_0) \cdot e^{\frac{-x}{l_c}}$$
$$l_c = \frac{\rho_a \cdot c_{pa} \cdot R_a}{B \cdot (\alpha_{up} + \alpha_{down})} \tag{2.15}$$

T_0 Undisturbed temperature far away from the air inlet $[°C, K]$.
T_{in} Inlet air temperature $[°C, K]$.
x Position inside the air gap, in the direction of the air [m].
l_c Characteristic length of the air gap [m].
ρ_a Density of air $[\frac{kg}{m^3}]$.
c_{pa} Specific heat capacity of air $[\frac{J}{kg \cdot K}]$.
R_a Air flow rate $[\frac{m^3}{s}]$.
B Width of the air gap [m].

2.4 U-value

The heat flow through a building envelope component, consisting of parallel layers, is transferred in straight lines from inside towards outside (Anderson, 2002).
U-value is the thermal transmittance of the component and it describes the total heat flow at steady state, that is transferred through one square meter of the component and at one degree of temperature difference. U-value has the unit $[\frac{W}{m^2 \cdot K}]$ and for a homogeneous component can be calculated by Equation 2.16. Figure 2.8 shows a homogeneous external wall consisting of two layers, and the corresponding network of thermal resistances.

$$U = \frac{1}{R_{se} + \sum R_i + R_{si}} \tag{2.16}$$

R_{se} External surface resistance, counting for both convection and long wave radiation $[\frac{m^2 \cdot K}{W}]$.
R_i Heat resistance, counting for each layer of the building envelope components $[\frac{m^2 \cdot K}{W}]$.
R_{si} Internal surface resistance $[\frac{m^2 \cdot K}{W}]$.

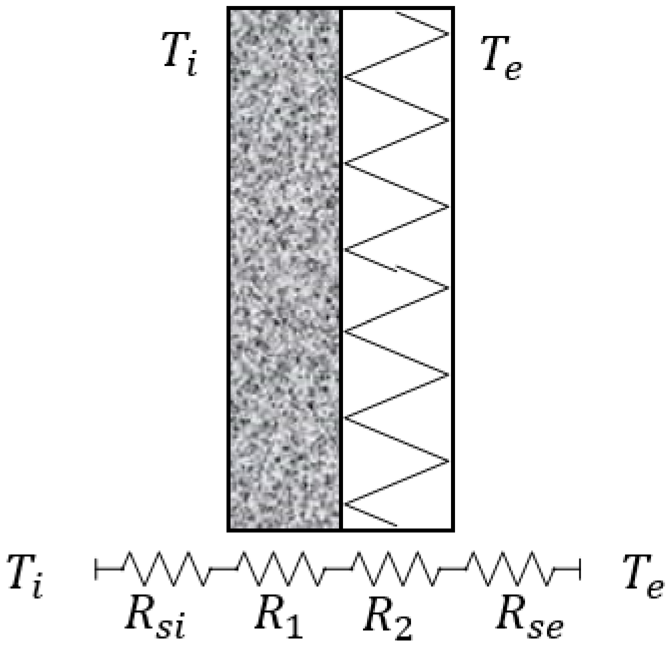

Figure 2.8: A homogeneous wall and the corresponding heat resistance network between indoor and outdoor.

Estimation of U-value by In-situ measurements

According to the standard ISO 9869-1, if the conditions of steady state are imposed, the thermal transmittance of a component can be estimated by in-situ measurements (Elements-In, 2014). To do that, temperatures on both sides and the heat flux trough the component have to be measured.
Creating steady-state conditions in practice is difficult to accomplish (Elements-In, 2014). One possible option to fulfill the criteria of steady-state in practice is by applying the hot-box method described in Chapter 2.11. Other options suggested by ISO 9869-1 are:

- To consider the fluctuations of temperatures and heat fluxes by a transient model.
- To run the analysis for a sufficiently long period of time to ensure that the mean values of temperatures and heat fluxes can be considered as good estimations of the steady-state. The requirements for this method is that the thermal properties of the materials used in the component are constant regardless the temperature variations during the analysis. In additional to that, the effects of thermal mass have to be negligible. This criteria can be fulfilled by long-term measurement and averaging the values over longer periods.

2.5 g-value

The g-value or the solar heat gain coefficient of a window, specifies the total incoming energy through the window, both from direct and diffuse solar radiation (Köster, 2004). The g-value which is expressed in percentage, includes the directly transmitted energy and secondary emissions from the window, see Figure 2.9.

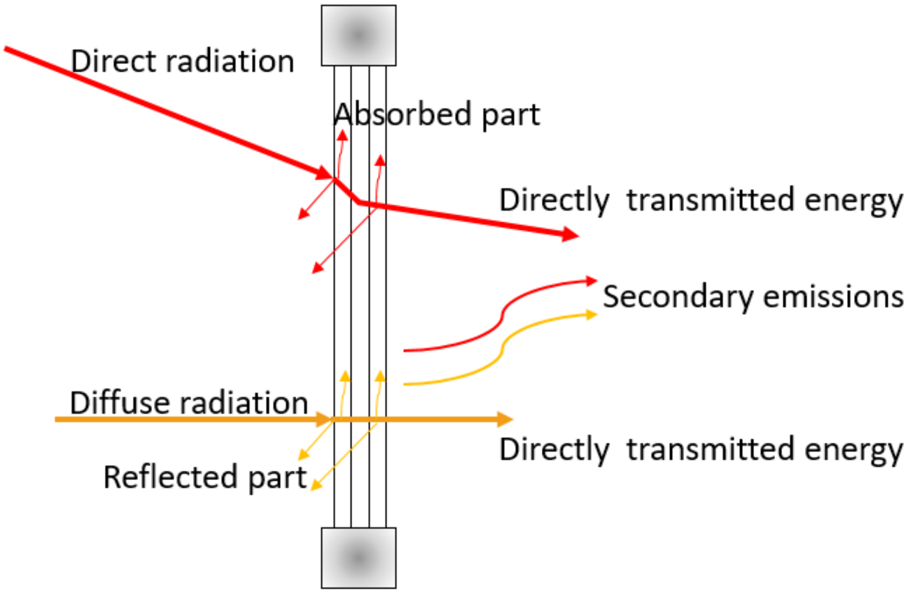

Figure 2.9: Division of incident radiation into directly transmitted energy and secondary emissions.

2.6 Transmission losses

The heat losses through the building envelope are expressed in term of transmission losses and can be calculated by Equation 2.17 (Petersson, 2007).

$$Q_{trans} = \sum U_i \cdot A_i \cdot \triangle T \tag{2.17}$$

U_i U-value for each part of the building envelope $[\frac{W}{m^2 \cdot K}]$.
A_i Area for each part of the building envelope $[m^2]$.
$\triangle T$ Temperature difference over the building envelope $[°C, K]$.

2.7 Ventilation losses

Any kind of air exchange between the warmer indoor and colder outdoor environment results in some heat losses. The air exchange might be via ventilation system in a controlled manner or via leakages that exist in the building (Hagentoft, 2001). The ventilation heat losses can be calculated by Equation 2.18.

$$Q_{ventilation} = n \cdot V \cdot \rho_a \cdot c_{pa} \cdot \triangle T \tag{2.18}$$

n Air change rate $[\frac{1}{s}]$ or $[\frac{1}{h}]$.
V Total interior air volume of the building $[m^3]$.
ρ_a Density of air $[kg/m^3]$.
c_{cp} Specific heat capacity of air at constant atmosphere pressure $[J/kg \cdot K]$.
$\triangle T$ Temperature difference between indoor and outdoor $[°C, K]$.

2.8 Thermal bridge

Thermal bridges are the local alterations in the homogeneous layout of the building envelop (Petersson, 2007). Thermal bridges result in higher heat losses in the areas containing a

thermal bridge, in comparison to other parts of the building envelope without any thermal bridges.
The local changes in building construction that create thermal bridges are normally one of the types listed below and shown in Figure 2.10:
(a) Connection between two materials with two different heat conductivity.
(b) Change of thicknesses in parts of the building envelope.
(c) Increment of cold areas in parts of the building envelope, for instance in corners and connections between walls, roofs and floors.

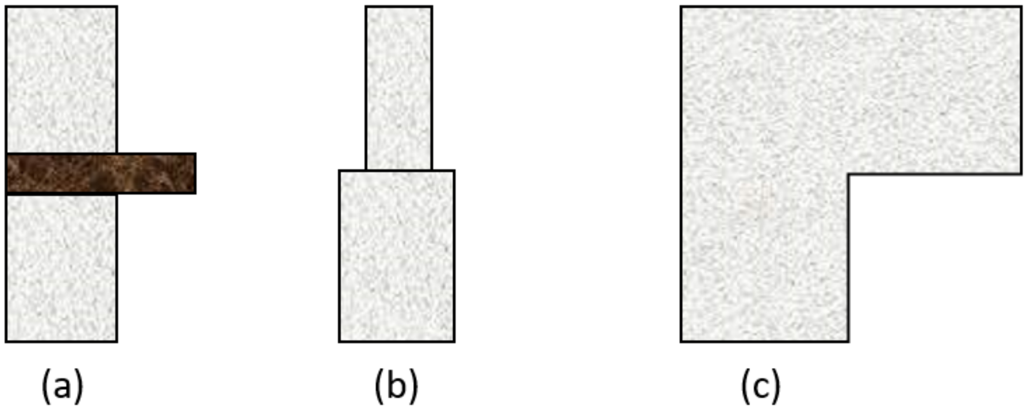

Figure 2.10: Different types of thermal bridges in building constructions.

The additional heat losses due to thermal bridges have to be considered when evaluating the thermal performance of the building envelope. Thermal bridge is normally designated by (Ψ) and has the unit $[\frac{W}{m \cdot K}]$.

2.9 Stationary and transient heat balance for a building

To reach a heat balance in a building, the heat gains inside the building have to be equal to the heat losses from the building (Bauwens and Roels, 2014). If the whole building can be considered as one zone with the same temperature, the heat balance of the building can be expressed by Equation 2.19:

$$C_i \cdot \frac{dT_i}{dt} = \sum Q_i \quad + c \tag{2.19}$$

C_i	Volumetric heat capacity of the indoor air and all components with the same temperature as indoor air $[\frac{J}{kg \cdot K}]$.
$\frac{dT_i}{dt}$	Temperature change in time.
Q_i	Total heat gains [W].
c	Heat loss term [W].

Considering the special case, where the indoor temperature is constant, the term $[\frac{dT_i}{dt}]$ in Equation 2.19 is equal to zero. This means that the stationary heat balance of the building becomes as shown in Equation 2.20:

$$\sum Q_i \quad + c = 0 \tag{2.20}$$

The method presented here to describe the heat balance of a building is called Lumped model (Hagentoft, 2001). In this model all interior layers inside a thermal insulated envelope, having the same temperature as indoor air, are lumped into one volumetric heat capacity. The volumetric heat capacity of interior layers can be calculated by Equation 2.21.

$$\mathrm{C} = \sum \mathrm{d_i} \cdot \rho_\mathrm{i} \cdot \mathrm{A_i} \cdot \mathrm{c_{p,i}} \tag{2.21}$$

C	Volumetric heat capacity of all the components with the same temperature as indoor air $[\frac{\mathrm{J}}{\mathrm{kg \cdot K}}]$.
$\mathrm{d_i}$	Thickness of interior layers [m].
ρ_i	Density of interior layers $[\mathrm{kg/m^3}]$
$\mathrm{A_i}$	Area of interior layers $[\mathrm{m^2}]$.
$\mathrm{c_{p,i}}$	Specific heat capacity of interior layers $[\mathrm{J/kg \cdot K}]$

The heat balance equation can be further developed by including the different heat loss and heat gain mechanisms directly in the heat balance equation (Bauwens and Roels, 2014). The heat balance equation becomes:

$$\mathrm{C_i} \cdot \frac{\mathrm{dT_i}}{\mathrm{dt}} = \mathrm{Q_{heat}} + \mathrm{Q_{solar}} + \mathrm{Q_{internal}} - \mathrm{Q_{trans}} - \mathrm{Q_{vent}} - \mathrm{Q_{latent}} \tag{2.22}$$

$\mathrm{Q_{heat}}$	Heat gains from heating or cooling system [W].
$\mathrm{Q_{solar}}$	Heat gains from solar radiation thorough windows [W].
$\mathrm{Q_{internal}}$	Internal heat gains from domestic appliance [W].
$\mathrm{Q_{trans}}$	Transmission heat losses through the building envelope [W].
$\mathrm{Q_{vent}}$	Ventilation heat losses, including leakages [W].
$\mathrm{Q_{latent}}$	Heat losses due to the drying of the construction damp (moisture) [W].

2.10 Outdoor temperature variations and its influence on indoor temperature

Due to Earth rotation around own axis but also around Sun, the outdoor temperature varies periodically on daily and seasonal bases (Hagentoft, 2001). One common way to describe the periodic variations of outdoor temperatures is by using trigonometric functions cos or sin.

In this report the outdoor temperature variations are described by cosine function including mean outdoor temperature, maximum and minimum temperatures that occur at regular intervals and time delay where the maximum outdoor temperature occurs, see Equation 2.23. In Figure 2.11 the outdoor temperature profile for the city Gothenburg in Sweden, with an annual mean outdoor temperature of 8 °C and an amplitude of 10 °C is shown. In Figure 2.11 it is assumed that the maximum outdoor temperature occurs in the middle of the year.

$$\mathrm{T_{out}(t)} = \mathrm{T_{out.mean}} + \mathrm{T_{out.A}} \cdot \cos(\frac{2 \cdot \pi}{\mathrm{t_p}} \cdot (\mathrm{t} - \mathrm{t_1})) \tag{2.23}$$

$T_{out.mean}$	Mean outdoor temperature over the time period [°C, K].
$T_{out.A}$	Amplitude of outdoor temperature over the time period [°C, K].
t_1	When the maximum outdoor temperature occurs [s, h, d].
t_p	Time period [s, h, d].

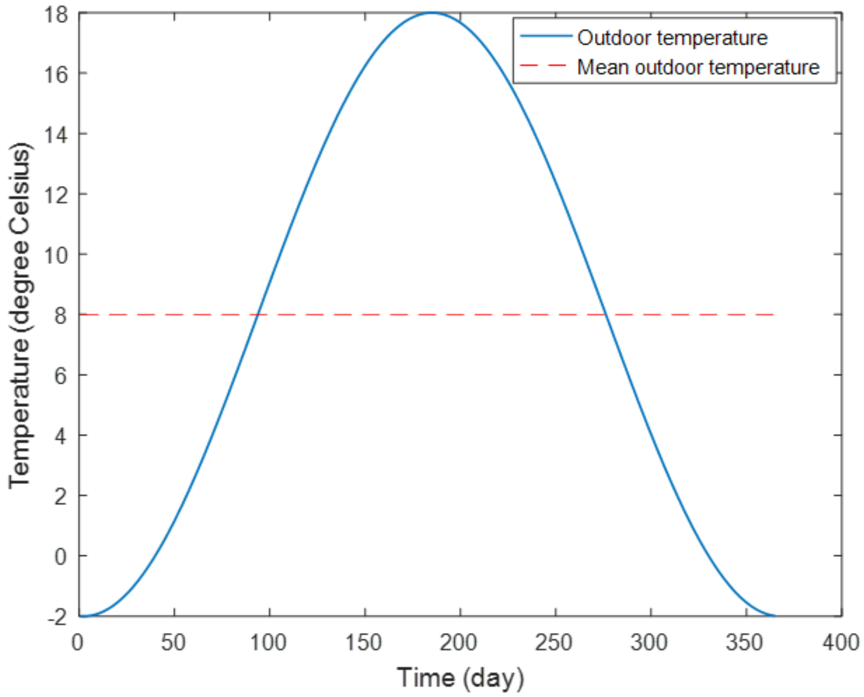

Figure 2.11: Periodic outdoor temperature variations in Gothenburg, described by cos function.

In accordance to the outdoor temperature variations, the indoor temperature also varies periodically and can be described by trigonometric functions (Hagentoft, 2001). Expression in 2.24 describes the periodic indoor temperature variations.

$$\begin{aligned}
T_{in}(t) &= T_{in.mean} + T_{in.A} \cdot \cos(\frac{2 \cdot \pi}{t_p} \cdot (t - t_2)) \\
T_{in.A} &= \frac{1}{\sqrt{1 + (\frac{2 \cdot \pi \cdot t_c}{t_p})^2}} \cdot T_{out.A} \\
t_2 &= (\frac{t_p}{2 \cdot \pi}) \cdot (\frac{2 \cdot \pi \cdot t_1}{t_p} + \arctan(\frac{2 \cdot \pi \cdot t_c}{t_p})) \\
t_c &= \frac{C}{K}
\end{aligned} \tag{2.24}$$

$T_{in.mean}$	Mean indoor temperature over the time period [°C, K].
$T_{in.A}$	Amplitude of indoor temperature over the time period [°C, K].
t_2	When the maximum indoor temperature occurs [s, h, d].
t_p	Time period [s, h, d].
C	Volumetric heat capacity of all the components with the same temperature as indoor air [$\frac{J}{kg \cdot K}$].
K	Overall thermal conductance of the building [$\frac{W}{K}$].
t_c	Time constant of the building [s, h, d].

As it can be seen in Equation 2.24, the indoor amplitude and phase shift are different from the outdoor ones. The reason for that is the thermal inertia of a building (Hagentoft, 2001). The time constant of a building, t_c, depends on the thermal inertia of the building and describes how fast the indoor temperature variations follow the outdoor temperature variations. For the special case when there is no heat gains in a building, the mean indoor temperature of the building is the same as the mean outdoor temperature, see Figure 2.12.

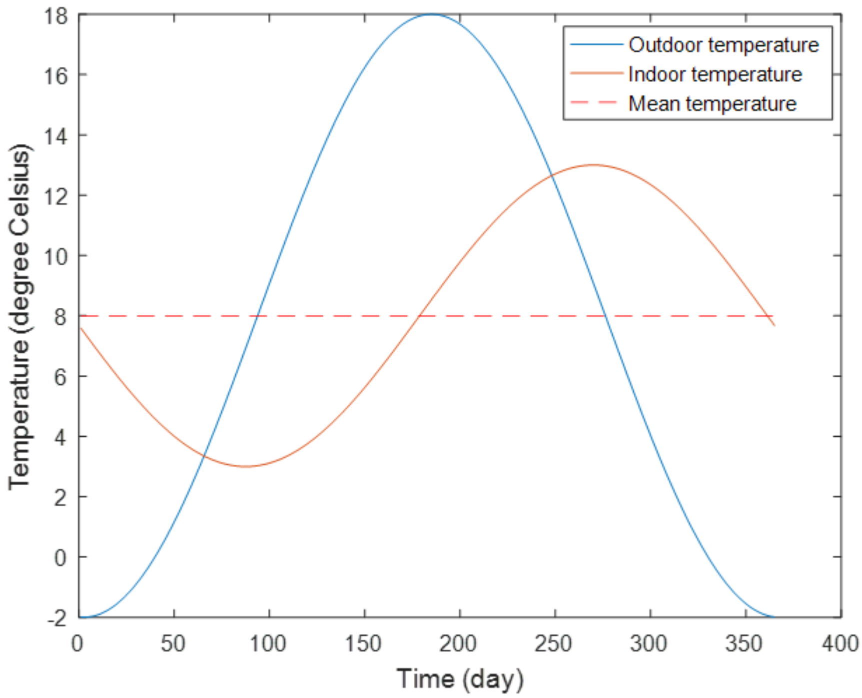

Figure 2.12: Schematic figure showing the periodic outdoor temperature variations in Gothenburg and the periodic indoor temperature variations for an unheated building located in Gothenburg.

2.11 Hot-box method

Hot-box method is a standard method to evaluate the thermal performance of a specific test specimen (ASTM-C1363, 2011). According to this method the thermal performance of a (building) component can be evaluated by designing a hot-box apparatus where there is a steady temperature difference across the component for a sufficient period of time. By sufficient period of time it means the time required to achieve a constant heat flux and steady temperatures. After achieving the constant heat flux and temperatures and depending on the desired accuracy, the time period of the measurements has to be extended additionally. This to quantify the evaluated parameters. Figure 2.13 shows a typical design of a hot-box apparatus.

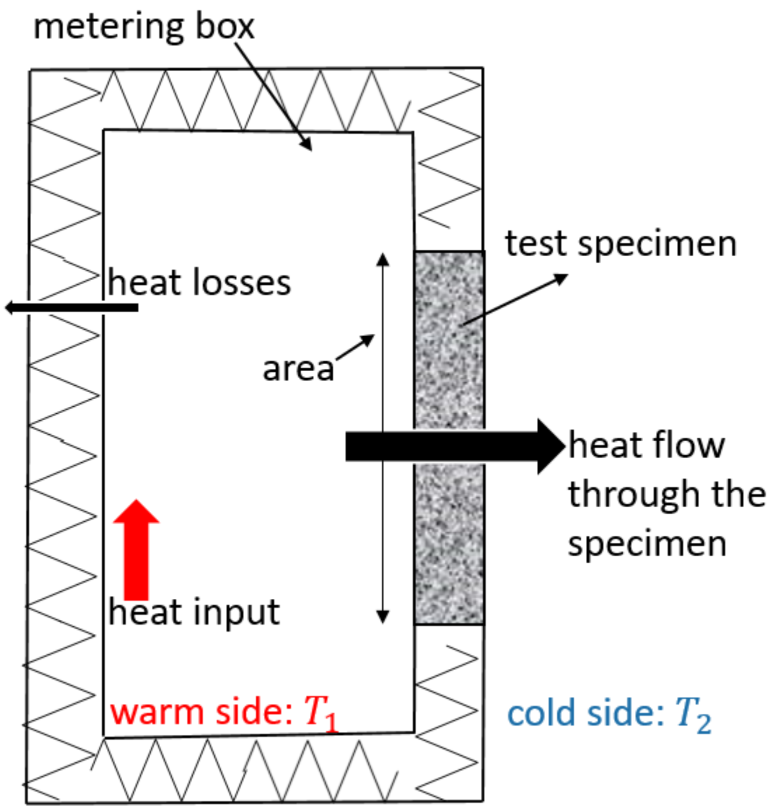

Figure 2.13: Schematic design of a hot-box apparatus to evaluate the thermal performance of a test specimen.

Assuming that the requirement of steady heat flow is fulfilled, the thermal resistance or thermal transmittance of a test specimen can be determined by the hot-box method if the total heat flux, area and temperature differences can be quantified (ASTM-C1363, 2011). Unlike area and temperatures, the heat flux can not be directly estimated. Instead, the net heat flux through the test specimen can be calculated by measuring the total energy input to the apparatus and the total heat losses thorough the envelope of the apparatus except for the part with the specimen. According to the hot-box method, the heat losses through the envelope should be minimized by for instance using highly insulated material in the envelope.

2.12 Blower door test

In order to evaluate and document the overall air tightness of a building or a part of a building, a blower door test can be performed (Energy Conservatory, 2012). Blower door test is a standardized test in which a pressure difference over the building envelope is created using a fan. By measuring the total pressure difference created over the fan, the total air flow through the fun can then be calculated. Considering the air mass conservation low described in Chapter 2.3.4, the total mass of air flowing through the fan has to be the

same as the total amount of air leaving the building through the leakages.
There are two different modes for operating a blower door test, pressurization or depressurization (Institute, 2015). If the inside pressure is higher than the outside pressure, a pressurization mode is performed and in the opposite case a depressurization mode is performed. In this project, the blower door test is performed according to the Swedish standard SS-EN ISO 9972:2015.

2.13 MATLAB/Simulink

Simulink is a block diagram software package for simulation and model-based design of dynamic systems (time dependent)(Karris, 2006). Simulink provides graphical editors and is integrated in MATLAB environment which makes it possible to simulate and analyze models in both environments, modelling in one environment and exporting the results to the other one for further analysis.

2.14 Comsol Multiphysics

Comsol Multiphysics is a software for modelling and numerical simulations (Zimmerman, 2006). In Comsol, systems of user-defined differential equations are solved by a semi-analytic approach. This is done by using finite element analysis. Comsol provides users some pre-designed models and templates which can be used for different modeling applications and to analyze different physical problems. Regarding building physics applications, Comsol Multiphysics can for instants be used to visualize and analyze different transport phenomena such as heat transport, numerically or by computational fluid dynamics(CFD).

3

Product description

The window curtains analyzed in this project consist of a curtain rod with 8 layers of textile, creating 7 layers of air. Two different designs of the curtain have been studied. In the first design, design A, upper and lower ledges are completely sealed and the certain is aimed to act just as an additional thermal insulation for the window. In the second conceptional design of the curtain, design B, the external surface is black with the aim to capture some solar radiation and then circulate the heated air back to the room via air ducts, see Figure 3.1 and 3.2. The air circulation is accelerated by 3 fans placed in the upper ledge of the curtain. The fans are controlled by a differential temperature control module with one temperature sensor inside the outermost air layer of the curtain and one sensor inside the rum. Each fan creates an air flow of $45.07\frac{m^3}{h}$ and is turned on whenever the air temperature in the outermost layer is higher than the indoor temperature. Both curtains have the dimensions [1.3m · 0.8m · 0.12m]. The structural components of the curtains are produced by 3D-printers of model "Zortaz M200". Further information about the materials used in the curtains can be found in Table 3.1.

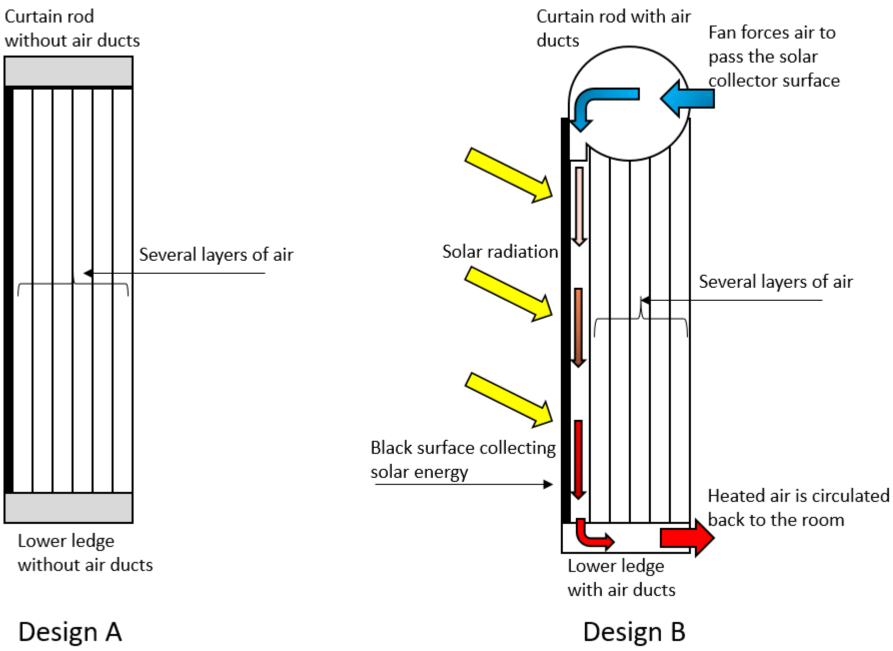

Figure 3.1: Schematic figure, not in scale, showing the design of Climate Curtain. Left: Design (A). Right: Design (B) with the solar collector and fan.

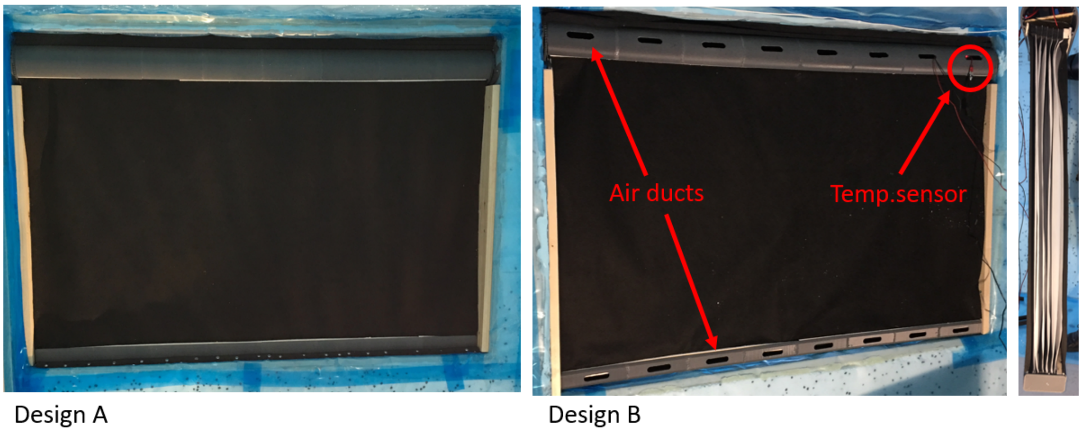

Figure 3.2: Photos showing the design of the Curtains. Left: Design (A). Middle :Design (B). Right: Design (B) side view

Table 3.1: Materials used in the curtains.

Material	**Information**
Textile	Fibertex SS PP, 40 g/m^2, Nevotex [1]
Textile	Fibertex 100 g/m^2, Black, Nevotex [2]
TowiTek diff.temp. control module	Conrad [3]
Chassis fan	Conrad [4], air flow rate: 45.07 m^3/h
Filament for 3D-printers	ABS filament 1.75 mm [5]

[1] http://ehandel.nevotex.se, Art. nr: 1904160
[2] http://ehandel.nevotex.se, Art. nr: 1941404
[3] www.conrad.com, Nr. 19 12 53, 9-12V (AC) or 12-15V (DC)
[4] www.conrad.com, Art.nr: 1169086, AK-FN076 Slimline Black, 80 x 80 x 10.8 mm
[5] https://www.3dprima.com/se/filament/abs-1-75mm/primavalue-abs-filament-1-75mm-1-kg-spool-svart/a-20642/

4

Performance of the pilot tests and prestudies in form of simulations to estimate the extension of the measurement campaign

To evaluate the energy performance of the curtains by in-situ measurements, a pilot study is performed. To do that, 3 identical test huts with one window in each hut are constructed. These test huts are placed in a large, partly unoccupied stable located in Färgelanda, Sweden, see Figure 4.1. The stable, with dimensions [40m · 10m · 6m], is built in 1960. Figure 4.2 shows the position of the test huts inside the stable. The building envelope of the stable is made of brick and the thickness of the external walls is roughly 40 cm.

Figure 4.1: Showing the coordinates of the city Färgelnada where the pilot studies are performed.

As the pilot studies are performed to evaluate the energy performance of the curtains according to the Hot-box method described in Section 2.11, the tests huts are constructed in such a way that aims to minimize all other heat losses than the ones through the windows. The test huts have the internal dimensions of [2.5m · 2.6m · 1.9m]. The entire building envelope of the test huts is made of Expanded polystyrene, EPS. The external walls of the test huts, that separate them from the indoor environment of the stable, have

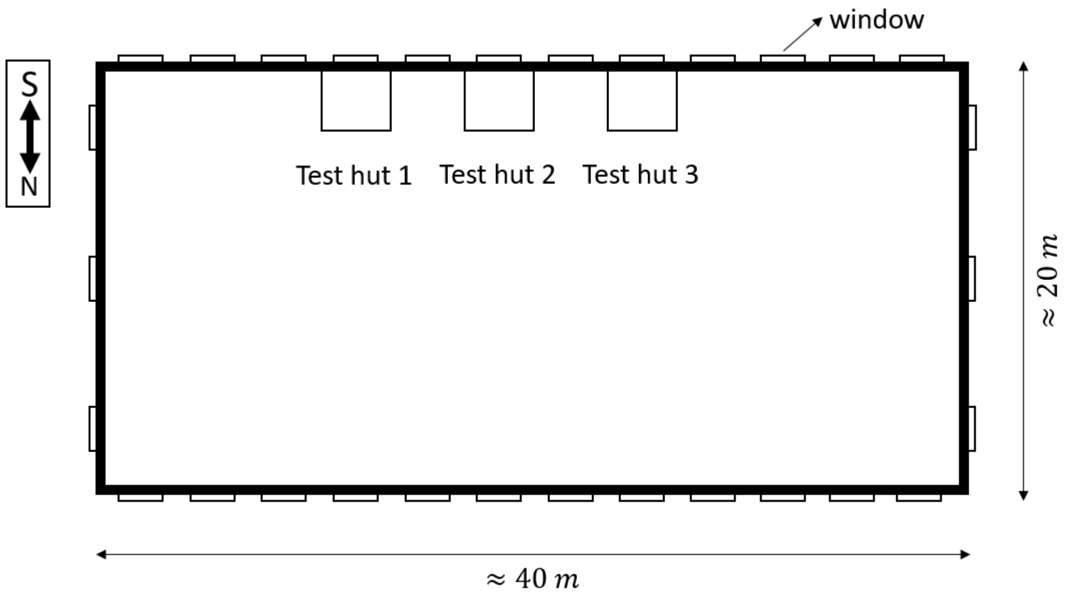

Figure 4.2: Figure, not in scale, showing the position of the test huts inside the stable.

a thickness of 200 mm. Roof and floors have a thickness of 300 mm. Additionally, the test huts are elevated by approximately 200 mm from the ground to create an air gap between the floor of the test huts and the ground. This to minimize the heat losses to the ground. The external walls of the test huts where the windows are positioned, and that separate the tests huts from the outdoor environment, consist of 100 mm EPS and 400mm Brick, see Figure 4.3.

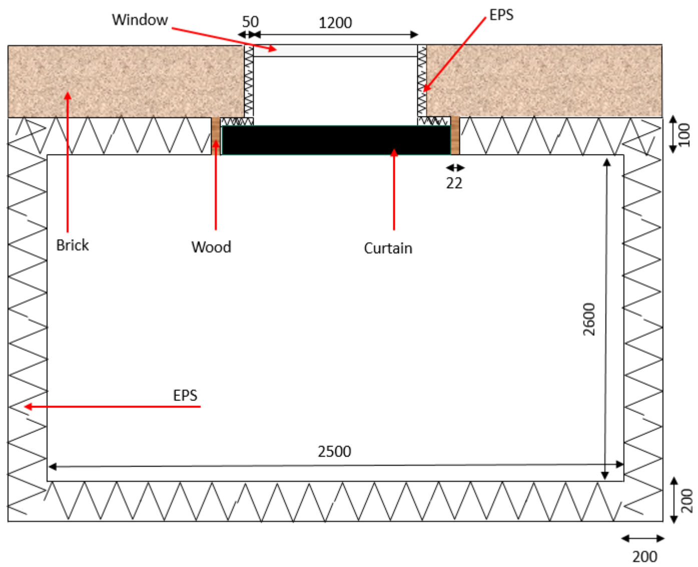

Figure 4.3: Principle sketch, not in scale, showing the construction and dimensions of the test huts [mm].

In each test hut, there is a gypsum board on the floor to ease the walking without damaging the EPS. There is also a gypsum board behind the plug socket as a fire safety measure. Windows are replaced by new ones with a U-value of 1.5 $\frac{W}{m^2 \cdot K}$, see Appendix 1. Table 4.1 presents all information concerning the dimensions and materials used in the construction of the test huts.

Table 4.1: Compilation of the material used in the construction of the test huts.

Component	Material	Dimension
External wall	EPS [1]	Thickness:200 mm
Roof/ Floor	EPS	Thickness: 300 mm
Nail	Distex plastic [2]	length 180 mm
Glue	Turbo Tack 291 [3]	-
plastic foil	Age-resistant air and vapour barrier	Thickness: 0.2 mm
Window	SP window, dubble glazing	120mm · 80mm
Gypsum board(floor)	Gypsum	240mm · 120mm · 13mm
Gypsum board(plug socket)	Gypsum	180mm · 55mm · 13mm
Door	EPS	1500mm · 800mm · 200mm

Figure 4.4 shows the final construction of the test huts. The distance between the test huts is approximately 2m.

Figure 4.4: Photos showing the construction and position of the test huts.

To evaluate the performance of the curtains, one curtain(design A) is placed in test hut 1, and one(design B) in test hut 3. Test hut 2 contains no curtain and is considered as the reference test hut. The different conditions in different huts are presented below:

- Test hut **number 1** has a window and the **design (A)** of the curtain, but **not exposed** to solar radiation.
- Test hut **number 2** has a window **exposed** to solar radiation **without** a curtain.
- Test hut **number 3** has a window and the **design (B)** of the curtain, and **exposed** to solar radiation.

[1] Thermal conductivity: 0.038 $[\frac{W}{m \cdot K}]$ according to the product specification provided by the producer.
[2] /produkt/isolerspik-isp-18048-distex-plast-180mm-48st-sb/
[3] http://www.danalim.se/produktkatalog/bygg/montage-kontaktlim/turbo-tack-291

To provide the desired condition in test hut 1, i.e no solar radiation, a wooden board is used as a shading for the window in test hut 1. The board is also painted white to decrease its absorptivity of solar radiation, see Figure 4.5.
The pilot study is run for a measuring campaign of approximately 4 weeks. During this period, the interior temperatures are kept constantly around 20°C and are measured by sensors. The different equipment used in the project are presented in Section 4.1.
Result from test hut 1 is used to estimate the thermal resistance of the curtain (A) and its contribution to the total thermal resistance of the window construction. The output from test hut 3 is used to estimate the thermal resistance of the curtain (B) and its contribution to the total thermal resistance of the window construction, i.e the window, the curtain and the air gap of approximately 30cm between them. In additional to that, the performance of the solar collector function of curtain (B) is estimated. This is done by evaluating the total amount of solar radiation that has been utilized in test hut 3 in comparison to test 2 where there is just a window. The output result from test hut 2 is used both to estimate the accuracy of the studies but also to compare to the results from test hut 1 and 3.

Figure 4.5: The wooden board painted in white, used as window shading in test hut 1.

4.1 Equipment used in this study

As described previously in this chapter, interior temperatures have to be kept constantly at approximately 20°C. To achieve the elevated temperatures in the test huts, one electrical radiator of model"ELRAD KABA 500W/230V" is used in each test hut. The radiator is equipped with an external thermostat that can be set to a certain temperature and by that regulate the temperature. According to the product specifications, the radiator has an accuracy of ±0.1°C. The radiators are placed in the middle of the test huts. In additional to the radiator, a floor fan is located in each test hut. This to circulate the interior air and to get a more even temperature distribution. The fan is of model "Rubicson floor fan ϕ 43 cm" with a maximum power consumption of 58 W, see Figure 4.6. The technical specification of the radiator can be seen in Appendix 2.

Figure 4.6: Electrical radiator and floor fan used in this study.

Temperature monitoring

For this pilot study, indoor temperatures in all three test huts, in the stable and outdoor temperatures are continuously monitored and logged by the concept of IoT, Internet of Things. More information about the fundamental concept of IoT can be read in (Yang, 2014).
Figure 4.7 shows the system used to measure and collect the temperatures during the measurement campaign.

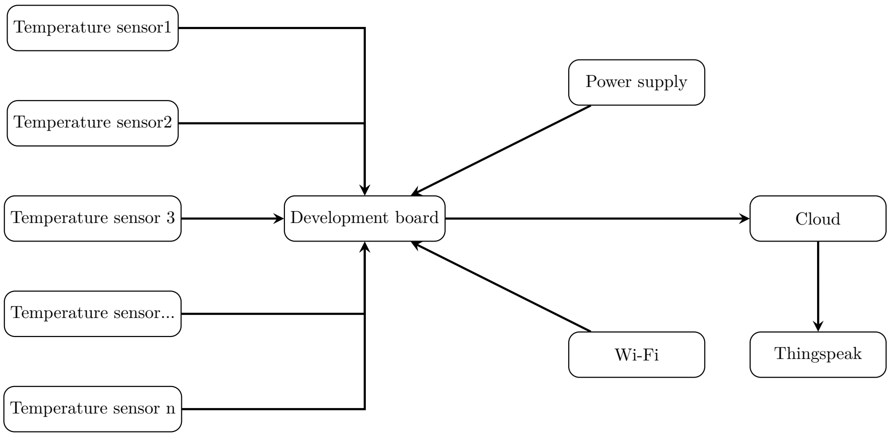

Figure 4.7: Temperature monitoring using development board and Thingspeak.

Figure 4.8 shows where all sensors are located. In each test hut three sensors at different heights are positioned. This to capture any deviation in the temperature distribution inside the test huts. Sensors number 1-9 are measuring indoor temperatures in the test huts, sensors 10-11 measuring the temperatures inside the stable and sensor 12 measures the outdoor temperatures. Sensors 10-12 are located on the opposite side of the stable to be protected from solar radiation.

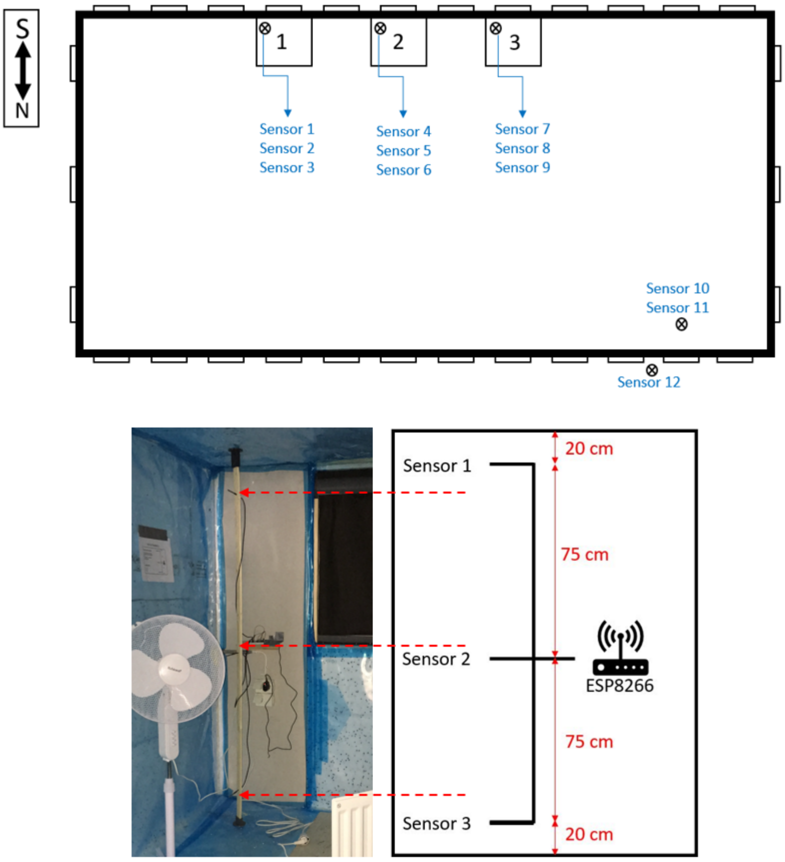

Figure 4.8: Up: Location of the sensors used in this project. Down: Vertical position of the sensors in test hut 1.

The system conducts of temperature sensors (ds18b20) that are connected to a development board (esp8266). Connection between the sensors and the development board is made by jump wires and a breadboard, see Figure 4.9.

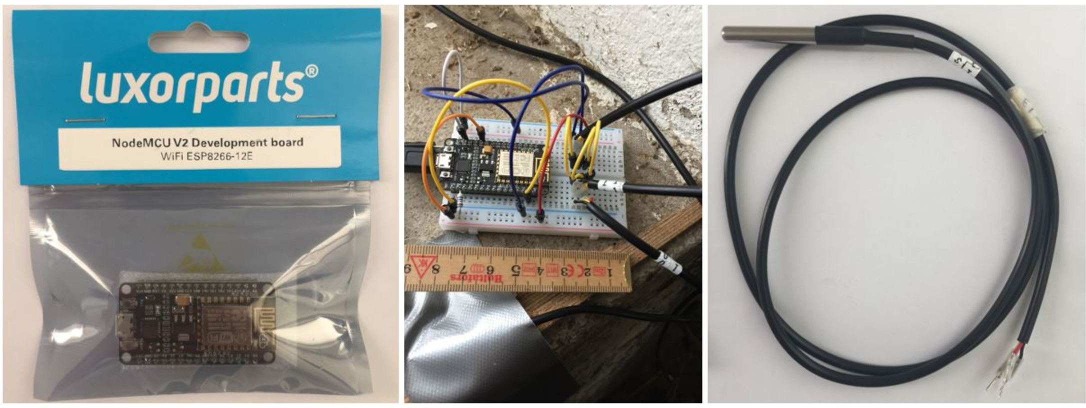

Figure 4.9: Equipment used for monitoring of temperatures. Left: Development board. Middle: Assembly of the components used for monitoring of temperatures in each test hut. Right: Sensor.

Once the sensors and the development board are connected, the development board can be programmed to send the collected data in a predefined interval, to an specific channel in Thingspeak, via Wi-Fi. Thingspeak is an open platform for IoT which has been used in this project to logg the measured data. The code used for programming of the development boards is written in Arduino IDE 1.8.5. All equipment used for monitoring of temperatures are compiled in Table 4.2.

Table 4.2: Equipment used to monitor the temperatures.

Equipment	Device	Accuracy
Temperature sensor probe	Luxorparts DS18B20	±0.5°C at −10 to 85°C
Breadboard	Luxorparts 400	-
jump wire	Luxorparts- male to male	-
Development Board	Nodemcu ESP8266	-

Calibration of temperature sensors

In order to check the accuracy of the temperature sensors used in this study, all sensors are calibrated based on the two point calibration method (Riga and Neag, 1991). For this purpose a climate chamber of model "Terchy: MHK-408 yk" [4], available at Chalmers university, is used to create the reference temperatures and to calibrate the sensors, see Figure 4.10. The climate chamber has an accuracy of ±0.2°C (the accuracy stated by producer) and it has been calibrated latest in 2017-10-10. All sensors are calibrated simultaneously at reference temperatures of $0, 10, 20$ and 30°C. The choice of these temperatures is based on the expected interval of temperatures during the measurement campaign. For the sensors measuring outdoor temperatures, it is highly expected to reach temperatures below 0°C. Duo to that, 3 out of 12 sensors are calibrated at one additional reference temperature, −10°C. The result of the calibration can be seen in Table 4.3 and Figure 4.11.

[4] https://www.quantel-global.com/sites/default/files/attachment/MHK_series_1.pdf

Figure 4.10: Photo showing the climate chamber used to calibrate the sensors.

Table 4.3: Results of the calibration of the temperature sensors.

Sensor \ Temperature (°C)	-10.00	0.00	10.00	20.00	30.00
Sensor 1	-	-0.37	9.63	19.62	29.69
Sensor 2	-	-0.44	9.63	19.50	29.50
Sensor 3	-	0.13	10.00	19.75	29.75
Sensor 4	-	-0.37	9.69	19.56	29.56
Sensor 5	-	-0.13	10.00	19.75	29.87
Sensor 6	-	-0.25	9.75	19.62	29.62
Sensor 7	-	-0.13	9.81	19.56	29.62
Sensor 8	-	-0.25	9.69	19.50	29.50
Sensor 9	-	0.00	9.94	19.69	29.75
Sensor 10	-9.13	0.13	10.00	19.75	29.69
Sensor 11	-9.50	-0.37	9.63	19.50	29.50
Sensor 12	-9.19	-0.31	9.69	19.50	29.56

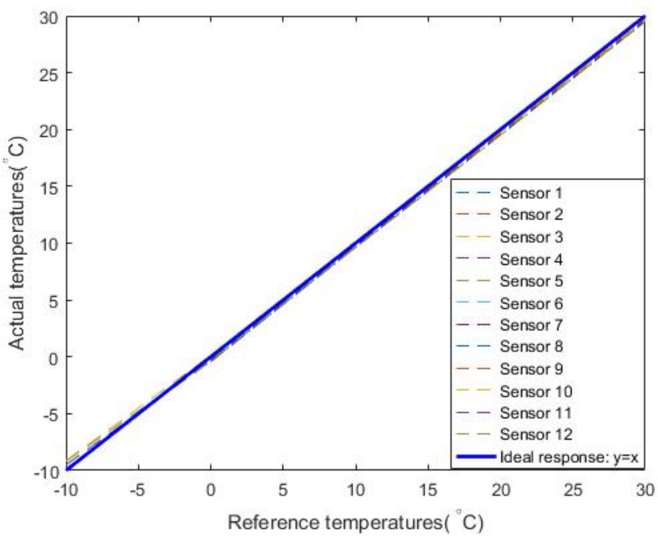

Figure 4.11: Plotted graphs showing the temperatures measured by the sensors at the reference temperatures.

To recalculate correct temperatures, linear equations, describing the condition in each interval of 10 degrees, i.e [-10 to 0], [0 to 10], [10 to 20] and [20 to 30] are calculated according to Equation 4.1.

$$\begin{aligned} y &= k \cdot x + m \\ k &= \frac{y_2 - y_1}{x_2 - x_1} \end{aligned} \tag{4.1}$$

$[x_1,y_1]$	Coordinates of point 1.
$[x_2,y_2]$	Coordinates of point 2.

Assuming that a temperature of 3°C is measured by sensor 1, the corrected value is recalculated by Equation 4.2:

$$\begin{aligned} k &= \frac{T_{actual.2} - T_{actual.1}}{T_{ref.2} - T_{ref.1}} \\ m &= T_{actual.2} - (k \cdot T_{ref.2}) \\ T_{corrected} &= \frac{T_{measured} - m}{k} \end{aligned} \tag{4.2}$$

0°C	Reference temperature 1, $[T_{ref.1}]$.
10°C	Reference temperature 2, $[T_{ref.2}]$.
−0.37°C	Temperature measured by the sensor at $[T_{ref.1}]$, $[T_{actual.1}]$.
9.63°C	Temperature measured by the sensor at $[T_{ref.2}]$, $[T_{actual.2}]$.
3°C	Temperature measured by the sensor at $[T_{measured}]$.
3.37°C	Corrected temperature of $[T_{measured}]$, $[T_{corrected}]$.

$$\begin{aligned} k &= \frac{9.63 - (-0.37)}{10 - 0} = 1 \\ m &= 9.63 - (1 \cdot 10) = -0.37 \\ T_{corrected} &= \frac{3 - (-0.37)}{1} = 3.37 \end{aligned} \tag{4.3}$$

Recalculations of correct temperatures are made by a MATLAB script. The input are the measured temperatures and the output are the corrected ones.

Energy logger

During the measurement campaign, energy consumption in all three test huts are measured and logged by a gateway and three power tags. The gateway is of model" Wiser energy gateway EER31800 " and the power tags are of model " Schneider A9MEM1520 ", see Figure 4.12. The technical properties of the gateway and the power tags can be found in Appendix 3.

Figure 4.12: Photos showing the gateway and the power tags used in site.

Figure 4.13 shows the system used to measure and collect the energy consumption during the measurement campaign. The total energy consumption in each test hut, is logged and send to an account at Wiser energy's website. The energy consumption of the fan and the sensors in each test hut correspond to approximately 30 Wh during one hour, i.e an effect of 30 W.

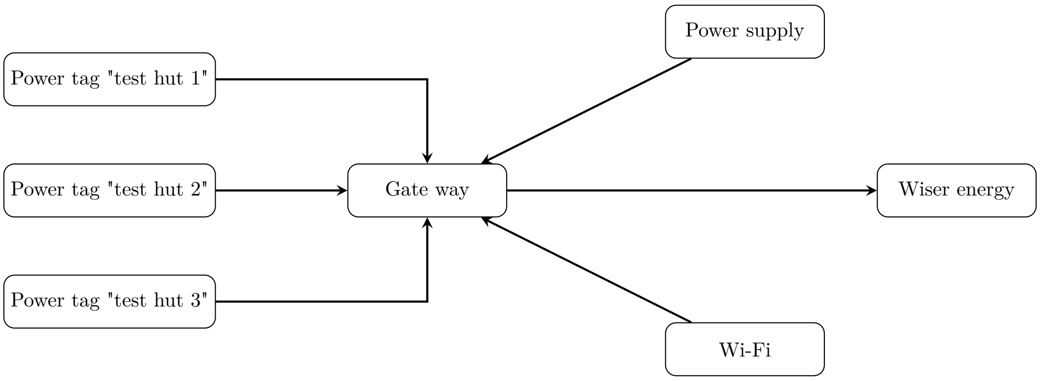

Figure 4.13: Showing the procedure for measuring of energy consumption in test huts.

Solarimeter

During the measuring campaign, the global solar radiation, i.e sum of direct and diffuse solar radiation, reaching the windows of the test huts is measured by a Solarimeter. The Solarimeter used in this project is of model " Kimo-SL200 " and has an accuracy of ±5%. The specific detail of the solarimeter and the calibration certificate can be found in Appendix 4. Sensor of the solarimeter is mounted on one of the windows in the stable (with no test hut behind), see Figure 4.14. The measuring interval of the solarimeter is from $1\frac{\mathrm{W}}{\mathrm{m}^2}$ to $1300\frac{\mathrm{W}}{\mathrm{m}^2}$.

Figure 4.14: Showing the solarimeter and how it is mounted on the exterior surface of a window with no test hut behind. .

4.1.1 Estimation of the extension of measurement campaign

As described in Chapter 2.4, the extension of the measurement campaign has to be long enough to minimize the dynamic effects of the thermal mass. As a roll of thumb, a period of 14 days in wintertime, is suggested by standards and is commonly implemented in practice (Biddulph et al., 2014). Duo to the special construction of the test huts (only insulation, i.e almost no thermal mass), the only possible locations where thermal mass might have a considerable effect is in the ground and in the external wall facing south. In order to make a rough estimation on how long the pilot test has to be run, the heat losses from the test huts to the ground and variation of the dynamic U-value of the external wall are studied. Both these studies are done by simulations in Comsol and Matlab and are described below.

U-value of the external wall of the test huts

Evaluation of the U-value of the external wall is done according to standard ISO 9869-1 (Elements-In, 2014) and based on the methods presented in (Biddulph et al., 2014), with the deviation that the evaluation in this study is done by simulation instead of in-situ measurements.
The first method to calculate the U-value is the "Average method" in which the effect of thermal mass can be neglected (Biddulph et al., 2014). This is based on the assumption of steady state which is valid only if the measuring period is long enough. The thermal resistance can be calculated by Equation 4.4, see Figure 4.15:

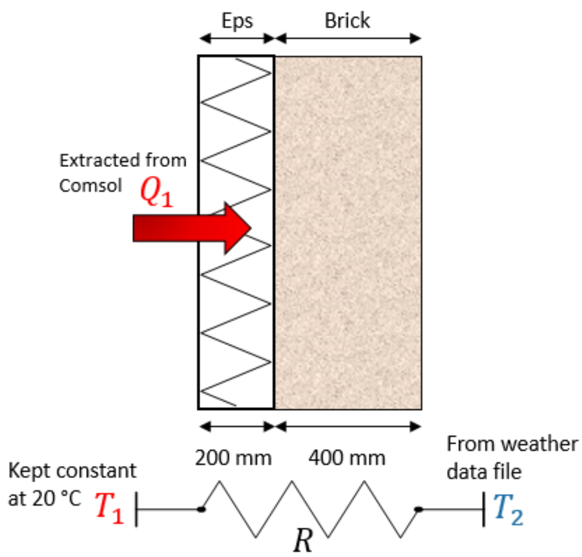

Figure 4.15: Model used for estimation of U-value based on the average method.

$$R_i = \frac{T_{1.i} - T_{2.i}}{Q_i} \tag{4.4}$$

R_i	Thermal resistance at time i.
$T_{1.i}$	Interior temperature at time i.
$T_{2.i}$	Exterior temperature at time i.
Q_i	Heat flux from interior towards exterior at time i.

The second method considers the effect of thermal mass and the corresponding time shift. To implement this method, in additional to the parameters needed in the average method, temperatures at a certain position inside the component are also needed (Biddulph et al., 2014). Figure 4.16 shows the schematic diagram of the simulated model and the parameters required for that. The thermal resistance can be estimated by applying Equation 4.5 and Equation 4.6 presented in (Biddulph et al., 2014):

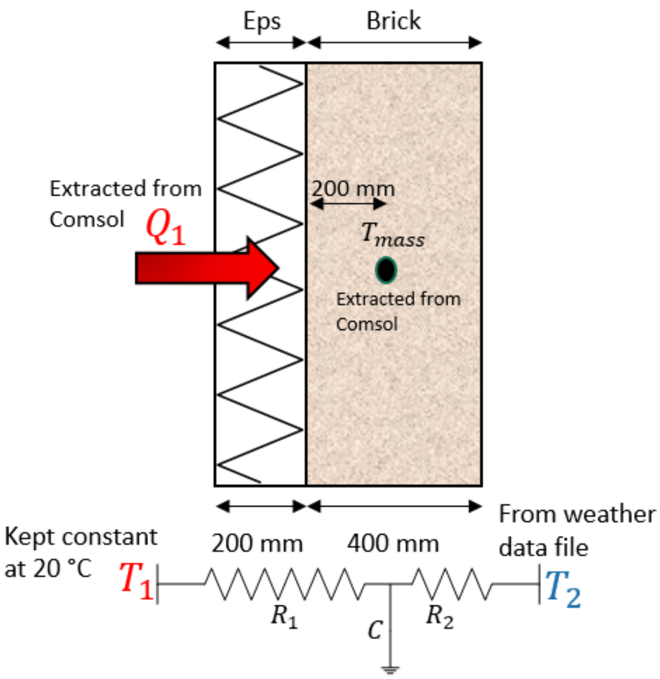

Figure 4.16: Model used for estimation of U-value, considering the effect of thermal mass.

$$Q_i = \frac{T_{1.i} - T_{mass.i}}{R_{1.i}} \tag{4.5}$$

$Q_{.i}$	Heat flux from interior towards exterior at time i.
$T_{1.i}$	Interior temperature at time i.
$T_{mass.i}$	Temperature of the chosen point inside the component, at time i.
$R_{1.i}$	Thermal resistance between interior and the chosen point inside the component, at time i.

$$C \cdot \frac{T_{mass.(i+1)} - T_{mass.(i)}}{t_{(i+1)} - t_{(i)}} = \frac{T_{1.(i+1)} - T_{mass.(i+1)}}{R_{1.i}} + \frac{T_{2.(i+1)} - T_{mass.(i+1)}}{R_{2.i}} \tag{4.6}$$

C	Volumetric heat capacity of the component.
$T_{mass.(i+1)}$	Temperature of the chosen point inside the component, at time i+1
$T_{mass.(i)}$	Temperature of the chosen point inside the component, at time i
$t_{(i+1)}$	Time step number i+1
$t_{(i)}$	Time step number i
$T_{1.(i+1)}$	Interior temperature at time i+1
$T_{2.(i+1)}$	Exterior temperature at time i+1
$R_{1.i}$	Thermal resistance between interior and the chosen point inside the component, at time i.
$R_{2.i}$	Thermal resistance between exterior and the chosen point inside the component, at time i.

The outdoor temperatures from last year, 2017, are collected from the open climate source SMHI [5]for the period over which simulations are run. As there is no weather station in Färgelanda, outdoor temperatures from the closest weather station located in Kroppefjäll-Granan A are used. The measuring campaign is planned to start 20th of Mars. The simulation is therefore run from 20th of Mars up to 40 days ahead.
All input data used in the Comsol model is compiled in Table 4.4 and Table 4.5. Dimensions are given in Figure 4.16. Material properties are based on tabulated values in (Hagentoft, 2001).

Table 4.4: Material properties used in simulations.

EPS	Thermal conductivity $[\frac{W}{m \cdot K}]$	0.038
	Density $[\frac{kg}{m^3}]$	30
	Heat capacity $[\frac{J}{kg \cdot K}]$	1500
Brick	Thermal conductivity $[\frac{W}{m \cdot K}]$	0.6
	Density $[\frac{kg}{m^3}]$	1500
	Heat capacity $[\frac{J}{kg \cdot K}]$	800

Table 4.5: Input data used in Comsol.

Initial temperature [°C]	$T_{out}(1)$ (Climate data file)
Internal heat transfer coefficient $[\frac{W}{m^2 \cdot K}]$	8
Internal temperature [°C]	20
External heat transfer coefficient $[\frac{W}{m^2 \cdot K}]$	25
External temperature [°C]	$T_{out}(t)$ (Climate data file)
Mesh size	Physics-controlled (Finer)

The U-values of the external wall, have been estimated using both methods described in (Biddulph et al., 2014) and the result is represented as graphs in Figure 4.17. When using the average method, the average over both 1 day and 2 days have been used. By average over 1 day, it means that the components used in Equation 4.5, $T_{1.i}$, $T_{2.i}$ and Q_i, represent the average interior temperature, exterior temperature and heat flux over 24 hours respectively. This is done for each single day during the whole period. The

[5] http://opendata-download-metobs.smhi.se

procedure is the same when averaging over 2 days but the averaging interval is 48 hours instead of 24 hours.
According to ISO 9869-1 and for such a component as the external wall studied here, the measurement campaign shall be ended if 72th hours have been passed and the deviation between the present U-value and the previous one is in between ±5% (Elements-In, 2014). However, since (Biddulph et al., 2014) has considered a deviation less than 1% as a measure of stability, this value is used in this study instead of 5% stated in ISO9869-1.
By using the average method, the stability is achieved at the 11th day, while by considering the effect of thermal mass, it occurs already at the 3rd day. But due to the second requirement, i.e longer period than 72 hours, the next occasion at 8th day is considered as the day in which the measurement can be ended.

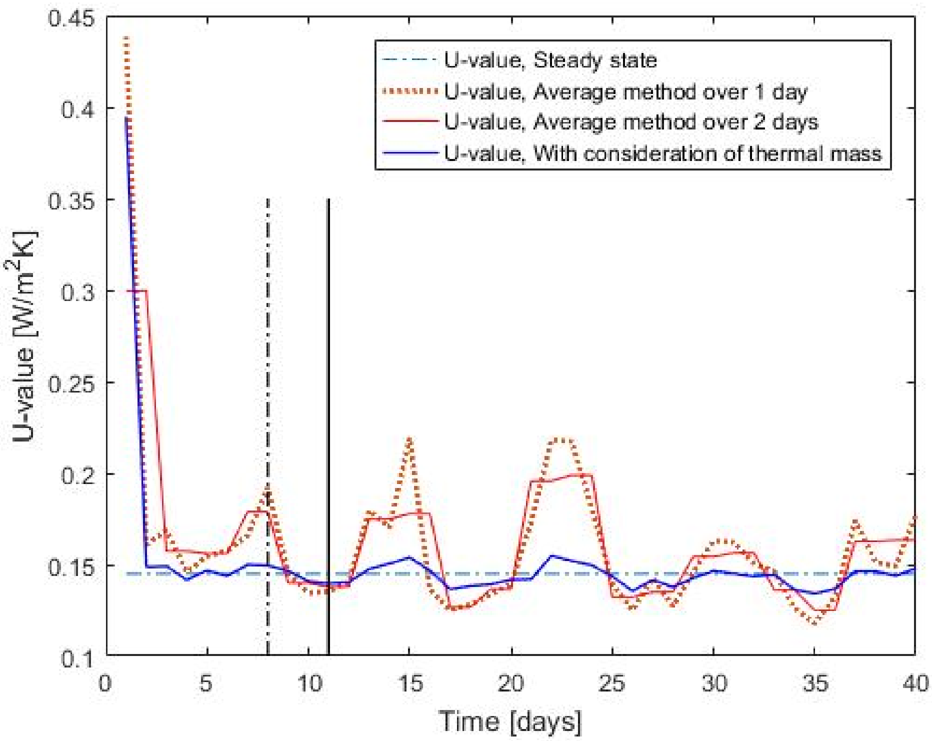

Figure 4.17: Variation of estimated U-values of the external wall, between 20th of Mars and 40 days ahead, using the average method and the second method in which the effect of thermal mass is considered. The vertical lines show when the measurement campaign can be ended, depending on the used method (Solid line: Average method).

As mentioned earlier in this chapter, the conditions used for this estimation, do not correspond to the actual ones during the real pilot tests. The result of this study should be considered as a rough estimation to check if the extension of the planned measurement campaign is sufficient or not. As the measurement campaign is about to be over 3-4 weeks, it can be considered as sufficient.

Heat exchange between test huts and ground

Test hut 2 is placed in between the two other test huts. Theoretically, if all 3 test huts are warmed up constantly and simultaneously, after a certain period of time and due to the heat losses from each hut to the ground, there is a risk that heat losses from test hut 2 in the middle, down to the ground, decrease in comparison to the others. This, if the ground temperatures underneath test hut 2 become higher than the rest of the ground, due to the heat losses from other two test huts.

In order to examine this and any effects of the thermal mass of the ground, a model is built in Comsol and run for the planned measuring campaign, i.e from 20$^{\text{th}}$ of Mars up to 40 days ahead. Same outdoor temperatures as the case for the external wall are used, see Section 4.1.1. The construction of the test huts and all dimensions are in accordance with the ones stated in Chapter 4. The only deviation is that the plywood board between the floors and the air gap underneath is neglected. Additionally, it is assumed that test huts are surrounded directly by the outdoor climate and all exterior surfaces are in contact with outdoor air directly. All input data used in the Comsol model is compiled in Table 4.6 and Table 4.7. Dimensions are given in Figure 4.16. Material properties are based on tabulated values in (Hagentoft, 2001).

Table 4.6: Material properties used in simulations.

EPS	Thermal conductivity [$\frac{W}{m \cdot K}$]	0.038
	Density [$\frac{kg}{m^3}$]	30
	Heat capacity [$\frac{J}{kg \cdot K}$]	1500
air	Thermal conductivity [$\frac{W}{m \cdot K}$]	0.025
	Density [$\frac{kg}{m^3}$]	1.2
	Heat capacity [$\frac{J}{kg \cdot K}$]	1000
Rock	Thermal conductivity [$\frac{W}{m \cdot K}$]	3
	Density [$\frac{kg}{m^3}$]	2700
	Heat capacity [$\frac{J}{kg \cdot K}$]	740

Table 4.7: Input data used in Comsol.

Initial temperature [°C]	$T_{out}(1)$ (Climate data file)
Internal heat transfer coefficient [$\frac{W}{m^2 \cdot K}$]	8
Internal temperature [°C]	20
External heat transfer coefficient [$\frac{W}{m^2 \cdot K}$]	25
External temperature [°C]	$T_{out}(t)$ (Climate data file)
Mesh size	User-controlled
Air gap - heat transfer coefficient [$\frac{W}{m^2 \cdot K}$]	0.8
Air gap - temperature [°C]	$T_{out}(t)$ (Climate data file)
Ground depth [m]	30

As seen in Table 4.7, the depth of the ground in the model is chosen to be 30m. This to ensure that the ground can be considered as semi-infinite. To decrease the simulation time, the area around the floors is given a denser mesh than the rest of the model, see Figure 4.19.

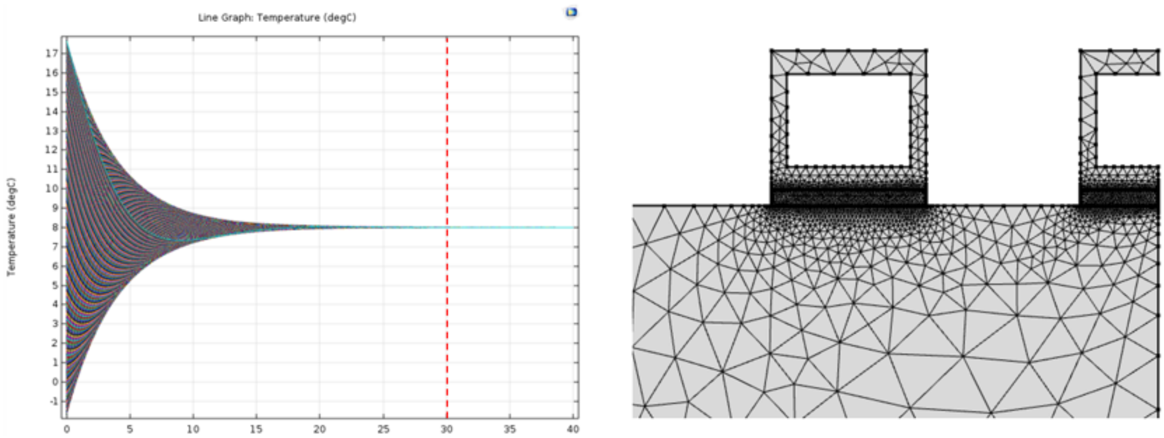

Figure 4.18: Left: Showing the result of the simulation made in Comsol to estimate the required depth of the ground. Right: Showing the chosen mesh size.

The result of the simulation is shown graphically in Figure 4.19. As it can be seen, the heat losses from both test huts are almost identical (a deviation less than 0.03 %) and this amount of deviation can be neglected.

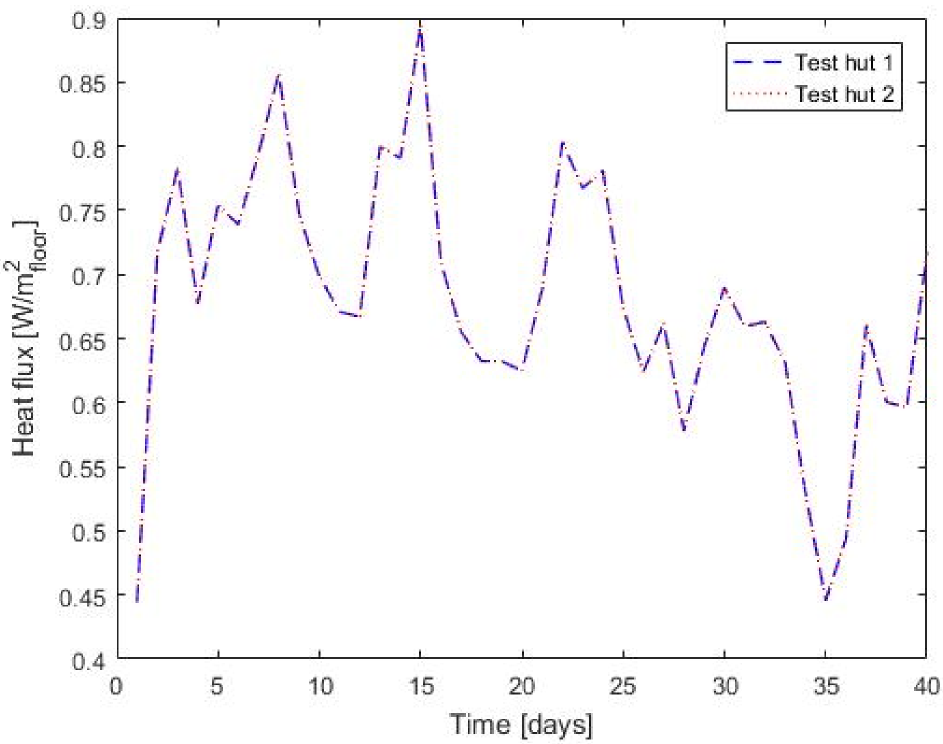

Figure 4.19: Heat flux to the ground from test hut 2 in the middle and test hut 1 at side, between 20th of Mars and 40 days ahead.

4.2 Validation of the test huts

As described in Section 2.12, and in order to evaluate the performance of the curtains, the results obtained from the test huts will be compared to each other. The optimal case is when all conditions in all test huts are exactly the same. However, this can be rather difficult to achieve in practice, mostly due to limitations described in Section 2.12, inaccuracy during the construction and other human factors. To minimize the effect of these source of errors and to calibrate the test huts, two measures are taken in this project. The first one is a blower door test and the second is an additional measurement campaign without the curtains.

4.2.1 Performance of Blower door test

To investigate the overall air permeability of the tests huts, a blower door test in each test hut is performed. A short description of blower door test can be read in Chapter 2.12. The equipment used in this project are a DG-700 Digital Gauge and a Minneapolis Blower Door (Model 3,110V) to create the required pressure differences, and the computer software TECTITE Express 5.1 to analyze and document the blower door test results. The TECTITE software provides several options for performing the tests in different manners. These options are described in (Energy Conservatory, 2012). In this project, all tests are performed at pressurization mode, i.e an over pressure is created inside the test huts. The tests are performed as multi-point automatic tests, in which the speed of the fan, air flow over the fan and choice of ring are automatically controlled by the software TECTITE. The software adjusts the fan speed for different pressure targets and takes multiple number of samples which will later be averaged to one certain air flow rate for each pressure target.

Figure 4.20 shows the arrangement of the equipment when performing the test in test hut 2. The fan is placed in a metal frame covered by a plastic sheet. The frame is then placed in the door opening. To avoid unintentional air flows between the frame and the door opening, the adjustment of the frame in the door opening has to be made properly.

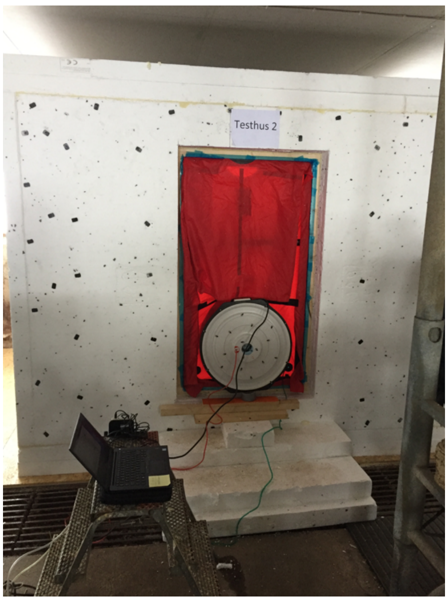

Figure 4.20: Assembling of the measuring equipment for the Blower door test.

Results from the first blower door tests, showed an unacceptably large amount of air leakages in all test huts. Due to that, all interior joints were filled with building sealants. In additional to that, all interior surfaces were covered by plastic foil and the area around the windows were sealed by tape, see Figure 4.21.

Figure 4.21: Covering of the interior surfaces by plastic foil and taping the windows as measures to reduce the amount of air leakages.

The results of the performed blower door tests, at 50 pascal pressure difference over the building envelope, can be seen in Table 4.8. Considering the test huts as facilities located in zone III and heated with electrical heating, the air tightness demand (q_{E50}) in Boverketsbyggregler, BBR, is $0.6\frac{l}{s\cdot m^2}$ of envelope area (Boverket, 2015). This means that all the test huts fulfill the requirement of air tightness described by BBR. However, the air tightness of the test huts varies and this will be taken into account in post processing of the final results.

Table 4.8: Test results from the Blower door tests.

Building / result	Test hut 1	Test hut 2	Test hut 3
Air flow q50 [l/s]	16	19	13
Air change rate n50 [1/h]	4.55	5.58	3.90
Air flow qF50 [l/s]	2.40	2.94	2.06
Air flow qE50 [l/s]	0.48	0.59	0.41

The detailed documentation of the test results can be found in Appendix 5.

4.2.2 Calibration campaign

In order to calibrate the test huts, an additional measurment campaign, without any curtains is carried out between the 5^{th} and $19^{\text{ th}}$ of Mars. The purpose of this measure is to identify and quantify the total amount of additional heat losses in each test hut through the thermal bridges and/or any other heat losses that can not be estimated directly. During the first days of the measurement campaign, it is discovered that the door in test hut 1 is not properly adjusted in the door opening. This issue is remedied on the 8^{th} of Mars. On the 15^{th} of Mars, the fan in test hut 2 stops working. This resulting in an uneven temperature distribution and a disturbance in the working schedule of the radiator in test hut 2. The fan is replaced by a new fan of the same model on the 18^{th} of Mars. Due to these issues, only the period between 9^{th} and 14^{th} of Mars is taken into account.
The process of estimating the additional heat losses can be seen in the heat mass balance equation, Equation 4.7 and Figure 4.22.

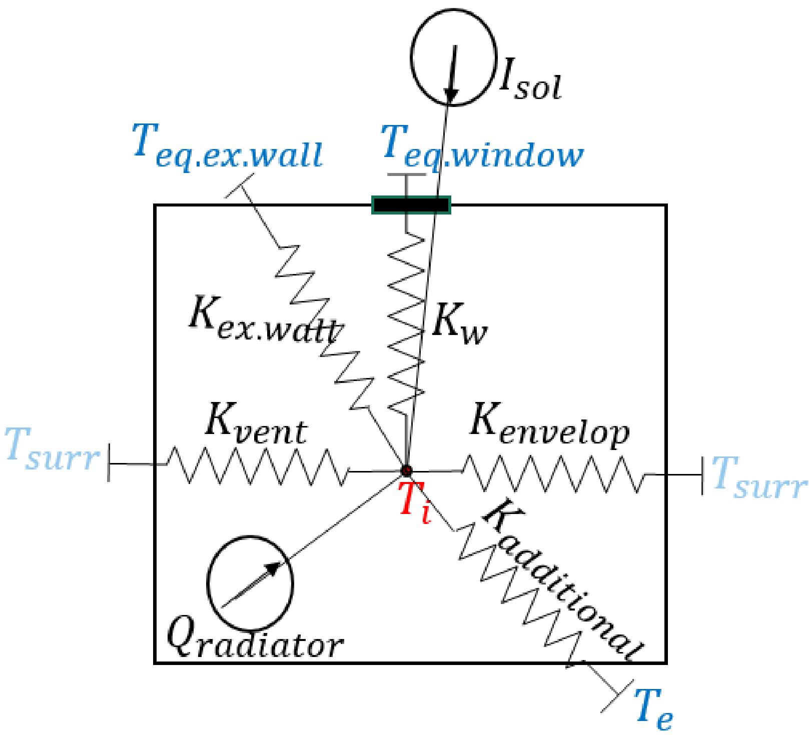

Figure 4.22: Thermal network for heat transfer through the building envelope.

$$\mathrm{C} \cdot \frac{\mathrm{dT_i}}{\mathrm{dt}} = \mathrm{Q_{radiator}} + \mathrm{Q_{sol}} - \mathrm{Q_{window}} - \mathrm{Q_{envelop}} - \mathrm{Q_{vent}} - \mathrm{Q_{ex.wall}} - \mathrm{Q_{additional}}$$
$$\mathrm{T_{eq}} = \mathrm{T_e} + \frac{\mathrm{I_{sol}} \cdot \cos(\theta) \cdot \alpha_{\mathrm{sol}} + \mathrm{g} \cdot \mathrm{r} + (\mathrm{T_{sky}} - \mathrm{T_e}) \cdot \alpha_{\mathrm{r}}}{\alpha_{\mathrm{c}} + \alpha_{\mathrm{r}}} \tag{4.7}$$

T_e	Exterior temperature.
T_{eq}	Equivalent temperature in which the effect of solar radiation and the radiation exchange between the sky and the window surface are included.
T_{surr}	Exterior temperature inside the stable.
T_i	Interior temperature.
T_e	Exterior temperature.
K_w	Thermal conductance of the window.
K_{walls}	Thermal conductance of the the walls,roof and floor.
K_{vent}	Ventilation conductance.
$K_{ex.wall}$	Thermal conductance of the the exterior wall facing south.
$K_{additional}$	Overall thermal conductance for additional losses.
$Q_{radiator}$	Heat surplus from the radiator.
$Q_{additional}$	Heat loss due to thermal bridges.
Q_{window}	Heat transfer through the window.
$Q_{envelop}$	Heat loss through the walls,floor and roof.
Q_{vent}	Heat loss due to leakages(ventilation).
$Q_{ex.wall}$	Heat loss through the external wall facing south.
α_c	Heat transfer coefficient for convection.
I_{sol}	Total amount of solar radiation striking the window.
θ	Angle between the normal of the window and the solar rays.
α_{sol}	Absorptivity of solar radiation of the window.
g	Density of the moisture flow rate.
r	Latent heat of evaporation.
T_{sky}	Sky temperature.
α_r	Heat transfer coefficient for radiation.

T_{eq} is a fictitious temperature which represents the impact of convection, long wave and short wave radiation, and latent heat transfer (Hagentoft, 2001). As the solarimeter is not available during this period, the total amount of solar radiation striking the window is unknown and has to be roughly estimated. The interior temperatures are considered to be increased due to solar radiation whenever the temperatures are increased drastically and there is no energy consumption by the radiator. These occasions correspond to the peaks in the graphs of "correction factor" in Figure 4.23. Based on the temperatures and the cloudiness for the first 5 days, shown in Figure 4.23, it can be concluded that the solar radiation for these 5 days is very low. To estimate the amount of solar radiation for these 5 days, a similar period during the later measurement campaign has been studied and a mean value of $20\frac{W}{m^2}$ has been chosen. This means that $I_{sol} = 20\frac{W}{m^2}$ in Equation 4.7.
Another simplification made in the analysis, is concerning the latent heat transfer which is set to be zero. The temperature of the sky is estimated according to the formulas stated in (Nik, 2017), see Equation 4.8. The total amount of cloudiness and the relative humidity of the outdoor air are collected from the open climate source SMHI for the period over which measurements are run. As there is no weather station in Färgelanda, data from the closest weather station located in Kroppefjäll-Granan A are used.

$$
\begin{aligned}
\mathrm{T_{sky}} &= \mathrm{C_a^{0.25}} \cdot \mathrm{T_{sky.clear}} \\
\mathrm{T_{sky.clear}} &= (\mathrm{T_e} + 273.15) \cdot (\epsilon_{\mathrm{clear}}^{0.25}) \\
\mathrm{C_a} &= 1 + 0.0224 \cdot \mathrm{C} + 0.0035 \cdot \mathrm{C}^2 + 0.00028 \cdot \mathrm{C}^3 \\
\epsilon_{\mathrm{clear}} &= 0.711 + 0.56 \cdot \frac{\mathrm{T_{dp}}}{100} + 0.73 \cdot (\frac{\mathrm{T_{dp}}}{100})^2 \\
\mathrm{T_{dp}} &= \frac{243.5 \cdot \mathrm{y}}{17.67 - \mathrm{y}} \\
\mathrm{y} &= \ln(\frac{\mathrm{RH}}{100}) + \frac{17.67 \cdot \mathrm{T_e}}{243.5 + \mathrm{T_e}} \\
\mathrm{T_{dp}} &= \frac{243.5 \cdot \mathrm{y}}{17.67 - \mathrm{y}}
\end{aligned}
\tag{4.8}
$$

$\epsilon_{\mathrm{clear}}$	Emissivity of a clear sky.
C	Total amount of cloudiness.
$\mathrm{T_{dp}}$	Dew point temperature.
RH	Relative humidity of the outdoor temperature.

Once the sky temperature is estimated, the heat transfer coefficient can be calculated according to 4.9, (Hagentoft, 2001). Usage of Equation 4.9, requires that the temperatures of the surfaces where radiation exchange occurs in between, are of the same order in Kelvin. In additional to that, the view factor between the two surfaces has to be one. Strictly speaking this is not fulfilled for the case studied here and it should be seen as a simplification.

$$
\begin{aligned}
\alpha_{\mathrm{r}} &= 4 \cdot (\frac{1}{\epsilon_1} + \frac{1}{\epsilon_2} - 1)^{-1} \cdot \sigma \cdot (\frac{\mathrm{T_{sky}} + \mathrm{T_{surface.exterior}}}{2})^3 \\
\sigma &= 4.567 \cdot 10^{-8}
\end{aligned}
\tag{4.9}
$$

σ	Stefan Boltzmann constant $[\frac{\mathrm{W}}{\mathrm{m^2 \cdot K^4}}]$.
$\mathrm{T_{surface.exterior}}$	Calculated surface temperature at the exterior of the window and the external wall [K].

The air change rate in each room is estimated based on the air change rate obtained by the blower door test and at 50 Pa in pressure difference. For the case studied here, a constant pressure difference of 2 Pa, over the building envelope is assumed.

Figure 4.23 shows the compiled result of the analysis. In order to take the additional heat losses into account, a correction factor $\Delta \mathrm{U}$ $[\frac{\mathrm{W}}{\mathrm{m^2 \cdot K}}]$for each test hut is defined. This correlation factor represents the relation between the total amount of additional heat losses ($\mathrm{Q_{additional}}$) and the temperature difference between indoor and outdoor, see Equation 4.10. Table 4.9 shows the calculated average value of the correction factor only for the first 5 days. The deviation between the additional losses in the test huts is approximately 5%.

$$
\Delta \mathrm{U_i} = \frac{\mathrm{Q_{additional_i}}}{(\mathrm{T_{i.i}} - \mathrm{T_e}) \cdot \mathrm{A_{envelop.i.tot}}}
\tag{4.10}
$$

ΔU_i	Correction factor for each test hut.
$A_{envelop.tot}$	Total area of the building envelope.

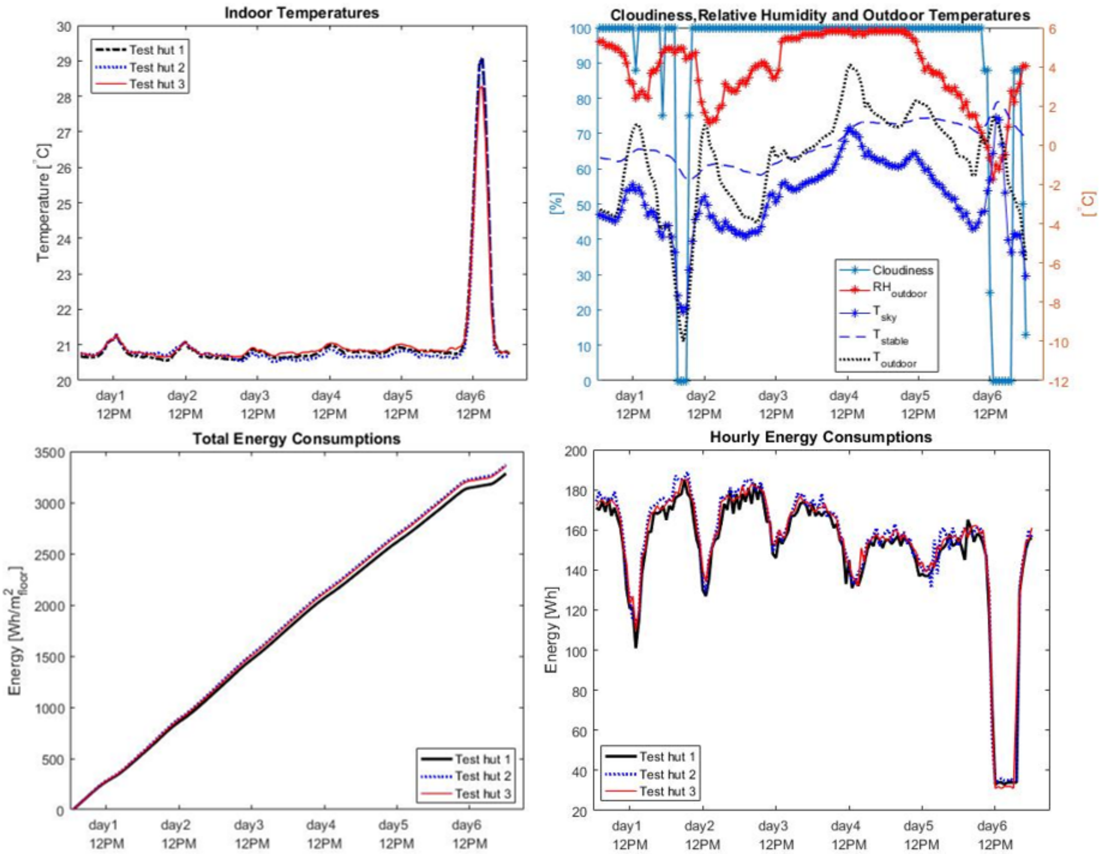

Figure 4.23: Compilation of all results obtained during the calibration campaign.

Table 4.9: Average value of the correction factor for each test hut.

Test Hut	$\Delta U\ [\frac{W_{additional}}{m^2_{envelop.tot} \cdot K}]$
1	0.0918
2	0.0883
3	0.0935

4.3 Measurement campaign

The 27 days long measurement campaign starts at the 27 $^{\text{th}}$ of Mars and continues until the 22 $^{\text{th}}$ of April. During this period, the pilot studies are performed as described in Chapter 4. Figures 4.24, 4.25 and 4.26 show the measured parameters for the entire measurement campaign. As it can be seen, the outdoor temperatures increases continuously during the entire period. However, this increment is slower during the first 10 days, which is also when the coldest outdoor temperatures occur. The temperatures inside the stable follow the outdoor temperatures with a certain delay and smaller bias, as expected.

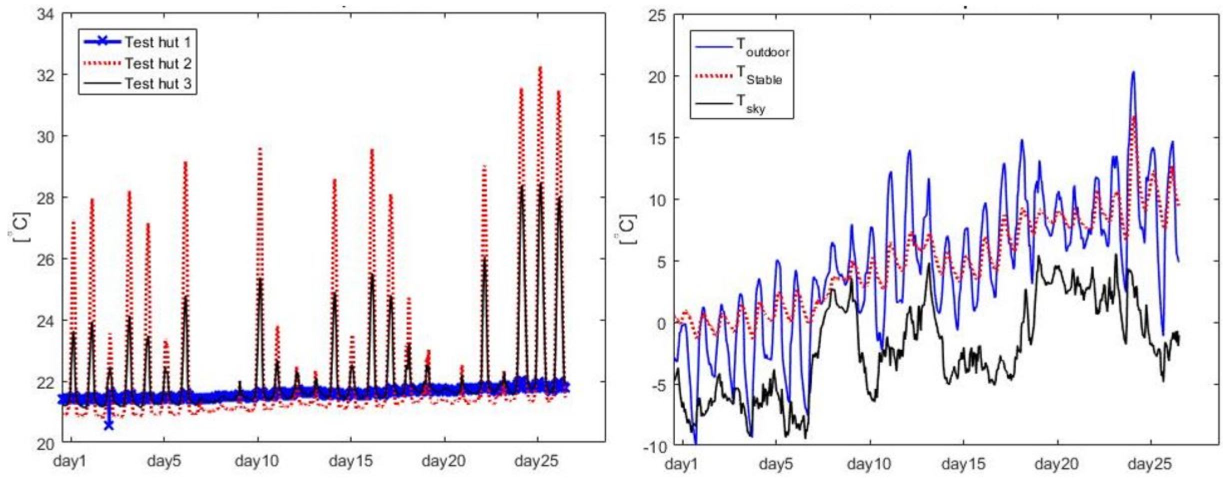

Figure 4.24: Hourly indoor and outdoor temperatures obtained during the 27 days of the measurement campaign.

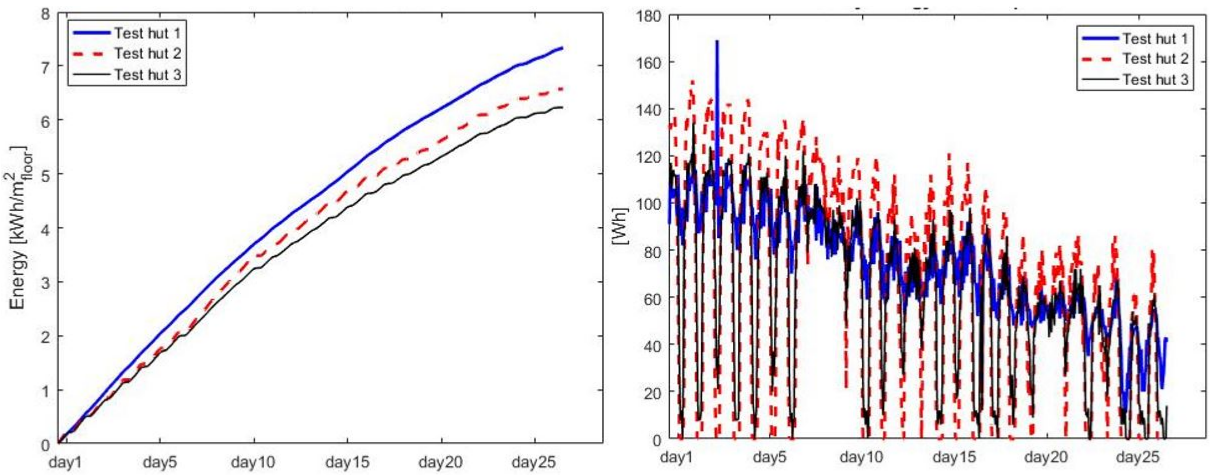

Figure 4.25: Hourly energy consumption during the 27 days of the measurement campaign.

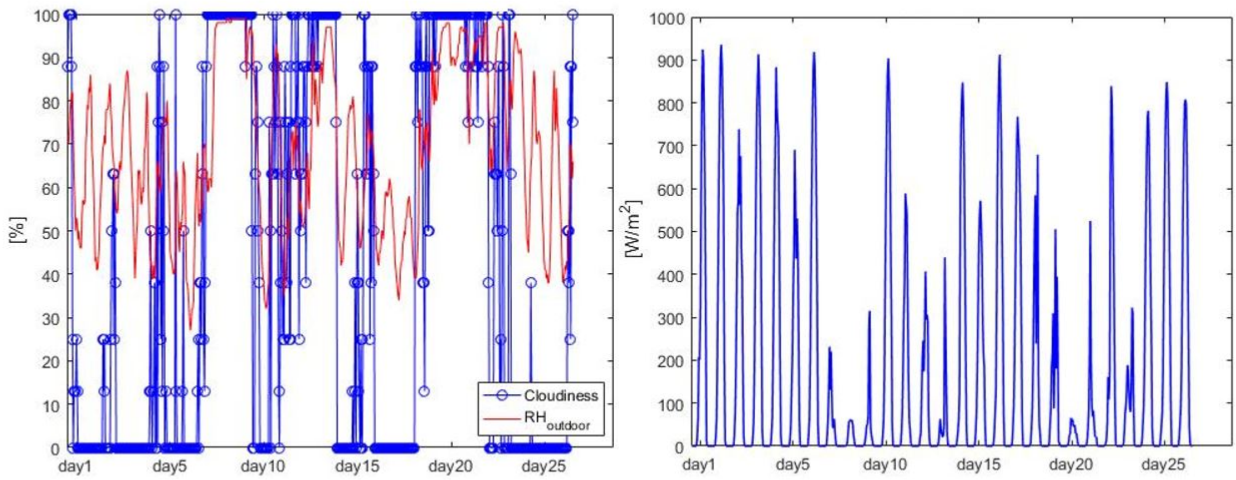

Figure 4.26: Left: Cloudiness and relative humidity, Right: Solar radiation, during the 27 days of the measurement campaign.

4.3.1 Test hut 2

U-value of the window in test hut 2, used as the reference case, is known to be 1.5 $\frac{\mathrm{W}}{\mathrm{m^2 \cdot K}}$, see Appendix 1. Based on the deviation between the U-value derived from the experiment and the correct U-value of the window in test hut 2, the accuracy of the experiment can be indicated.

The procedure for calculating the U-value is the same as described in Section 4.2.2. Using Equation 4.11 and the measured data in Figure 4.24, 4.25 and 4.26, the total amount of heat losses through the window and thus its U-value can be estimated.

$$\begin{aligned} \mathrm{Q_{window}} &= \mathrm{Q_{radiator}} + \mathrm{Q_{sol}} - \mathrm{Q_{envelope}} - \mathrm{Q_{vent}} - \mathrm{Q_{ex.wall}} - \mathrm{Q_{additional}} \\ \mathrm{U_{window}} &= \frac{\mathrm{Q_{window}}}{(\mathrm{T_i} - \mathrm{T_{eq.window}}) \cdot \mathrm{A_{window}}} \end{aligned} \tag{4.11}$$

$\mathrm{Q_{window}}$	Heat loss through the window.
$\mathrm{Q_{radiator}}$	Heat surplus from the radiator.
$\mathrm{Q_{additional}}$	Heat loss due to additional losses.
$\mathrm{Q_{sol}}$	Heat surplus from solar radiation that reaches the indoor environment.
$\mathrm{Q_{envelop}}$	Heat loss through the walls,floor and roof.
$\mathrm{Q_{vent}}$	Heat loss due to leakages(ventilation), with an assumption of a constant pressure difference of 2 Pa, over the building envelope.
$\mathrm{Q_{ex.wall}}$	Heat loss through the external wall facing south.
$\mathrm{T_i}$	Interior temperature.
$\mathrm{T_{eq.window}}$	Equivalent outdoor temperature in which the effect of the radiation exchange between the sky and the window surface is included.
$\mathrm{A_{window}}$	Area of the window.

As the measured data are on hourly basis, Equation 4.11 can be implemented for every hour and thus calculate the U-value at each hour. However, as the radiators are tuned off at times, during some hours the amount of heat gains are less than the amount of heat losses. To get around this issue but also in order to minimize the effect of thermal mass of the materials in the test huts, the calculations are not made for each hour. Instead, they are averaged over a period of starting from 1 day up to 27 days. This means that the value shown for day 1 in Figure 4.27 is the average over the first 24 hours, day 2 over the first 48 hours and day 27 is the average over the whole period. The average U-value of the first 10 days is $1.48\frac{W}{m^2 \cdot K}$, i.e an underestimation by 2 %, while the average U-value of the whole period is $1.92\frac{W}{m^2 \cdot K}$, corresponding to an overestimation by 27 %. Comparing the average of all values, 1.74 $\frac{W}{m^2 \cdot K}$, to the correct U-value, 1.5 $\frac{W}{m^2 \cdot K}$, an accuracy of 84 % is achieved.

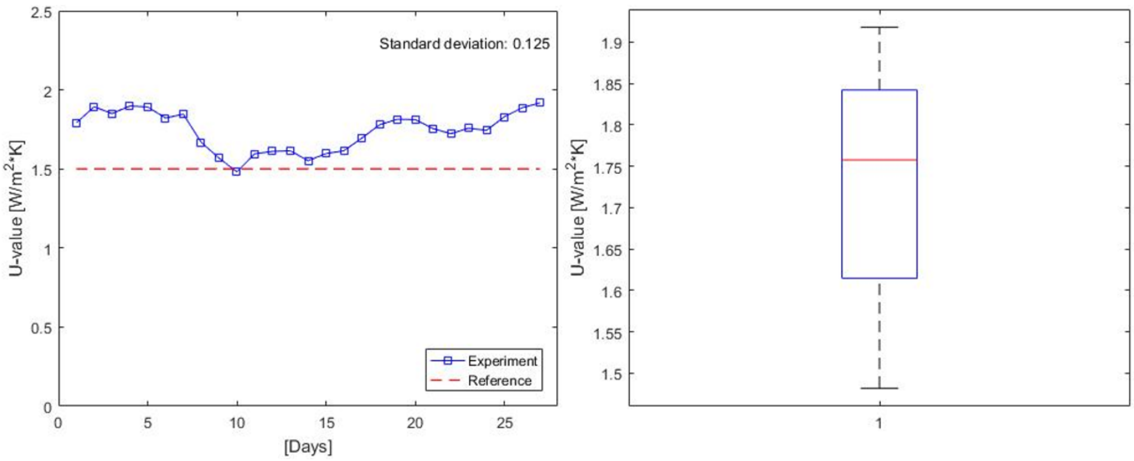

Figure 4.27: Graphs showing the U-value of the window in test hut 2, estimated by experiment.

Accuracy and precision of the experiment

Equation 4.12 and 4.13, describe how the error and standard deviation of the experiments performed in this project are calculated. As the U-value of the window in test hut 2 is the only known actual value, the accuracy of all results is based on the accuracy achieved in test hut 2.

$$\mathrm{Error}[\%] = \frac{\mathrm{Value_{Experimental}} - \mathrm{Value_{Actual}}}{\mathrm{Value_{Actual}}} \cdot 100 = 16\% \qquad (4.12)$$

$$\mathrm{Standard \quad deviation} = \sqrt{\frac{\sum(\mathrm{x_i} - \mathrm{x_{average}})^2}{\mathrm{n} - 1}} = 0.125 \qquad (4.13)$$

4.3.2 Test hut 1

In test hut 1, curtain design (A) is mounted in front of the window. The procedure is the same as for test hut 2 but with two differences. The first is that the U-value estimated here represents the U-value for the Window, the curtain and the air gap in between, all three together. The second one is that the additional heat losses in test hut 1 are considered by calculation of the total amount of thermal bridges instead. The main reason for that is the alteration of the conditions in test hut 1 by including the curtain and eliminating the solar radiation. The U-value of the window including the curtain and the air gap in between is calculated according to Equation 4.14 and Figure 4.28 and 4.29.

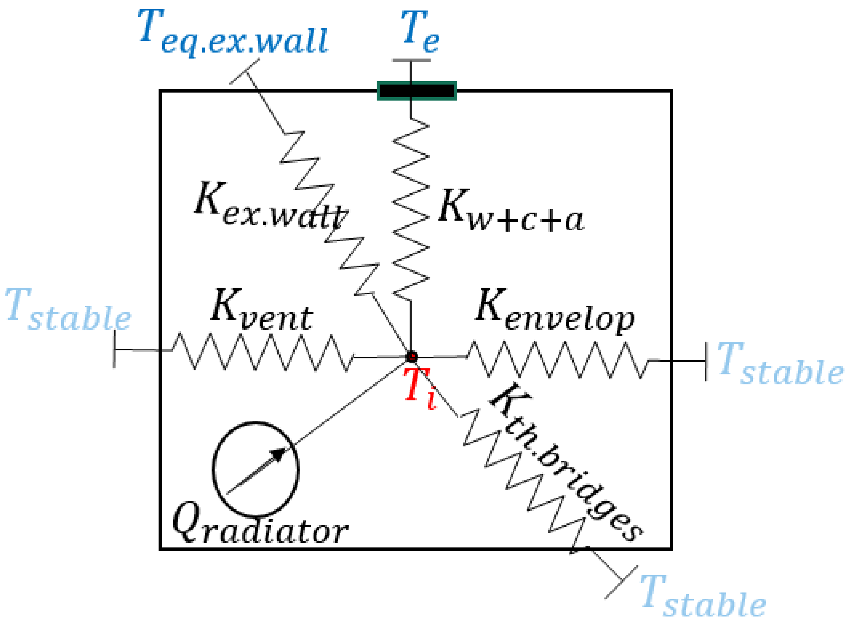

Figure 4.28: Thermal network for heat transfer through the building envelope of test hut 1.

$$
\begin{gathered}
\mathrm{Q_{w+c+a} = Q_{radiator} - Q_{envelope} - Q_{vent} - Q_{ex.wall} - Q_{w.side} - Q_{th.bridges}} \\
\mathrm{U_{window} = \frac{Q_{w+c+a}}{(T_i - T_e) \cdot A_{window}}}
\end{gathered}
\tag{4.14}
$$

$\mathrm{Q_{w+c+a}}$	Heat loss through the window including the curtain and the air gap in between.
$\mathrm{Q_{radiator}}$	Heat surplus from the radiator.
$\mathrm{Q_{th.bridge}}$	Heat loss due to thermal bridges.
$\mathrm{Q_{envelop}}$	Heat loss through the walls,floor and roof.
$\mathrm{Q_{vent}}$	Heat loss due to leakages(ventilation).
$\mathrm{Q_{ex.wall}}$	Heat loss through the external wall facing south.
$\mathrm{Q_{w.side}}$	Heat loss through the walls around the window.
$\mathrm{T_i}$	Interior temperature.
$\mathrm{T_e}$	Exterior temperature.
$\mathrm{A_{window}}$	Area of the window.

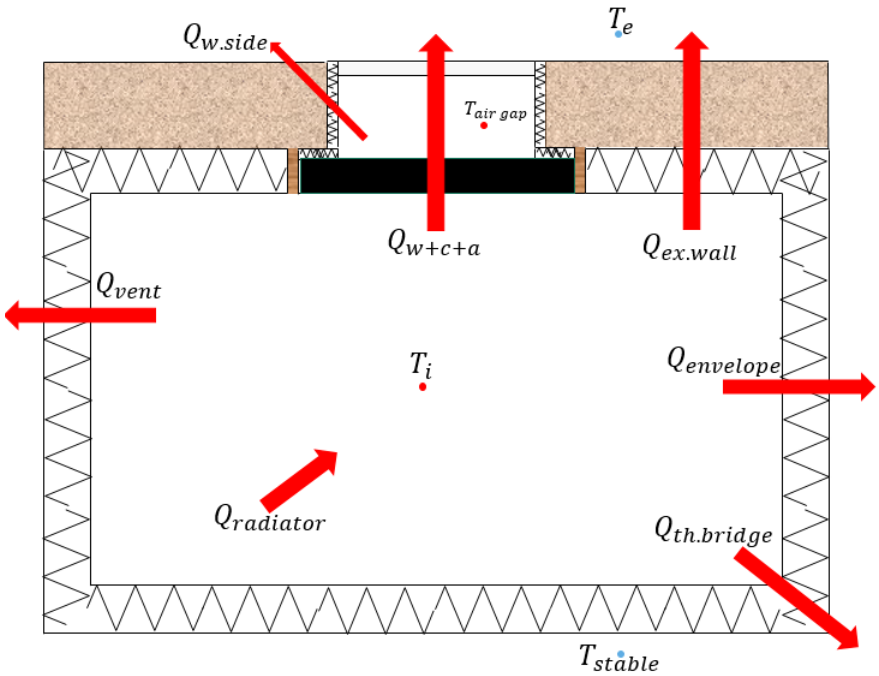

Figure 4.29: Components included in the energy balance of test hut 1.

Numerical Estimation of thermal transmittance ψ $[\frac{W}{m \cdot K}]$

As the whole construction is made of EPS, the major part of the thermal bridges are of the type geometric thermal bridges, i.e type (c) and (b) described in Chapter 2.8. Therefore, one thermal transmittance ψ is defined and used for the whole construction.

Figure 4.30 illustrates the steady-state model designed in Comsol. The model represents a floor/wall junction. (C) represents the thermal transmittance ψ, (A) and (B) represents the thermal coupling coefficient for the floor and wall respectively $[\frac{W}{m \cdot K}]$.

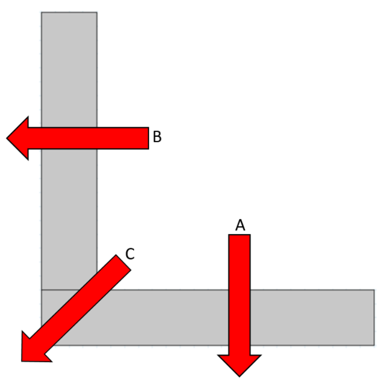

Figure 4.30: Sketch showing the edge designed in Comsol.

The thermal transmittance ψ is calculated according to Equation 4.15:

$$\begin{aligned} \psi &= (\mathrm{A} + \mathrm{B} + \mathrm{C}) - \mathrm{A} - \mathrm{B} \\ \\ \mathrm{A} &= \mathrm{U_{floor}} \cdot \mathrm{L_{floor}} \\ \mathrm{B} &= \mathrm{U_{wall}} \cdot \mathrm{L_{wall}} \end{aligned} \tag{4.15}$$

The Input data used in the model is represented in Table 4.10

Table 4.10: Input data used in Comsol for estimation of ψ.

Initial temperature [°C]	0
Internal temperature [°C]	1
External temperature [°C]	0
Mesh size	Extremely fine
EPS: Thermal conductivity $[\frac{W}{m \cdot K}]$	0.038

Figure 4.31 shows the final temperature distribution and the chosen mesh size in Comsol.

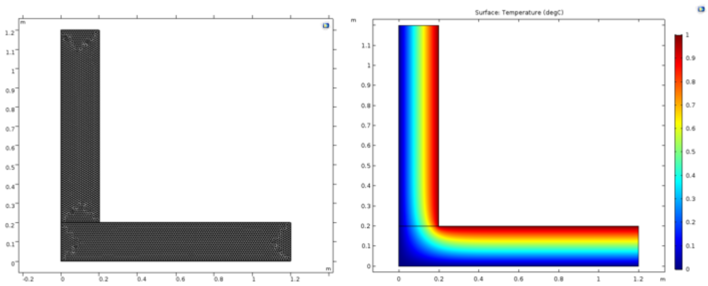

Figure 4.31: Sketch showing the corner junction designed in Comsol.

The output of the model, i.e sum of A, B and C is equal to 0.40127 $\frac{W}{m \cdot K}$, and the thermal transmittance ψ is estimated to 0.0213 $\frac{W}{m \cdot K}$. The additional heat losses through thermal bridges can then be calculated by Equation 4.16:

$$\begin{aligned} \mathrm{Q_{th.bridges}} &= \psi \cdot \mathrm{L_{th.bridge}} \cdot \Delta \mathrm{T} \\ \psi &= 0.0213 \frac{\mathrm{W}}{\mathrm{m} \cdot \mathrm{K}} \end{aligned} \tag{4.16}$$

$\mathrm{Q_{th.bridge}}$ Heat loss due to thermal bridges.
$\mathrm{L_{th.bridge}}$ Total length of thermal bridges.
$\Delta \mathrm{T}$ temperature difference over the building envelope.

Numerical Estimation of $\mathrm{Q_{w.side}}$

The presence of the curtain changes the conditions around the window. The curtain works as a insulation barrier resulting in different temperatures in the air gap than the rest of the test hut. The walls surrounding the air gap have a total area of 1.6 m^2.
In order to calculate the heat losses through the walls of the air gap, a steady-state model in Comsol, as shown in Figure 4.32 is built. Due to symmetry, only half of the construction

is designed. The simulations are run 27 times at which indoor and outdoor temperatures correspond to the mean temperatures for the whole period until then. As an example, the temperatures at simulation number 10 represent the mean temperature of the period between day 1 until day 10. Table 4.11 and 4.12 shows the input data used in Comsol. For the thermal conductivity of the window in Table 4.11, the U-value is converted to thermal conductivity. For the thermal conductivity of the curtain, the theoretical resistance of the curtain (assuming no air leakages) is converted to thermal conductivity.

Table 4.11: Input data used in Comsol for estimation of $Q_{w.side}$.

Initial temperature [°C]	0
Interior heat transfer coefficient[$\frac{W}{m^2 \cdot K}$]	25
Exterior heat transfer coefficient[$\frac{W}{m^2 \cdot K}$]	25
EPS: Thermal conductivity [$\frac{W}{m \cdot K}$]	0.038
Brick: Thermal conductivity [$\frac{W}{m \cdot K}$]	0.6
Curtain: Thermal conductivity [$\frac{W}{m \cdot K}$]	0.09
Window: Thermal conductivity [$\frac{W}{m \cdot K}$]	0.04
Mesh size	Extremely fine

Table 4.12: Mean indoor and outdoor temperatures used in the simulations (steady-state).

Temperature (°C) / Time(Day)	Indoor	Outdoor
1	21,43	-2,41
2	21,42	-2,87
3	21,41	-2,43
4	21,42	-2,40
5	21,42	-2,30
6	21,42	-1,92
7	21,43	-1,87
8	21,43	-1,65
9	21,43	-0,97
10	21,44	-0,47
11	21,45	-0,12
12	21,46	0,29
13	21,47	0,83
14	21,48	1,23
15	21,49	1,39
16	21,49	1,54
17	21,50	1,76
18	21,51	2,08
19	21,52	2,47
20	21,53	2,79
21	21,53	3,06
22	21,54	3,27
23	21,55	3,51
24	21,56	3,75
25	21,57	4,09
26	21,58	4,31
27	21,59	4,45

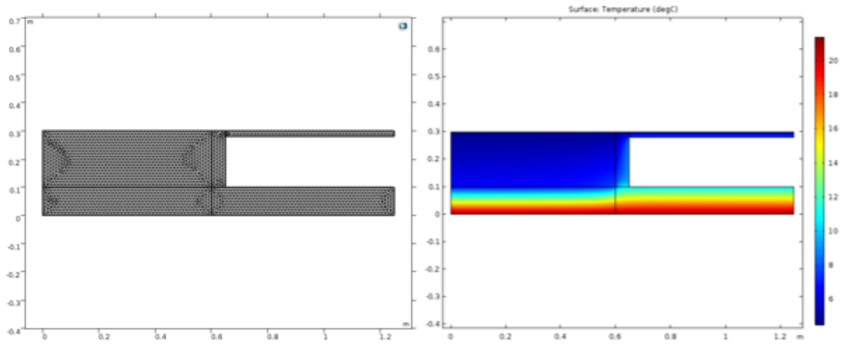

Figure 4.32: Sketch showing the model designed in Comsol. Left : Chosen mesh size. Right: temperature distribution at the final step.

U-value of the curtain design (A)

Figure 4.33 shows the U-value of the curtain including the window and the air gap in between. In similarity to the case in test hut 2, the results are averaged and the U-value at day 10 is the average over the 10 first days. The average U-value for the first 10 days is 0.62 $\frac{W}{m^2 \cdot K}$, while the average U-value for the whole period is 0.73 $\frac{W}{m^2 \cdot K}$. This means that the contribution of the curtain and the air gap, corresponds to 51 % reduction of the U-value for the case with only a window.

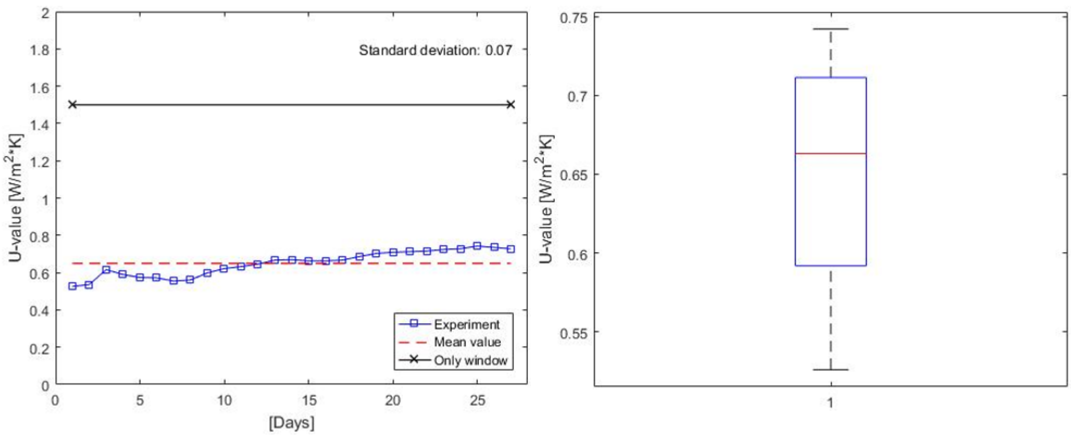

Figure 4.33: Graphs showing the U-value of the curtain in test hut 1 estimated by in-situ measurement, including the window and the air gap in between.

4.3.3 Test hut 3

Test hut 3 contains the curtain design (B). Again, the procedure is the same as the one in test hut 2 but with two differences. The first is that the U-value estimated here represents the U-value for the window, the curtain and the air gap in between, all three together. The second one is that in test hut 2, the g-value of the window and thus the total amount of solar radiation that reaches the indoor environment is known. In test hut 3, as the curtain is positioned in front of the window, the amount of solar radiation that passes through the window, reaches the curtain and the air gap first. Some part of it will be absorbed by the outmost layer of the curtain and will eventually reach the indoor environment. Some part of it will be lost to the outdoor environment. This means that for test hut 3, two

different parameters have to be estimated: a U-value representing the thermal resistance of the window, curtain and the air gap in between, but also a new g-value representing the total amount of solar radiation that can be utilized by the window, curtain and the air gap. To find out these two parameters, two equations have to be solved at the same time. The first one is the heat balance equation for test hut 3 and the second is the equation representing the relationship between the temperatures and solar radiation in test hut 2 and test hut 3.
Unlike the calculations in test hut 1, the additional heat losses in test hut 3 are estimated using $\Delta U_{additional}$, obtained from the calibration campaign. In test hut 1, due to the alteration of the conditions by including the curtain, and the fact that solar radiation is totally blocked, the additional heat losses are estimated by calculating the total amount of thermal bridges. In test hut 3, despite the presence of a curtain, and as the solar radiation reaches the interior of the test hut, the additional heat losses are estimated using $\Delta U_{additional}$, i.e as for the case in test hut 2.

Heat balance equation: Test hut 3

Figure 4.34 and Equation 4.17 describe the heat balance in test hut 3 and how the U-value of the window including the curtain and the air gap is calculated.

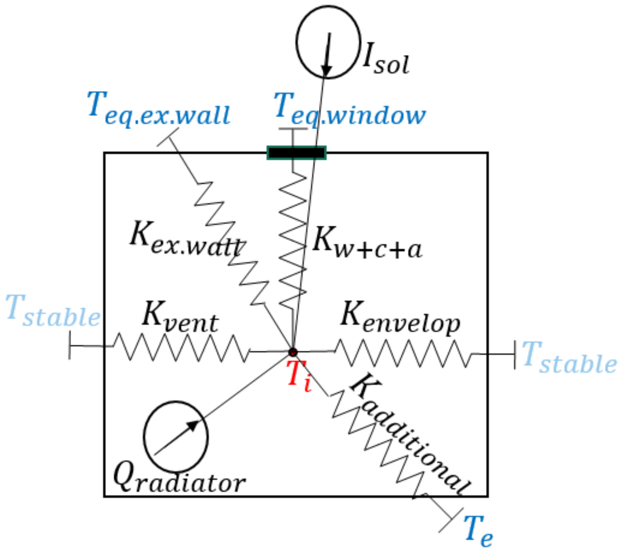

Figure 4.34: Thermal network for heat transfer through the building envelope of test hut 3.

$$
\begin{aligned}
&\mathrm{Q_{w+c+a} = Q_{radiator} + Q_{sol} - Q_{envelope} - Q_{vent} - Q_{ex.wall} - Q_{additional}} \\
&\mathrm{U_{window} = \frac{Q_{w+c+a}}{(T_i - T_e) \cdot A_{window}}}
\end{aligned}
\tag{4.17}
$$

g-value: Test hut 3

The new g-value, representing the total amount of solar radiation utilized in test hut 3, is calculated according to equation 4.18. To eliminate the effect of the radiator, the Equation below is solved for the hours at which the radiators are turned off and the solar intensity is more than $150\frac{\mathrm{W}}{\mathrm{m}^2}$.

$$\begin{aligned}
K_{tot.2} &= \Delta U_{additional.2} \cdot A_{tot} + U_{envelope} \cdot A_{envelope} + U_{ex.wall} \cdot A_{ex.wall} \\
&\quad + U_{window.2} \cdot A_{window} + n_2 \cdot V_{tot} \cdot \frac{\rho_{air} \cdot c_{air}}{3600} \\
K_{tot.3} &= \Delta U_{additional.3} \cdot A_{tot} + U_{envelope} \cdot A_{envelope} + U_{ex.wall} \cdot A_{ex.wall} \\
&\quad + U_{w+c+a} \cdot A_{window} + n_3 \cdot V_{tot} \cdot \frac{\rho_{air} \cdot c_{air}}{3600}
\end{aligned}$$

$$\begin{aligned}
T_{i.2} &= T_e + \frac{Q_{sol.2}}{K_{tot.2}} = T_{e.2} + \frac{g_2 \cdot I_{sol} \cdot A_{window}}{K_{tot.2}} \\
T_{i.3} &= T_e + \frac{Q_{sol.3}}{K_{tot.3}} = T_{e.3} + \frac{g_3 \cdot I_{sol} \cdot A_{window}}{K_{tot.3}} \\
\frac{T_{i.2} - T_{i.3}}{I_{sol} \cdot A_{window}} &= \frac{g_2}{K_{tot.2}} - \frac{g_3}{K_{tot.3}}
\end{aligned} \tag{4.18}$$

$$\boxed{g_3 = K_{tot.3} \cdot (\frac{g_2}{K_{tot.2}} - \frac{T_{i.2} - T_{i.3}}{I_{sol} \cdot A_{window}})}$$

$K_{tot.2}$	Overall thermal conductance for test hut 2 $[\frac{W}{K}]$.
$K_{tot.3}$	Overall thermal conductance for test hut 3 $[\frac{W}{K}]$.
$T_{i.2}$	Indoor temperatures in test hut 2 [°C].
$T_{i.3}$	Indoor temperatures in test hut 3 [°C].
g_2	g-value of the window in test hut 2 [-].
g_3	Representative g-value in test hut 3 for the window, curtain and the air gap in between [-].

Figure 4.35 shows the indoor temperature variations in test hut 2 and 3, during the 89 hours at which the radiators are turned off and the solar intensity is more than 150 $\frac{W}{m^2}$.

Equations 4.18 and 4.17 are solved at the same time and based on a guessed U-value. By multiple iterations, a consistent g-value and U-value is obtained. Figure 4.36 shows the compiled results from test hut 3. The total amount of solar radiation utilized in test hut 3 correspond to a mean g-value of 0.57 $[-]$, witch corresponds to approximately 20 % reduction in comparison to the g-value of the window (0.65). The mean U-value of the curtain design (B) is 0.8 $\frac{W}{m^2 \cdot K}$, which is higher than the U-value of design (A).

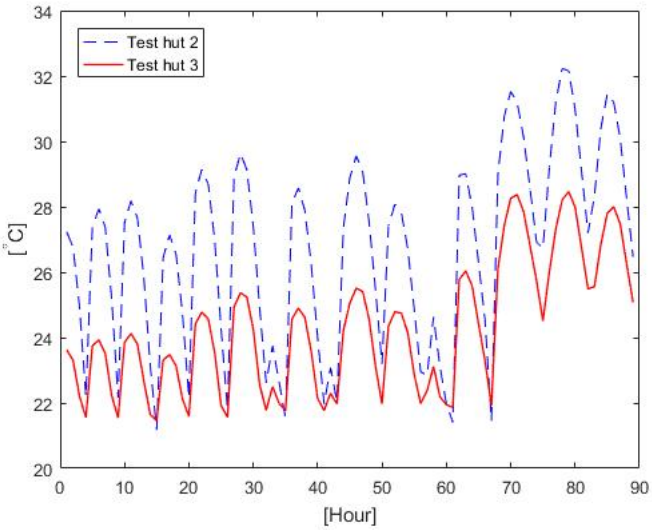

Figure 4.35: Indoor temperature variations when the radiators are turned off and the solar intensity is more than 150 $\frac{W}{m^2}$.

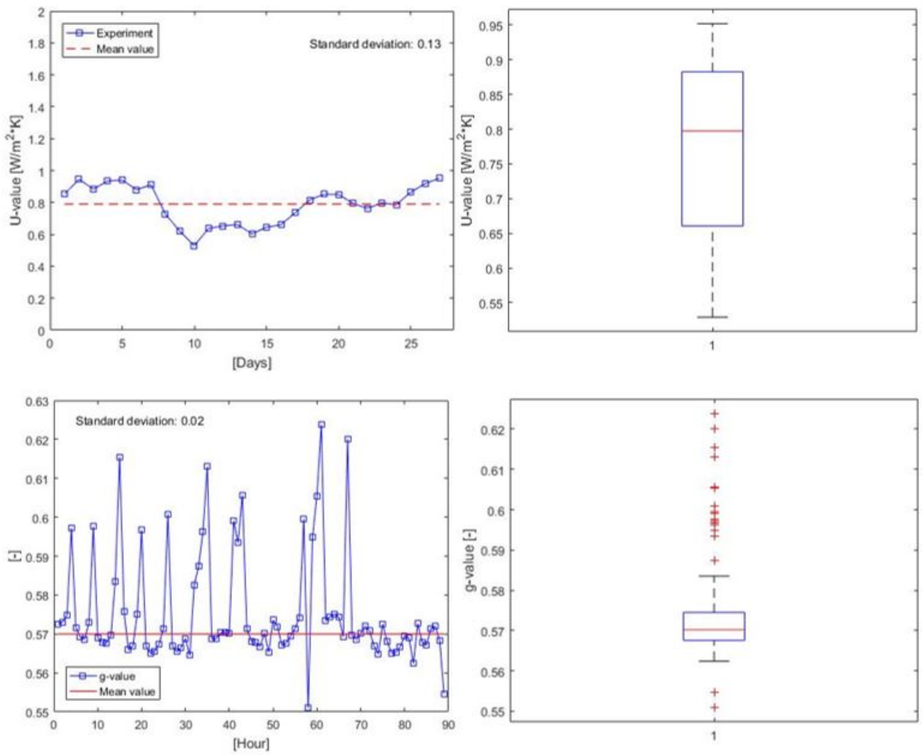

Figure 4.36: Graphs showing the obtained results from test hut 3. Up: U-value of the curtain design (B) including the window and the air gap in between. Down: g-value.

4.3.4 Estimation of the effect of the air gap in between the window and curtain

The air gap between the curtain and window is approximately 40 cm. For such an air gap, there is a long wave radiation exchange between the interior surface of the window and the exterior surface of the curtain. In additional to that, heat is transferred both due to natural but also forced convection, if there is any air movements. As the air gap studied here is 40 cm wide, heat transfer due to conduction can be neglected.
The fact that neither the temperature distribution nor the air velocity in the air gap are known, increases the difficulty for a precise estimation of the thermal properties of the air gap. In this project a simplified model is used to estimate the thermal resistance of the air gap. Figure 4.37 shows the thermal network used in the model. The calculations are based on two assumptions: The first one is that there is no forced air movements in the air gap, i.e the curtain is completely sealed and has no leakages. The second one is that the air has same temperature in every position in the air gap.

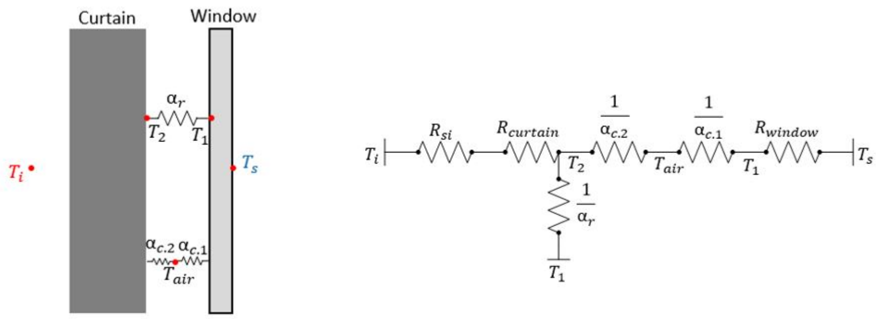

Figure 4.37: Different components in the thermal network solved to estimate the thermal properties of the air gap.

The heat transfer coefficients $\alpha_{\mathrm{c.1}}$, $\alpha_{\mathrm{c.2}}$ and α_{r} are calculated according to Equation 4.19 and 4.20, (Hagentoft, 2001):

$$\begin{aligned} \alpha_{\mathrm{c.1}} &= 2 \cdot |\mathrm{T_{air}} - \mathrm{T_1}|^{0.25} \\ \alpha_{\mathrm{c.2}} &= 2 \cdot |\mathrm{T_{air}} - \mathrm{T_2}|^{0.25} \end{aligned} \tag{4.19}$$

$$\alpha_{\mathrm{r}} = 4 \cdot \left(\frac{1}{\epsilon_1} + \frac{1}{\epsilon_2} - 1\right)^{-1} \cdot \sigma \cdot \left(\frac{\mathrm{T_1} + \mathrm{T_2}}{2} + 273.15\right)^3 \tag{4.20}$$

And the total thermal resistance for the air gap is calculated by Equation 4.21:

$$\mathrm{R_{airgap}} = \left(\alpha_{\mathrm{r}} + \frac{1}{\frac{1}{\alpha_{\mathrm{c.1}}} + \frac{1}{\alpha_{\mathrm{c.2}}}}\right)^{-1} \tag{4.21}$$

The problem is solved by multiple iterations for the interior and exterior temperatures at each hour during the 27 days of the measurement campaign. As it can be seen in Figure 4.38, the thermal resistance of the air gap is estimated to approximately 0.22 $\frac{\mathrm{m^2 \cdot K}}{\mathrm{W}}$.

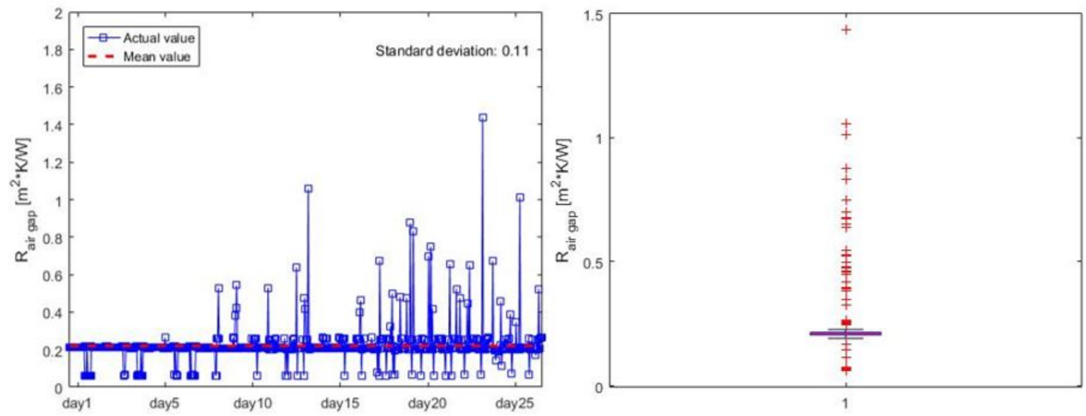

Figure 4.38: Estimated value for the thermal resistance of the air gap during the entire measurement campaign.

4.3.5 Estimation of the surface to surface resistance of the curtains

As the thermal properties of the window are known and based on the estimated resistance for the air gap, a thermal resistance for the curtain can be defined as shown in Figure 4.39 and Equation 4.22:

Figure 4.39: Thermal network of resistance to estimate the resistance of the curtain.

$$\begin{aligned} \mathrm{R_{curtain}} &= \frac{1}{\mathrm{U_{tot}}} - \mathrm{R_{si}} - \mathrm{R_{se}} - \mathrm{R_{airgap}} - \mathrm{R_{glass}} \\ \mathrm{R_{glass}} &= \frac{1}{\mathrm{U_{window}}} - \mathrm{R_{si}} - \mathrm{R_{se}} \end{aligned} \tag{4.22}$$

In Table 4.13 the surface to surface resistances for both designs of the curtain are presented. The values are based on the total U-value ($\mathrm{U_{tot}}$)for the curtain including the window and the air gap in between estimated by in-situ measurements. The calculation is done for the average value over the first 10 days, over the entire 27 days and the average of all 27 values.

Table 4.13: Surface to surface resistance for different designs of the curtain.

Resistance ($\frac{m^2 \cdot K}{W}$) / **Curtain type**	**10 Days**	**27 Days**	**Average**
Design (A)	0.73	0.49	0.65
Design (B)	1.00	0.17	0.38

Comparison between the results from the pilot study and the tests performed by RISE

As mentioned in Chapter 1, a similar design of the curtain is partially tested at the testing institute RISE in Borås, Sweden. The technical details of the curtain tested at RISE and the documentation of the test can be found in Appendix 8.
The tested curtain at RISE consists of 11 layers and the corresponding 10 air gaps, with an estimated surface to surface resistance of 0.83 $\frac{m^2 \cdot K}{W}$. The curtain studied in this project, design (A), is on the other hand somehow different than the one tested at RISE. This curtain consists of 8 layers and the corresponding 7 air gaps, with an estimated surface to surface resistance of 0.65 $\frac{m^2 \cdot K}{W}$. Assuming a linear relation between the number of air gaps and the total thermal resistance of the curtain, adding 3 additional air gaps to the curtain design (A), i.e 10 air gaps, increases the resistance of the curtain from 0.65 $\frac{m^2 \cdot K}{W}$ to approximately 0.90 $\frac{m^2 \cdot K}{W}$. Comparing the theoretical surface to surface resistance of the curtain design (A) with 10 air gaps, with the result from the test performed at RISE, shows an overestimation of the resistance of the curtain by approximately 8 % by the pilot study performed in this project.

Sensitivity analysis

As described in Section 4.2.2, the amount of heat losses due to leakages and ventilation is based on the total air permeability of the test hut obtained from the blower door test and the assumption of a constant pressure difference of 2 Pa over the building envelope.
As the ventilation losses is the only parameter in the heat mass balance equations solved in this project, that is not directly measured during the measurement campaign, a sensitivity analysis is performed to evaluate the impact of different air flow rates, n[$\frac{1}{h}$], and thus different ventilation losses on the estimated U-value of the window construction in test hut 1, 0.65 $\frac{W}{m^2 \cdot K}$.
The other parameter considered in the sensitivity analysis, is the solar intensity, $Q_{sol}[\frac{W}{m^2}]$, measured by the solarimeter used in this project and the impact of it on the estimated U-value of the window in test hut 2, 1.74 $\frac{W}{m^2 \cdot K}$. Table 4.14 shows the results of the sensitivity analysis performed.

Table 4.14: Sensitivity analysis of air flow rate in test hut 1 and solar intensity in test hut 2.

Parameter	**Change**	**Acronym**	**New U-value** [$\frac{W}{m^2 \cdot K}$]	**Difference** [%]
Air flow rate, n [$\frac{1}{h}$]	Increment by 100 %	$2.0 \cdot n$	0.1	85
	Increment by 20 %	$1.2 \cdot n$	0.54	17
	Decrement by 20 %	$0.8 \cdot n$	0.76	17
	Decrement by 50 %	$0.5 \cdot n$	0.92	42
Solar intensity, Q_{sol} [$\frac{W}{m^2}$]	Increment by 10 %	$1.1 \cdot Q_{sol}$	2.12	22
	Increment by 5 %	$1.05 \cdot Q_{sol}$	1.93	11
	Decrement by 5 %	$0.95 \cdot Q_{sol}$	1.55	11
	Decrement by 10 %	$0.9 \cdot Q_{sol}$	1.4	22

As it can be seen in Table 4.14, the result of the parameter study performed in this project seams to be very sensitive to the accuracy of measured solar radiation and even more sensitive to the changes of air flow rate. In test hut 1 where the curtain design (A) is located, the total amount of heat losses is reduced and any minor changes, for instance changes of the heat losses through leakages, affect the heat losses through the window construction and the corresponding U-value.

5

Parametric study to optimize the design of the curtain

In this project, two different parameters and their effect on the thermal performance of the curtains have been studied. The first parameter is the emissivity of the material used in both designs of the curtain. The second one is the air flow rate created by fans in the solar collector function of design (B).

5.1 Emissivity of the material

To evaluate how much the thermal resistance of the curtain can be increased if all layer of the curtain are replaced by low-emissivity material, a model as shown in Figure 5.1 is studied. The model represents a curtain with 8 layers, i.e 7 air gaps in between, which is completely sealed. Assuming that there is no air movement inside the air gaps, i.e stagnant air, and due to the very narrow width of the air gaps, the heat transfer due to convection can be neglected. The heat transfer process is thus due to heat conduction and long-wave radiation. In the cases studied here, a temperature difference of 1 °C is assumed. An other simplification made in the model is that the temperatures on both sides of each layer are equal. This means that the thermal resistance of the material has been neglected. Equation 5.1 shows how different parameters used in this study are defined, (Hagentoft, 2001).

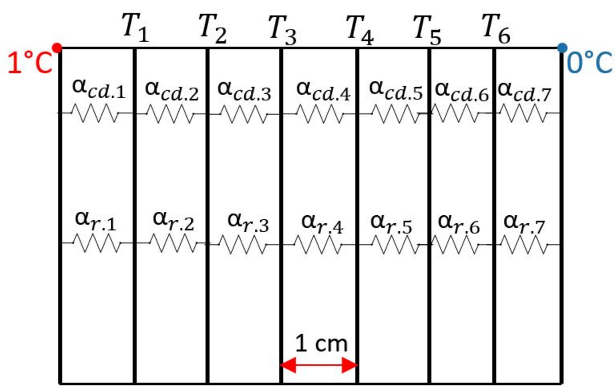

Figure 5.1: Modeled studied to investigate the effect of low-emissivty material in the curtain.

The thermal resistance between layers is calculated according to Equation 5.1:

$$\begin{aligned}
\mathrm{R_{tot}} &= \sum \mathrm{R_i} \\
\mathrm{R_i} &= \frac{1}{\alpha_{\mathrm{r.i}} + \alpha_{\mathrm{cd.i}}} \\
\alpha_{\mathrm{r.i}} &= 4 \cdot \sigma \cdot \left(\frac{1}{\epsilon_{\mathrm{i}}} + \frac{1}{\epsilon_{\mathrm{i+1}}} - 1\right)^{-1} \cdot \left(\frac{\mathrm{T_i} + \mathrm{T_{i+1}}}{2} + 273.17\right)^3 \\
\alpha_{\mathrm{cd.i}} &= \frac{\lambda_{\mathrm{air}}}{\mathrm{d_{air}}} = \frac{0.025}{0.01} = 2.5 \frac{\mathrm{W}}{\mathrm{m^2 \cdot K}}
\end{aligned} \tag{5.1}$$

These equations have been solved iteratively for different emissivity in MATLAB and the result is presented in Table 5.1 and Figure 5.2:

Table 5.1: Thermal Resistance of the curtain at different emissivities.

Emissivity(ϵ) / **Temperature** [°C] / **Resistance**[$\frac{m^2 \cdot K}{W}$]	**0.9**	**0.7**	**0.5**	**0.3**	**0.1**
T_1	0.86	0.86	0.86	0.86	0.86
T_2	0.71	0.71	0.71	0.71	0.71
T_3	0.57	0.57	0.57	0.57	0.57
T_4	0.43	0.43	0.43	0.43	0.43
T_5	0.29	0.29	0.29	0.29	0.29
T_6	0.14	0.14	0.14	0.14	0.14
R_1	0.1584	0.1996	0.2467	0.3010	0.3643
R_2	0.1585	0.1997	0.2468	0.3011	0.3643
R_3	0.1587	0.1999	0.2470	0.3012	0.3644
R_4	0.1588	0.2001	0.2471	0.3013	0.3644
R_5	0.1590	0.2002	0.2473	0.3014	0.3645
R_6	0.1591	0.2004	0.2474	0.3015	0.3645
R_7	0.1593	0.2005	0.2476	0.3017	0.3646
R_{tot}	1.1118	1.4004	1.7298	2.1092	2.5508
Improvement [%]	0	26	55	90	129

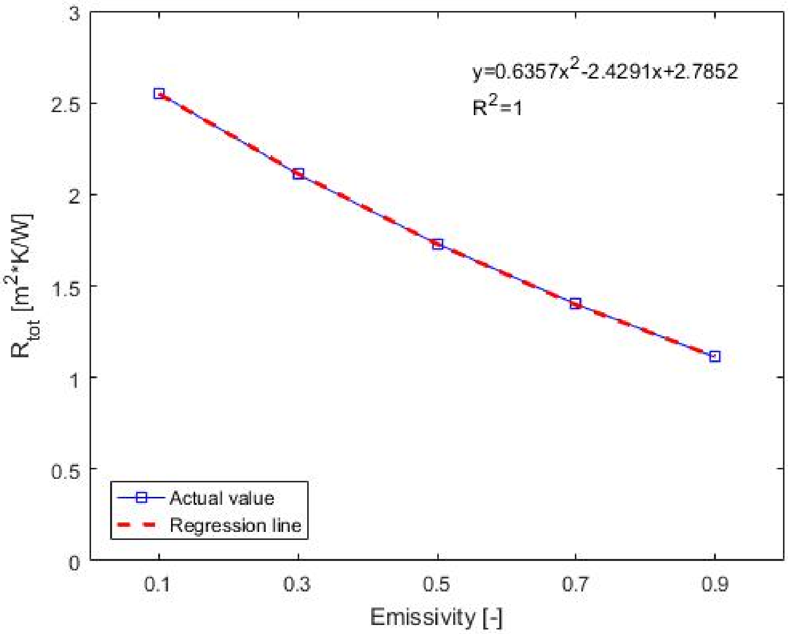

Figure 5.2: Graph showing the relation between emissivity of the material and the total resistance of the curtain.

As it can be seen in Table 5.1, the maximum theoretical resistance of the curtain made by materials with an emissivity of 0.9, is equal to approximately 1.11 $\frac{m^2 \cdot K}{W}$. The surface to surface resistance of the curtain, obtained from the pilot study performed in this project corresponds to 0.65 $\frac{m^2 \cdot K}{W}$, i.e 40 % less than the maximum theoretical resistance. This can be seen as an indicator for possibilities to improve the design and production of the curtain and by that improve the thermal performance of the curtain.

5.2 Air velocity of the fans

To evaluate the impact of different air velocities of the fans, on the performance of the solar collector function of design (B) and per one meter window in horizontal direction, a relationship between the total amount of heat losses through the window and the convectional heat gains to the room is defined. The problem is solved analytically and the equations used in this study are in accordance with the equations presented in (Hagentoft and Karim, 2018)

Equation 5.2 represent the net heat gain in the room by the solar collector function of the curtain and forced convection:

$$\begin{aligned} &\mathrm{Q_{in}} = (\mathrm{q_s} - \frac{\mathrm{T_i} - \mathrm{T_e}}{\mathrm{R_f}}) \cdot \mathrm{H} \cdot \frac{\mathrm{R_f}}{\mathrm{R_g} + \mathrm{R_f}} \cdot (\frac{\mathrm{R_g}}{\mathrm{R_f}} \cdot \frac{\mathrm{l_c}}{\mathrm{H}} \cdot (1 - \mathrm{e}^{-\frac{\mathrm{H}}{\mathrm{l_c}}}) + 1) \\ &\mathrm{l_c} = \frac{\mathrm{q_a} \cdot \rho_\mathrm{a} \cdot \mathrm{c_{pa}}}{\frac{1}{\mathrm{R_f}} + \frac{1}{\mathrm{R_g}}} \end{aligned} \tag{5.2}$$

Equation 5.3 represent the net heat gain in the room if no curtain is used, i.e only a window:

$$Q_{\mathrm{in.window}} = Q_s \cdot 1 \cdot H - \frac{1 \cdot H}{R_f} \cdot (T_i - T_e) \tag{5.3}$$

And Equation 5.4 describes the relation between the net heat gain with and without curtain, i.e if only having a window:

$$\eta = \frac{Q_{\mathrm{in}}}{Q_{\mathrm{in.window}}} = \frac{(q_s - \frac{T_i - T_e}{R_f}) \cdot H \cdot \frac{R_f}{R_g + R_f} \cdot (\frac{R_g}{R_f} \cdot \frac{l_c}{H} \cdot (1 - e^{-\frac{H}{l_c}}) + 1)}{Q_s \cdot 1 \cdot H - \frac{1 \cdot H}{R_f} \cdot (T_i - T_e)} \tag{5.4}$$

Q_{in}	Heat gain per one meter window (Horizontally), for the case with curtain $[\frac{W}{m}]$.
$Q_{\mathrm{in.window}}$	Heat gain per one meter window (Horizontally), for the case without curtain $[\frac{W}{m}]$.
R_f	Thermal resistance between screen where solar radiation is absorbed to external temperature $[\frac{m^2 \cdot K}{W}]$.
R_g	Thermal resistance between screen where solar radiation is absorbed to internal temperature $[\frac{m^2 \cdot K}{W}]$.
H	Height of window (length of air path) [m].
q_a	Airflow rate $[\frac{m^3}{ms}]$.
$\rho_a c_{pa}$	Heat capacity of air.
q_s	Absorbed solar radiation at the screen $[\frac{W}{m^2}]$.
Q_s	Solar radiation transmitted through the window[W].
T_e	External air temperature.
T_i	Internal air temperature.

Figure 5.3 shows the net heat gain in the room (Equation 5.2) at different air flow rates. The solar intensity striking the window is assumed to be 800 $\frac{W}{m^2}$, dimensions of the curtain and window are set to [1.0m · 1.0m], absorptivity of the curtain is 0.9 and indoor and outdoor temperatures are set to be 20 and 0 °C respectively. As it can be seen in Figure 5.3, for air flows higher than 0.1 $\frac{m^3}{s}$ the efficiency of the solar collector function is rather independent of the air velocity created by fans. For air flows lower than 0.1 $\frac{m^3}{s}$, the increment of Q_{in} starts from 0 $\frac{m^3}{s}$ and stops at 0.04-0.05 $\frac{m^3}{s}$. This means that for the specific case studied here, increasing the the air flow of the fans above 0.05 $\frac{m^3}{s}$ does not have a major effect on the total heat gain in the room. Worth to be mentioned is that in reality, and for a curtain with these dimensions, it is rather impossible to achieve an air flow rate higher than 0.1 $\frac{m^3}{s}$

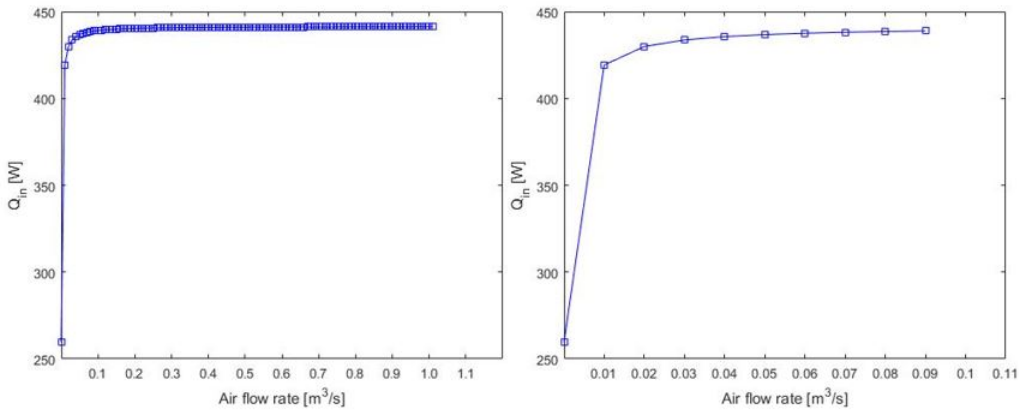

Figure 5.3: Graphs showing the relation between air flow rate and the net heat surplus into the room. Left : from 0 to 1.0 $\frac{\mathrm{m}^3}{\mathrm{s}}$, Right: from 0 to 0.1 $\frac{\mathrm{m}^3}{\mathrm{s}}$.

Looking at the comparison between the cases with and without a certain (Equation 5.4), the relation seems to be below 1, regardless the dimensions of the window and air flow rates. As it can be seen in Figure 5.4, having a curtain and its solar collector function is more efficient for windows with lower height. For the specific case studied here, and regarding the solar collector function, it is more profitable to just have a window without a curtain and its solar collector function. The case studied here is based on the assumption that the absorptivity of the curtain is equal to 1, i.e a best case scenario for the curtain.

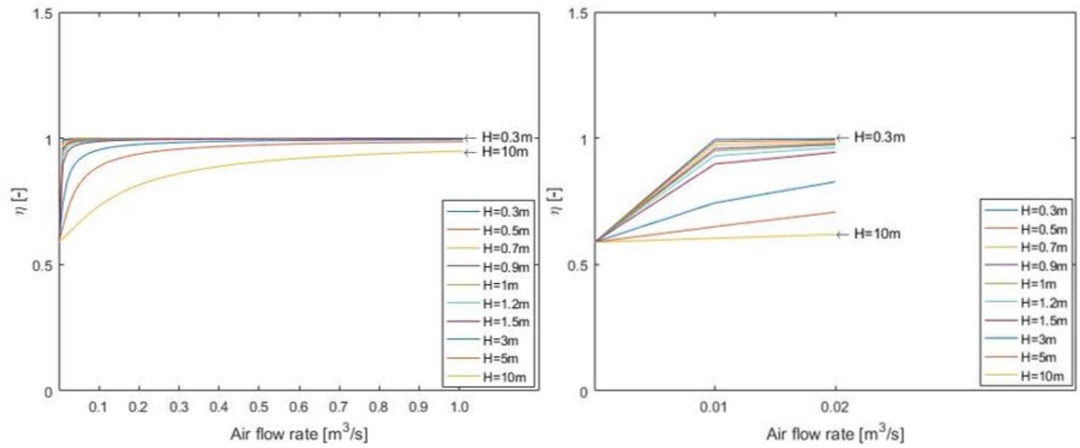

Figure 5.4: Graph showing the relation between air flow rate, height of the window and the net efficiency of the solar collector function. Left : from 0 to 1.0 $\frac{\mathrm{m}^3}{\mathrm{s}}$, Right: from 0 to 0.02 $\frac{\mathrm{m}^3}{\mathrm{s}}$.

Case study: Forced convection

A Simulink model is built to evaluate the performance of the solar collector function at different air flow rate in a fictitious test room. The room is considered as a hot box and the simulations are run for 1 hour, i.e 3600 steady state iterations, one for each second. The unknown parameter at each step is the indoor temperature inside the room, and the initial temperature at each step is the result of the previous one. The dimensions of the test room are [8m · 10m · 3m] and it has only one window. The room is considered to be very well insulated (no other heat losses than the ones through the window are considered) and the effect of thermal mass of the materials in the room is not considered either. Initial indoor temperature is set to 20 °C. The curtain and window has the dimensions [1m · 1m]. The solar radiation striking the window is constant during 1 hour and has the intensity of 800 $\frac{W}{m^2}$. Absorptivity of the curtain is 0.9 and g-value of the window is 0.65. More detail about the model built in Simulink can be found in Appendix 6. The simulations are run for different air flow rates and the results are presented in Table 5.2. The instantaneous indoor temperature is calculated according to Equation 5.5.

$$C_{air} \cdot \frac{dT_{in}}{dt} = Q_{in} + 0 \tag{5.5}$$

Table 5.2: Results from simulation made in Simulink for variable air flow rate.

Air flow rate$[\frac{m^3}{s}]$	l_c [m]	**Temperature** [°C]	**Energy** [Wh]
0.01	3.74	25.20	416
0.03	11.22	25.38	430
0.05	18.70	25.42	433
0.10	37.40	25.45	435
0.20	74.80	25.46	436
1.00	374.02	25.47	438
5.00	1870.10	25.47	438

Natural convection

The second case studied here is to have the solar collector function of the curtain without any fans and just consider the air flows created by the pressure difference, due to different temperatures in the curtain and indoor. Equation 5.6, describes how the air flow rate due to natural convection is calculated (Hagentoft and Karim, 2018). The equation has to be solved by multiple iterations and an initial guess on the air flow rate.

$$\begin{aligned} \Delta P &= H \cdot 3456 \cdot (\frac{1}{T_i} - \frac{1}{T_{mean.airgap}}) \\ T_{mean.airgap} &= \frac{1}{H}\int_0^H T(s)ds \\ q_a &= A_1 \cdot 0.84 \cdot \sqrt{\Delta P} \end{aligned} \tag{5.6}$$

ΔP	Pressure difference [Pa].
T_i	Indoor temperature [K].
$T_{mean.airgap}$	Mean temperature in the air gap [K].
$T(s)$	Temperature at position s in the air gap [°C].
H	Height of window (length of air path) [m].
A_1	Area of the holes in the entrance of the air gap $[\frac{m^3}{ms}]$.
q_a	Airflow rate $[\frac{m^3}{ms}]$.

Same model with the same conditions as the model for the case with forced convection is designed in MATLAB and solve by multiple iterations. Simulations are run for 1 hour and the result is presented in Table 5.3. As the air flow rate and other parameters varies for each step, mean values are presented instead.

Table 5.3: Results from simulation for the case with natural convection.

Mean air flow rate[$\frac{m^3}{s}$]	$l_{c.mean}$ [m]	**Temperature** [°C]	**Energy** [Wh]
0.0075	3.00	25.22	417

6

Case study

In this chapter, the energy performance of the curtain design (A) and its influence on the energy consumption of a fictitious house located in Gothenburg is studied by the means of simulations. In this study, the energy consumption of four cases listed below are studied.

- **Windows facing south**
- **Case I**: Total energy consumption of the house without covering the windows by curtains, during 3 month(Jan-Mars) and with a indoor set temperature of 20 °C.

- **Case II**: Total energy consumption of the house with covering the windows by curtains, during 3 month(Jan-Mars) and with a indoor set temperature of 20 °C. Curtains are rolled-up whenever solar radiation reaches an intensity above 90 $\frac{W}{m^2}$.

- **Windows facing north**
- **Case III**: Total energy consumption of the house without covering the windows by curtains, during 3 month(Jan-Mars) and with a indoor set temperature of 20 °C.

- **Case IV**: Total energy consumption of the house with covering the windows by curtains, during 3 month(Jan-Mars) and with a indoor set temperature of 20 °C. Curtains are rolled-up whenever solar radiation reaches an intensity above 90 $\frac{W}{m^2}$.

Description of the house

The fictitious house studied here is a single-detached dwelling made entirely of concrete, mineral wool and gypsum. It is located in Gothenburg and has the dimensions [8m · 10m · 3m]. In this house, there are two windows once facing south and once north, having the dimensions [1.5m · 1.5m]. The details of the house are presented in Table 6.1. All material properties are according to given data in (Hagentoft, 2001).

Table 6.1: Details of the house.

$d_{concrete}[m]$	0.200	$\lambda_{concrete}\ [\frac{W}{mK}]$	1.7
$d_{min.wool}[m]$	0.100	$\lambda_{min.wool}\ [\frac{W}{mK}]$	0.033
$d_{gypsum}[m]$	0.013	$\lambda_{gypsum}\ [\frac{W}{mK}]$	0.22
$\tau_{window.diffuse}[-]$ [1]	0.5	$n_{ventilation}\ [\frac{1}{h}]$	0.5
$U_{window}[\frac{W}{m^2K}]$	3.0	$R_{curtain}\ [\frac{m^2K}{W}]$	0.65

[1] $\tau_{window.diffuse}$ is the window transmittance for diffuse radiation. Window transmittance for direct radiation is dependent on the angle of incidence, see Appendix 7.

Validation of the model

A model in Simulink is designed to simulate the cases. Detail of the model can be found in Appendix 7 (The Simulink library used in the model is originally written by Pepe Tan, PhD student at Chalmers University of Technology, and modified by the author of this report). The model in Simulink is validated against the indoor temperatures in test hut 2 during the measurement campaign. The input data for the model is the same conditions measured in test hut 2 during the measurement campaign. Figure 6.1 shows the measured indoor temperatures in test hut 2 and the indoor temperatures from the model in Simulink. Looking at the graphs on left, it can be seen that the result from simulation converges, with a sufficient accuracy, to the experimental one. The graphs on the Right can be somehow deceptive. During the measurement campaign, the radiator is turned on and off at times. This can for instance happen in the middle of one hour so the heat gain from the radiator is only for 30 minutes. However since the input data to the model is on hourly bases, the model interpret the heat gain from radiator, for the whole hour and distribute it evenly during this hour. In additional to that, the manner that the Simulink model treats radiation exchange in the room is limited and simplified. These two factors result in an almost constant delay during the whole period and also bigger deviations at the peaks. These two issues can be possible explanations for the big dispersion shown in the graphs on the right side. For the scope of this case study, the accuracy of the model is considered to be sufficient and no further measures are taken.

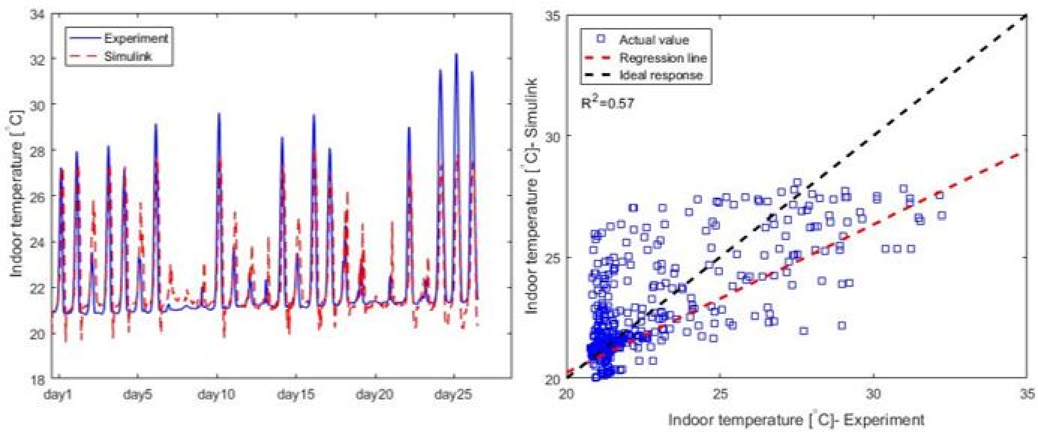

Figure 6.1: Left: Indoor temperatures in test hut 2 from measured on site and simulated by Simulink-model. Right: Convergence of the model against experimental data.

Result of the simulation

As described earlier, the simulations are run for 3 month, January, February and Mars for a representative year in Gothenburg. Figure 6.2 shows the outdoor temperatures and the total solar radiation (south and north direction, vertical), for the simulated period.

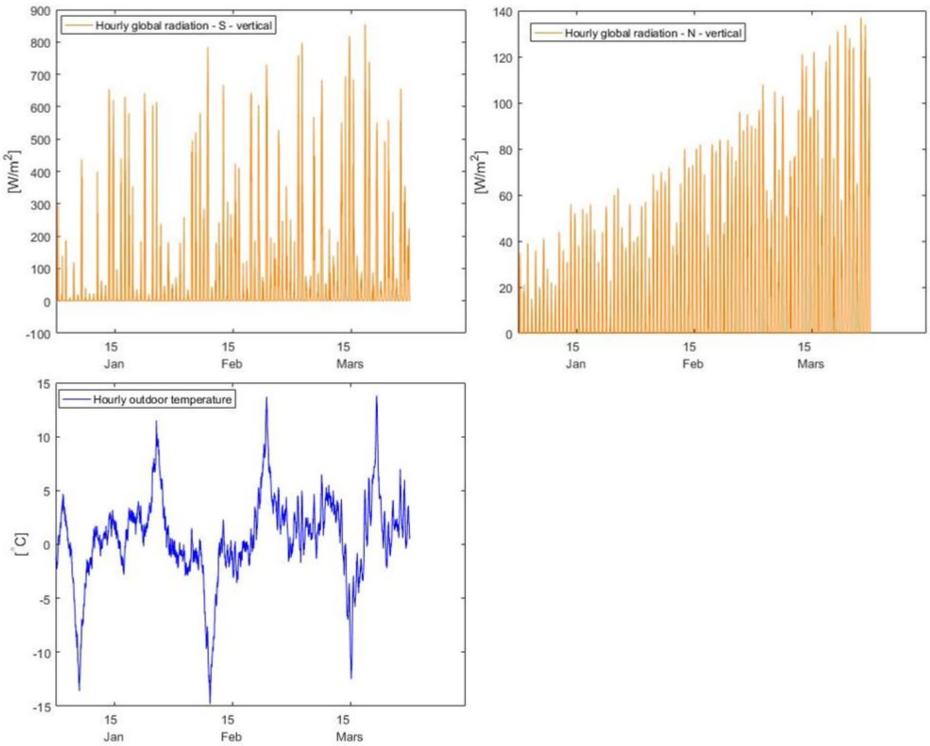

Figure 6.2: Down: Hourly Outdoor temperatures in Gothenburg between 1^{th} of January until 31^{th} of Mars. Up, Left: Total vertical solar radiation in the direction of south. Up,right: Total vertical solar radiation in the direction of north, and for the same period.

Windows facing south

In Figures 6.3 and 6.4 the complied results from the simulation of both cases I and II, are presented. In both cases the power of the heater is adjust so the indoor temperatures never undergo 20 °C, except for the few occasions where the lowest sinks of the outdoor temperature occur. At these occasions, temperatures above 19.8 °C have been accepted. In case II, variable U-value for the windows is used. Whenever the curtains are rolled-down, U-value is reduced to 1.02 $\frac{\mathrm{W}}{\mathrm{m}^2{\cdot}\mathrm{K}}$. This value corresponds to the new U-value of the window including the curtain, and the resistance of the air gap in between is neglected. At these occasions the solar radiation is set to zero as the curtains are rolled-down.

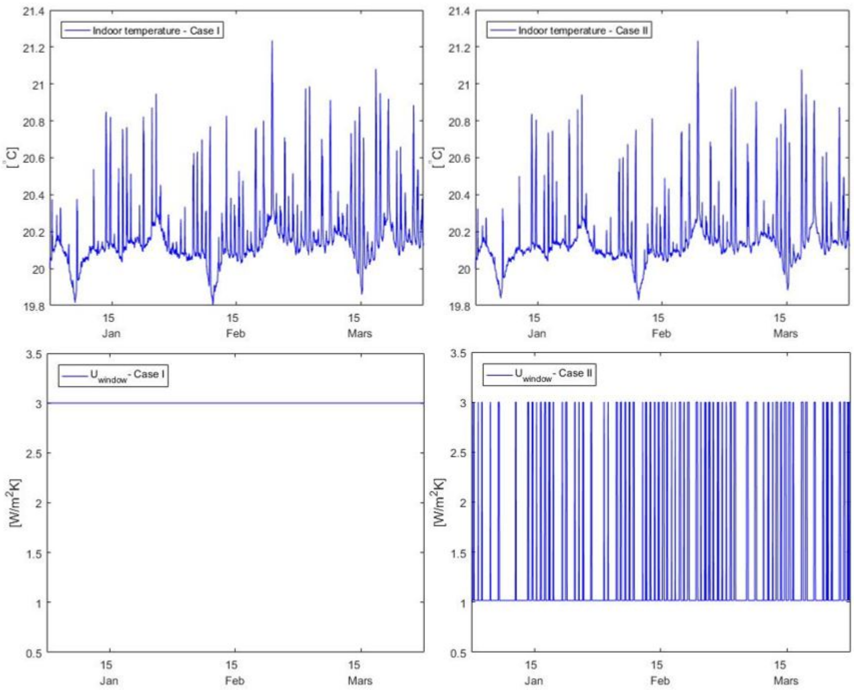

Figure 6.3: Indoor temperatures and U-value of the windows. Left: Case I. Right: Case II.

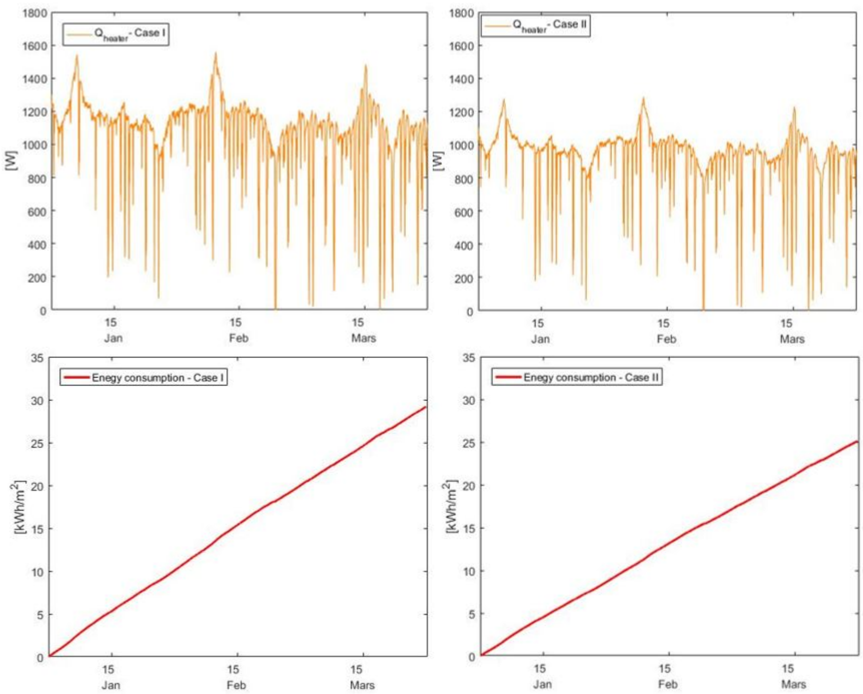

Figure 6.4: Power of the heaters and the total energy consumption. Left: Case I. Right: Case II.

The comparison between two cases shows that by using the curtains in case II, the energy consumption during the whole 3 month is reduced by approximately 14 %, see Figure 6.5.

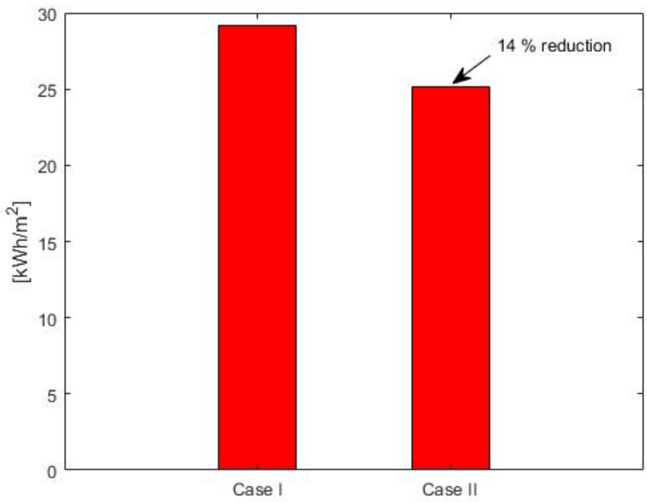

Figure 6.5: Energy consumption per square meter floor area in Case I and Case II.

Windows facing north

For case III and IV, simulations are run exactly as for case I and II. The only difference is the position of the windows, witch are facing north now. Figure 6.6 and Figure 6.7 Shows the results from simulations for case III and IV. As it can be seen in Figure 6.8, the energy consumption in case IV is 16 % less than case III.

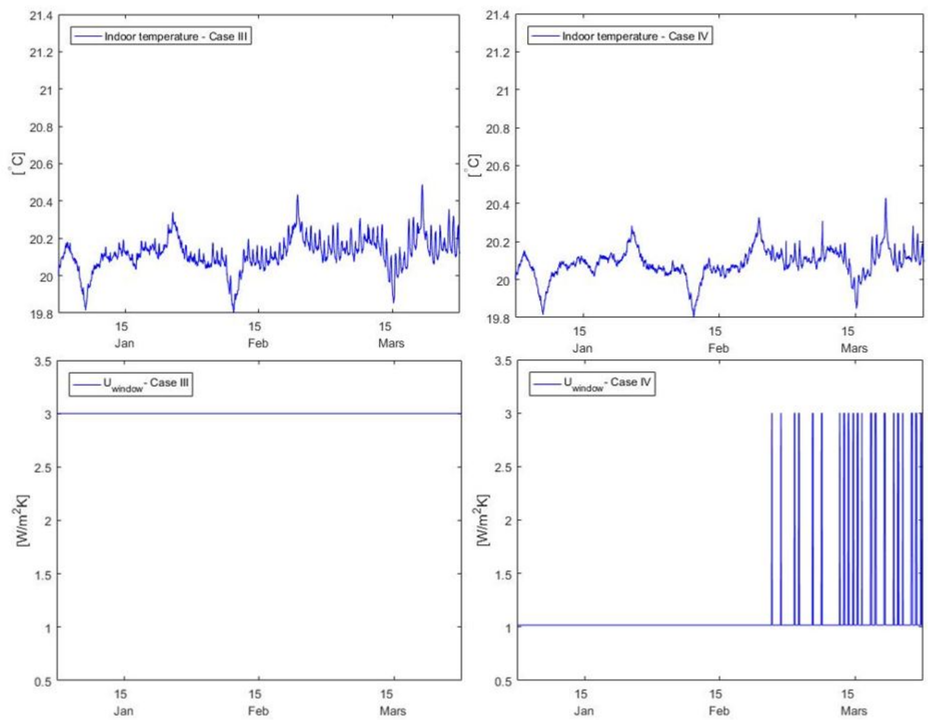

Figure 6.6: Indoor temperatures and U-value of the windows.Left: Case III. Right: Case IV.

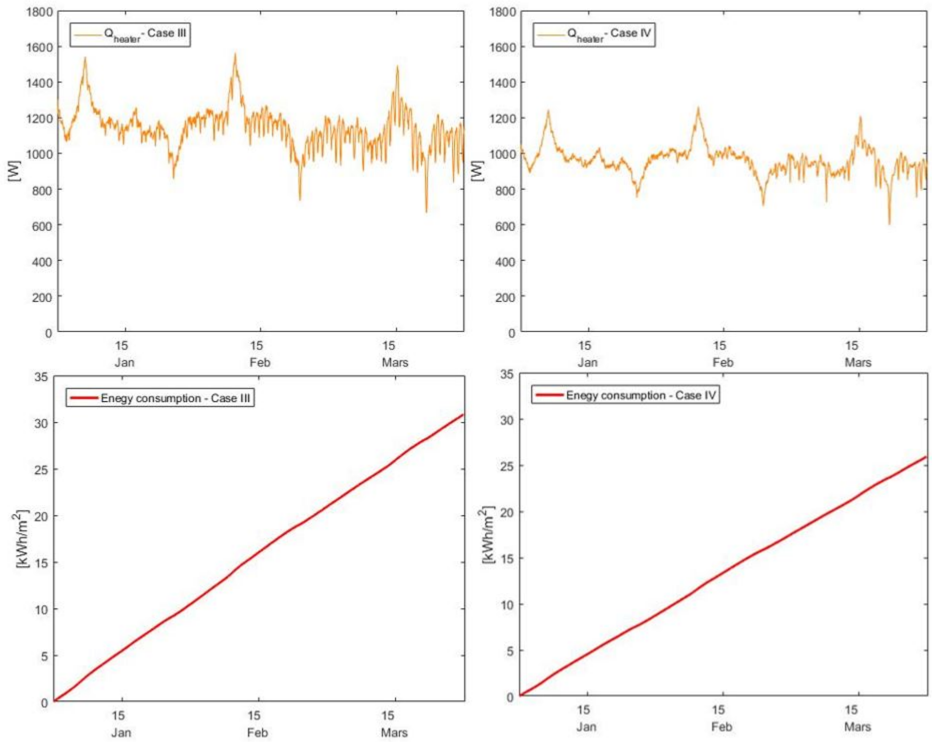

Figure 6.7: Power of the heaters and the total energy consumption. Left: Case III. Right: Case IV.

6.5.

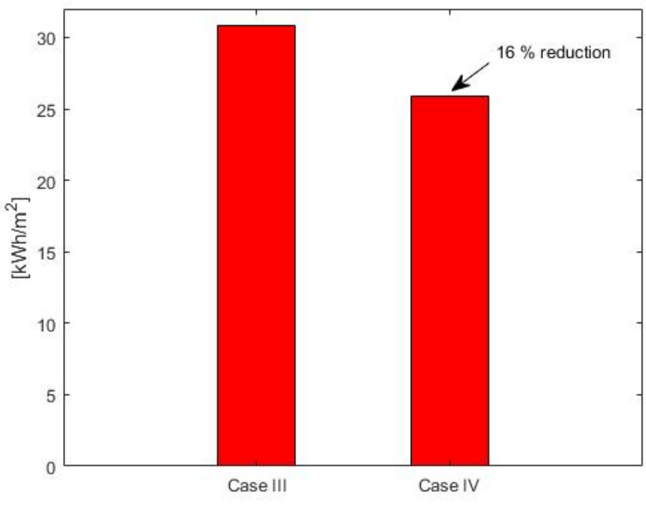

Figure 6.8: Energy consumption per square meter floor area in Case III and Case IV.

7

Conclusions and discussions

Conclusions

The energy performance of 2 different designs of the energy smart window curtain, called Climate Curtain, is evaluated by in-situ measurement. Curtain design (A) has the aim to increase the overall thermal resistance of window constructions and by that decrease the heat losses through windows. Curtain design (B) has an additional solar collector function which is aimed to capture some part of solar radiation striking windows and warm up the indoor temperatures.
The pilot study performed in this project consists of 3 identical test huts with one window in each test hut. 2 test huts are equipped by curtain design (A) and (B), and 1 test hut is used as reference case. The interior temperatures are kept at constant temperatures using radiators with thermostat. Interior and exterior temperatures, energy consumption in each test hut, and solar radiation are measured continuously. Possible deviations between the test huts are evaluated by performing a Bloower door test and an additional measurement campaign.

The results from pilot study show that both design (A) and (B) increase the overall thermal resistance of the window. For curtain design (A), the mean thermal resistance is estimated to 0.65 $\frac{\mathrm{m}^2\cdot\mathrm{K}}{\mathrm{W}}$ and for design (B) to 0.40 $\frac{\mathrm{m}^2\cdot\mathrm{K}}{\mathrm{W}}$. The effect of the curtain on the total resistance of the window construction in percentage, is incident to type of the window and its U-value. For a window with high U-value, it is more profitable to have the curtain while for very good windows with low U-value, the effect of the curtain decreases. Curtain design (B) and its associated solar collector function shows that it has the possibility to capture some part of the solar radiation striking the window. The total amount of solar radiation than has been utilized by design (B) corresponds to a g-value of 0.57, while the window has a g-value of 0.65. This means that regarding solar radiation, a window without a curtain design (B) is more efficient to utilize the solar radiation and to increase the indoor temperatures.
The parameter study performed, shows a rather week relation between the efficiency of the solar collector function and the air velocity of the fans. Regarding the material used in the curtain, it is shown that the efficiency of the curtain can be further improved by using low emissivity material. Decreasing the emissivity of the material from 0.9 to 0.5 can theoretically improve the thermal properties of the curtain by almost 55 %.

Discussions

Regarding the pilot studies performed in this project and the air gap between the curtain and window, it is worth mentioning that there will always be an air gap between the curtain and window. The created air gap can have a positive effect on the total thermal resistance of window construction. The effect of that is however very much case dependent and depends on for instance the distance between the window and air gap, air movements and also the air temperatures inside the gap. This makes the estimation of the impact of the air gap, rather difficult.
The additional heat losses in test hut 1 are considered by calculation of the total amount of thermal bridges instead of using $\Delta U_{\text{additional}}$ obtained from the calibration campaign. The main reason for that is the alteration of the conditions in test hut 1 by including the curtain and eliminating the solar radiation. Considering the additional losses in test hut 1 by $\Delta U_{\text{additional}}$ would result in an unacceptable amount of heat losses and unreasonable negative U-values for the window construction.

The accuracy of the pilot study performed in this project is set to $\pm 16\%$. This value is based on the accuracy obtained in the test hut used as reference. The fluctuation of the results obtained in test hut 2 and 3, where solar radiation is not blocked, is much more than the ones obtained in test hut 1. Beside that, the results from test hut 2 show an almost constant over estimation of the result. Due to some delay in the production of the curtains but also the test huts, the measurement campaign started later than what it was initially planned. Due to this issue, major part of the experiment was conducted in April where outdoor climate become warmer. The warmer outdoor conditions and the presence of solar radiation might have created some unintentional disturbance in the performed study, as the heat transfer is no longer in one direction(from interior to exterior) anymore. As the solar radiation is blocked by a shading in test hut 1, where curtain deign (A) is used, and as the fluctuation of the result is much less, the accuracy should be better than the one obtained in the reference test hut, test hut 2.

To get an even indoor temperature distribution in the test huts, one floor fan was used in each test hut. As the total air volume of the test huts are low(12 m^3), the air flows created by the fans are not representative for air flows in a normal room without fans. Air flows created by fans might have result in some additional air movements in the curtains and thus reduced the thermal resistance of the curtains. This is of course also case dependent and in order to minimize the effect of this issue, the curtain should optimally be completely sealed to prevent any unintentional leakages.

The temperatures in the stable were measured by 2 sensors at different heights and far away from the test huts. The stable is still used as a storage by the owners of the stable and can be used form time to time. In order to prevent the sensors to be effected by that and also to protect them from solar radiation, the sensors were positioned far away from the test huts(approximately 20 m). As there are some windows between the test huts, solar radiation can reach the air around the test huts and increase the temperatures. This can be considered as a source of error in the experiment as the sensors do not measure the exact temperatures around the test huts. By covering the windows located between the test huts, this issue could be solved.

The exterior walls where the windows are located, can also be a possible source of error.

The exterior wall is considered as homogeneous wall of brick with the same conditions in all 3 test huts. The construction of the external wall can however be different at different positions, resulting in different conditions for the test huts. Due to economical and time limitations of the project, the external wall is used exactly as it is. The calibration campaign is however conducted to capture any possible deviations between the test huts.

Regarding the performed blower door tests, as it can be seen in Appendix 4, there is a deviation from standard ISO 9972. According to the standard, (Institute, 2015), the minimum pressure difference shall be 10 Pa(±3 Pa) or five times the ΔP_{01}. This requirement is however not fulfilled for the tests performed in test hut 1 and 3. The combination of low leakage area and low air volume of the huts, result in that the blower door equipment can not take any samples at such a low pressure as 10 Pa. According to Paula Wahlgren, Associate professor at Chalmers University of Technology and expert in airtightness of buildings, this is not considered as a major issue and despite this deviation from the standard, the test results are still valid.

8

Recommendations for further research

The studies performed in this project have been based on the scope of the thesis, and have been highly influenced by the time and economical limitations of the project.
The conclusions of the thesis are based on the limited studies performed, but in order to fully capture the behaviour of the curtains, further research is required. Suggestions for some further research are listed below:

- A pilot study during a pure winter period with less solar radiation, to minimize the disturbances and uncertainties of the study.
- A pilot study with more test huts to evaluate different parameters simultaneously, and/or same parameters but with and without solar radiation.
- A pilot study to investigate the performance of the curtain if low emissivity material is used.
- A pilot study during a longer period to evaluate the long term performance of the curtain.
- A pilot study with two curtains, one completely sealed and the other one sealed as it is today.
- A pilot study during summer time.
- A pilot study with variable air flow rate to evaluate the impact of it on the efficiency of the design.
- More simulation studies for longer period, different climates and different directions for the windows.

Bibliography

Brian Anderson. *Conventions for U-value calculations*. CRC, 2002.

ASTM-C1363. Standard test method for thermal performance of building materials and envelope assemblies by means of a hot box apparatus. *West Conshohocken, Pennsylvania: ASTM International*, 2011.

GK Batchelor. An introduction to fluid mechanics (cambridge mathematical library), 2000.

Geert Bauwens and Staf Roels. Co-heating test: A state-of-the-art. *Energy and Buildings*, 82:163–172, 2014.

Phillip Biddulph, Virginia Gori, Clifford A Elwell, Cameron Scott, Caroline Rye, Robert Lowe, and Tadj Oreszczyn. Inferring the thermal resistance and effective thermal mass of a wall using frequent temperature and heat flux measurements. *Energy and Buildings*, 78:10–16, 2014.

Boverket. Boverkets byggregler, bbr avsnitt 9 bfs 2011:6 t.o.m. bfs 2015:3. *Avsnitt 9 Energihushållning*, 2015.

ISO Thermal Insulation-Building Elements-In. situ measurement of thermal resistance and thermal transmittance (iso 9869-1), 2014.

Minneapolis Blower Energy Conservatory. Operation manual for model 3 and model 4 systems. *Energy Conservatory*, 2012.

Carl-Eric Hagentoft. *Introduction to building physics*. External organization, 2001.

Carl-Eric Hagentoft and Ali Karim. Assessment of energy smart window curtains and the effect of variable air flow rate on the performance of the curtains. *[To be published]*, -:–, 2018.

Swedish Standards Institute. Thermal performance of buildings – determination of air permeability of buildings – fan pressurization method (iso 9972:2015). *Avsnitt 9 Energihushållning*, 2015.

Muhammad Iqbal. *An introduction to solar radiation*. Elsevier, 2012.

Steven T Karris. *Introduction to Simulink with engineering applications*. Orchard Publications, 2006.

Helmut Köster. *Dynamic daylighting architecture: basics, systems, projects*. Springer Science & Business Media, 2004.

Mahmoud Massoud. *Engineering thermofluids*, volume 2005. Springer, 2005.

Vahid M Nik. Application of typical and extreme weather data sets in the hygrothermal simulation of building components for future climate–a case study for a wooden frame wall. *Energy and Buildings*, 154:30–45, 2017.

BÅ Petersson. Tillämpad byggnadsfysik 3rd ed. *Studentlitteratur. ISBN*, pages 978–91, 2007.

Alan T Riga and C Michael Neag. *Thermal characterization of polymeric materials*. ASTM Philadelphia, PA, USA, 1991.

Claude-Alain Roulet. *Ventilation and airflow in buildings: methods for diagnosis and evaluation*. Routledge, 2012.

J Straube. Understanding and controlling air flow in building enclosures. *Unviversity Waterloo*, 2002.

Iain S Walker, David J Wilson, and Max H Sherman. A comparison of the power law to quadratic formulations for air infiltration calculations. *Energy and Buildings*, 27(3): 293–299, 1998.

Shuang-Hua Yang. Internet of things. In *Wireless Sensor Networks*, pages 247–261. Springer, 2014.

William BJ Zimmerman. *Multiphysics modeling with finite element methods*, volume 18. World Scientific Publishing Company, 2006.

.1 Appendix 1 - Window

Sidohängt fönster

Utåtgående 2-glas isolerruta.

VIRKESKVALITET:

Lamellimmad furu

SPRÖJS:

Löstagbar spröjs finns för utvändig montering.

UTFÖRANDE & BESLAGNING

- In- och utsida i trä.
- Lamellimmad enkelbåge med monterad 2-glas isolerruta.
- Karmförband limmade och spikade/skruvade.
- Bågförband limmade och spikade.
- Spårmonterad tätningslist i bågen.
- Utanpåliggande persienn kan monteras på bågens rumssida. Ej fabriksmonterad.
- Kan förses med infälld spaltventil i karmen, 40 cm^2.
- 2 st ytbehandlade bärgångjärn av metall. 3st gångjärn från höjd 13M.
- Blankförnicklad stormkrok 1 st per båge.
- Blankförnicklade fönsterlås 2 st per båge.

YTBEHANDLING:

Allt trä genomgår en skyddsbehandling som motverkar röta och blånad.

TÄCKMÅLADE
Komponenterna ytbehandlas med en 1-komponent vattenburen grundfärg och en 1-komponent vattenburen täckfärg på samtliga ytor.

LASERADE
Komponenterna behandlas med en vattenburen lasyr och en vattenbaserad lasyrlack på samtliga ytor.

MONTERING:

Karmsidorna är förborrade för karminfästning.
Täckpluggar medföljer.

GLASNING:

- Glasad med 2-glas isolerruta D4-16.
- Energiglas som standard.
- Monterad enligt MTK-system 3
- Glaslist av aluminium i bågbottenstycket monterad med snäppbeslag. Vitlackad på fönster med vitmålad utsida, vid övriga kulörer anodiserad.
- Avståndet mellan aluminiumprofilen och bågbottenstycket min. 6mm.
- Övriga glaslister av skummad PVC på fönster med vitmålad utsida, övriga kulörer träglaslist i samma utvändiga kulör som fönstret.
- U-värde 1,5

Modul BREDD	1-luft	2-luft	3-luft
Min	4M	8M	13M
Max	11M	20M	30M

Modul HÖJD	1-luft	2-luft
Min	4M*	10M
Max	18M**	27M

*) 4M på överkantshängda
**) t.o.m. bredd 10M. Bredd 11M = maxhöjd 16M

Sidohängt

Utåtgående 2-glas isolerruta

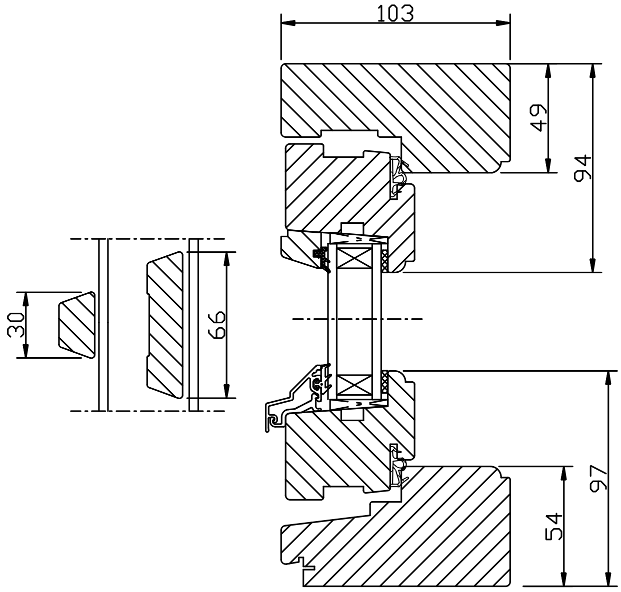

Vertikalsnitt

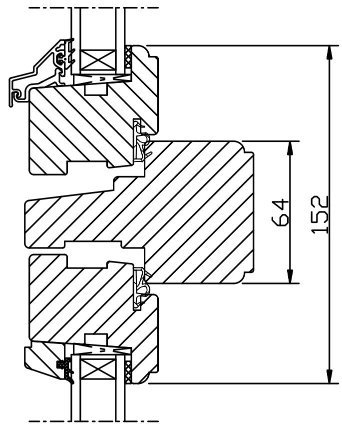

Vertikalsnitt karm tvärpost

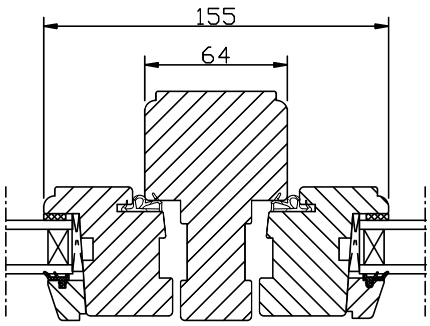

Horisontalsnitt karm mittpost

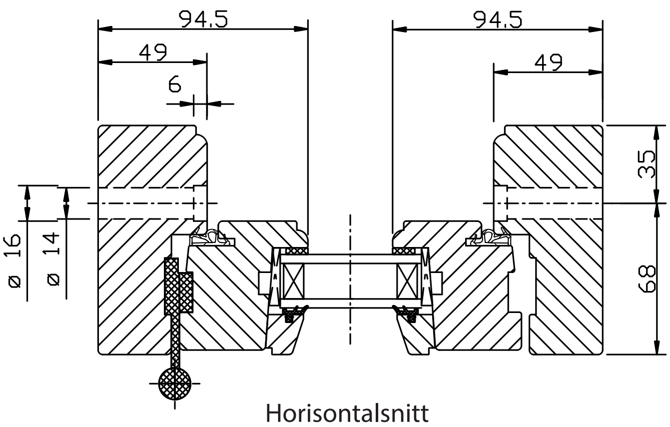

Horisontalsnitt

.2 Appendix 2 - Radiator

8500077 ELRAD KABA 0507 500W/230V

Artnr.:	8500077	RSK-nr.:	0000000
Typbeskrivning:	KABA P 0507 010 230 05 1	Frp. strl::	1
Leverantör:	LVI	ALEM09:	N

Artikelegenskape

Längd	700mm	Höjd	500mm
Vikt	11kg		

Kort beskrivning:

ELRAD KABA 0507 500W/230V

Mediumbeskrivning:

Kaba P oljefylld elradiator med elektronisk termostat för väggmontage alt fristående placering. 500W, 230V, 500 mm hög stickpropp

Lång beskrivning:

Kaba är en perfekt extra värmekälla för de utrymmen i hemmet som inte används så ofta eller till exempel i garaget eller arbetsrummet. Platser där du kanske inte tillbringar så mycket tid regelbundet behöver också värme för en så behaglig vistelse som möjligt. Kaba P levereras med stickproppsanslutning och golvkonsoler så att den också kan användas som en flyttbar enhet. Ett enkelt temperaturvred gör den till ett okomplicerat val för de utrymmen i hemmet som bara behöver en liten extra uppvärmning då och då.

Punkttext:

Egenskaper

Oljefylld radiator med vegetabilisk olja.
Frostskydd
Tillverkad av hållfast stål av högsta kvalitet.
Beständig vit epoxylackering (vit RAL 9016).
Enkel att använda, snabb uppvärmning och jämn temperatur på hela ytan.
System för låsning av fästanordning.
Luktfri, tystgående och ej allergiframkallande.
För väggmontage (400 V) alternativt fristående placering med stickproppsanslutning (230 V).
Produkten saknar konvektionsplåt
Monteras med termostaten till höger.
Elektronisk termostat med kalibreringsmöjlighet.
Låsbar termostatenhet.
Termostathus av slagtålig polykarbonat.
Levereras med väggkonsoler och skruv för fast montage.
Ingen kopplingsdosa ingår, tillval e-nr. 85 000 33.
Kaba P levereras med golvkonsoler för fristående placering.

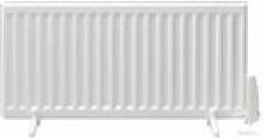

3. DRIFT

- Sätt på radiatorn genom att trycka på knappen till läge I (bild 4 A). Önskad rumstemperatur ställs in med termostatvredet (bild 4 B). Radiatorn ska inte slås "på" förrän den är korrekt installerad och säkert fastsatt i väggfästena (bild 5A). Den gröna ledlampan (bild 4 C) lyser när radiatorn drar effekt. Om den inställda temperaturen inte motsvarar den uppnådda temperaturen kan termostaten justeras genom att dra termostatvredet (bild 4 B) rakt ut och trycka tillbaka det så att pilen pekar på den uppmätta rumstemperaturen.
- Om den röda ledlampan lyser eller blinkar (bild 4 D) har elektroniken upptäckt ett fel. Kontakta din leverantör.
- Radiatorn levereras med en låsbar panel. Den kan låsas genom att flytta spärren enligt bild 5B.

4. UNDERHÅLL, REPARATION OCH KASSERING

- **VARNING**: Koppla ur strömmen innan du utför underhåll av något slag.
- Produkten kan rengöras med en mjuk fuktig trasa. Använd INTE kemiska eller nötande rengöringsmedel eftersom de skadar ytbeläggningen.
- Elradiatorn är försedd med ett överhettningsskydd som inte kan återställas (smältsäkring). Detta överhettningsskydd kopplar bort strömmen om elradiatorn blir för het (t.ex. om det täcks över) eller, om den är fristående, välts och blir liggande.
- Om anslutningskabeln är skadad måste den för att undvika risker bytas ut av tillverkaren, dennes servicerepresentant eller annan kvalificerad person.
- För att radiatorn ska fungera korrekt måste den innehålla rätt mängd vegetabilisk olja. Eventuella reparationer som kräver att radiatorn öppnas får därför bara utföras av tillverkaren eller godkänd servicetekniker.
- Om det uppstår en läcka, kontakta tillverkaren eller servicetekniker.
- När radiatorn kasseras ska oljan avfallshanteras enligt lokala bestämmelser.

5. GARANTI

Produkten har 10 års garanti utom för elektriska och elektroniska komponenter, som har 2 års garanti.

6. TEKNISKA SPECIFIKATIONER

MÄTNOGGRANNHET	0.1°C
OMGIVNINGSFÖRHÅLLANDEN: **- Drifttemperatur** **- Transport- och förvaringstemperatur**	 -30°C till +50°C -30°C till +70°C
INSTÄLLNINGSINTERVALL FÖR TEMP: **- Komfort** **- Frysskydd**	 +5°C till +30°C +7°C
ISOLATIONSKLASS	Klass I
KAPSLINGSKLASS	IP 44
STRÖMFÖRSÖRJNING	230 VAC eller 400 VAC - 50 Hz enligt produktens typskylt
DIREKTIV OCH NORMER: **Produkten har konstruerats för att uppfylla följande direktiv och normer.**	• EN 60730-1 • EN 60335-1 • EN 60335-2-30 • EN 62233 • EN 55014-1 • EN 55014-2 • EN 61000-3-2 • EN 61000-3-3 • EN 60529 • Lågspänningsdirektivet 2006/95/EC • EMC-direktivet 2004/108/EC • RoHS-direktivet 2002/95/EC

.3 Appendix 3 - Power tag/gateway

Produktdatablad
Egenskaper

A9MEM1520
Strömtrafo Power Tag sensor 1P

E-nummer : 4262737
EAN-kod : 3606480909122
Lagerkod : Lagerförd

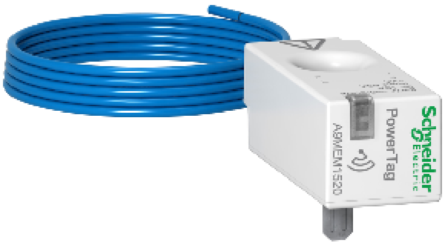

Produktdata

Produktfamilj	PowerTag
Produktnamn	PowerTag A9 M63
Typ av produkt eller komponent	Energisensor
Antal poler	1P
Tillåten ström	63 A
[In] märkström	10 A
Mätström	40 mA
Mättad ström	130 A
Specifik produktanvändning	Kostnadsfördelning Larm överbelastning Lastövervakning Strömövervakning
Produktkompatibilitet	Acti 9 Smartlink SI B Acti 9 Smartlink SI D
Marknadssegment	Brytarens spänningsövervakning Kostnadsfördelning Larm överbelastning
Kompatibilitetsintervall	Multi 9 C60 Multi 9 ID Acti 9 iK60 Acti 9 iKQ Acti 9 iID Acti 9 iID K Acti 9 K60 Acti 9 iKQE RCBO Acti 9 Reflex iC60 Multi 9 C32N Acti 9 iC65 Multi 9 C65 Acti 9 DT60 Acti9 iC enkelanslutning
Protkoll kommunikationsport	Modbus TCP/IP via Smartlink SI D Modbus TCP/IP via Smartlink SI B

Noggrannhetsklass	Klass 1 ström IEC 61557-12 Klass 0,5 spänning IEC 61557-12 Klass 1 Aktiv effekt IEC 61557-12 Klass 1 aktiv energi IEC 61557-12 Klass 1 effektfaktor IEC 61557-12
Placering (vid montage)	Ovansida eller undersida
Montagefästen	På brytare
Montering	Skruvade i anslutningar
Produktdestination	Ställverk
Typ av mätning	Aktiv energi Effektfaktor Ström Aktiv effekt Spänning
Typ av larm	Spänningsförlust (med uppmätt ström vid spänningsförlust)
Överföringsbärarmedium	Radiofrekvens 2.4...2.4835 GHz i överensstämmelse med IEEE 802.15.4

Teknisk data

Elektrisk anslutning	Kontaktdon tand och kabel
Anslutningar - plintar	Solid kabel, 1x 1.5...16 mm² Fåtrådig kabel, 2x 1.5...2.5 mm² Solid kabel, 2x 1.5...2.5 mm² Fåtrådig kabel, 1x 1.5...16 mm²
Kabellängd	1 m
Kabelkomposition	1 x 0.33 mm²
[Us] driftspänning	230 V AC +/- 20 %
Nätverksfrekvens	50/60 Hz
Energiförbrikning i VA	2 VA
Mätningskategori	Category III enligt IEC 61010-2-30
Höjd	16.5 mm
Bredd	17.7 mm
Djup	42.7 mm
Produktens vikt	16.4 g
Färg	Vit RAL 9003

Miljö

Arbetshöjd över havet	0...2000 m
Omgivningstemeperatur vid drift	-25...60 °C
Omgivande lufttemperatur för lagring	-40...85 °C
Överspänningskategori	III enligt IEC 61010-1
IP-kapslingsklass	IP20 enligt IEC 60529
IK-skyddsgrad	IK05
Föroreningsgrad	3
Relativ fuktighet	0...95 % (i drift) vid 45 °C enligt IEC 60721-3-3
Vibrationsbeständighet	3M4 enligt IEC 60721-3-3
Miljökarakteristik	Dammsäker: klass 3S3 enligt IEC 60721-3-3 Saltdimma: class 3C2 enligt IEC 60721-3-3

Hållbarhetsinformation

Erbjudandets hållbarhetsstatus	Green Premium produkt
RoHS (datumkod: ÅÅVV)	Kompatibel - sedan 1605 - Schneider Electric declaration of conformity Schneider Electric declaration of conformity
REACh	Produkten innehåller inte SVHC över tröskelvärdet Produkten innehåller inte SVHC över tröskelvärdet
Miljöprofil	Tillgänglig

Information om uttjänta produkter	Tillgänglig

Produktdatablad
Egenskaper

EER31800
Wiser Energy Gateway för trådlös kommunikation med 20 st Power Tag.

E-nummer : 4262741
EAN-kod : 3606481216182
Lagerkod : Lagerförd

Produktdata

Produktfamilj	Wiser
Produktområde	Wiser Link
Typ av produkt eller komponent	IP kommunikationsmodul
Produktnamn	MIP
Färg	Vit (RAL 9003)

Teknisk data

[Us] driftspänning	110/230 V AC (+/- 15 %) 2 A
Nätverksfrekvens	50/60 Hz
Energiförbrikning i VA	5 VA
Montagesätt	Clip-on
Montagefästen	DIN-skena
Sändningshastighet	9600 bit/s 0...24 V 2-tråds icke polariserad kabel 50 m Wiser EM5 energimätare
Webbtjänster konfiguration	Bluetooth
Kommunikations protokoll	Zigbee
Komunikationsinterface	Ethernet 10/100BASE-T 6 STP 100 m
Integrerad anslutningstyp	DHCP client (Ethernet port)
Lokal indikering	Produktstatus : grön, orange och röd LED Ethernet status (LAN ST) : grön och orange LED
Överspänningskategori	III
Elektrisk anslutning	Screw terminal block for main supply Screw terminal block for communication
Material	PC (polykarbonat)
Höjd	84 mm
Bredd	54 mm
Djup	67 mm

Produktens vikt	133 g
Kompatibilitetsintervall	Wiser energy meter EM5 Acti 9 energisensor (PowerTag)

Miljö

IP-kapslingsklass	Infälld : IP40 består av IEC 60529 Kapslad : IP20 består av IEC 60529
Föroreningsgrad	2
IK-skyddsgrad	IK05 överensstämmer med IEC 62262
Relativ fuktighet	93 % (at 40 °C)
Arbetshöjd över havet	0...2000 m
Omgivningstemeperatur vid drift	-25...50 °C
Standarder	IEC 61000-6-1 : 2005 IEC 61000-6-3 : 2005
Elektromagnetisk kompabilitet	Elektromagnetisk immunitet överensstämmer med IEC 61000-6-1 Elektromagnetisk emission överensstämmer med IEC 61000-6-3
Brandtålighet	30 s at 650 °C

Hållbarhetsinformation

Erbjudandets hållbarhetsstatus	Green Premium produkt
RoHS (datumkod: ÅÅVV)	Kompatibel - sedan 1735 - Schneider Electric declaration of conformity Schneider Electric declaration of conformity
REACh	Produkten innehåller inte SVHC över tröskelvärdet Produkten innehåller inte SVHC över tröskelvärdet
Miljöprofil	Tillgänglig
Information om uttjänta produkter	Tillgänglig

.4 Appendix 4 - Solarimeter

KIMO INSTRUMENTS

Technical Data Sheet

Pressure / Temperature / Humidity / Air Velocity / Airflow / Sound level

Solarimeter
SL 200

TECHNICAL FEATURES

• SL 200 Instrument

Solar irrigation measuring range	from 1 W/m² to 1300 W/m²
Energetic exposure measuring range	from 1 Wh/m² to 500 kWh/m²
Frequency of the measure	2 / s
Accuracy	5% of measurement
Calculation frequency (W/m²)	1 / min (average on 60 seconds)
Storage capacity	31 days, 44640 saved recording points
Fast datas download	1000 values/second
Detection	out of range and sensor default
Operating temperature	from -10°C to +50°C
Storage temperature	from -10°C to +55°C
Package dimensions	58 x 120 x 33 mm
Autonomy	more than 72 hours in continuous mode Unlimited with power supply adapter
Power supply	3 LR3-AAA batteries
Electronic	Digital
Electronic card	Varnish
Conformity	in accordance with RoHS directive

• Solar cell

Spectral response	from 400 to 1100 nm
Nominal sensitivity	100mv for 1000W/m² *
Response in cosine	corrected until 80°
Coefficient in temperature	+0,1% /°C
Effective area	1 cm²
Operating temperature	from -30°C to +60°C
Humidity dependence	100% RH
UV performance	excellent (PMMA filter)
Mode	photovoltaic
Material	polycristallin silicon
Front face	translucent PMMA
Tightness	Polyurethane resin and housing in PMMA and polyacetol
Cell weight	60g
Cell dimensions	30 x 32 mm
Cable length	1,25 m (can be unplugged)

* SL200 is supplied with a calibration certificate in reference to the WRR (World Radiometric Reference).
** Timed : duration of dataset is expressed in DD/HH/MM/SS

The portable autonomous solarimeter measures the solar irrigation for the control of photovoltaic and thermal installations on test or on site:

- **Measurement and spot check of the solar irrigation in W/m²**
  (instantaneous, average, time-recording, min/max values, hold function)
- **Calculation of the energetic exposure in Wh/m²**
  during the timed measures campaign*
- **Storage and saving of average values**
  of power and updating the energetic exposure calculation every minutes
- **Recorded datas can be read on the display, and the graphic function allows a fast interpretation of the measure file**

SL 200

- Easy to use, for immediate informations
- Evaluation of the produced electric powers, optimum orientation of solar panels and performances follow-up.
- Analysis of sunshine on site, on short and long-term period.
- Choice and determination of the thermal or photovoltaic generators features
- Storage and saving of average values of power; update of energetic exposure calculation every minute
- Easy use of datas stored in memory,
- Reading and graphical approximation of datas by 24 hours via transfer data software.

For the QualiSOL, QualiPV certificated professionals, the office control for the Guarantee of Solar Result

1 2 3 **Functions** keys
4 **Delete and Back screen** key
5 **Screen** key
6 **On/Off** key

1. Measurement

Instantaneous W/m²
Maximum value
Minimum value
Pause - Hold

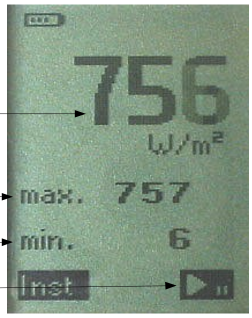

Instantaneous W/m²
Average W/m²
Energetic exposure
Time
Duration

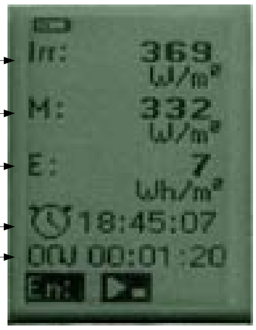

2. Reading

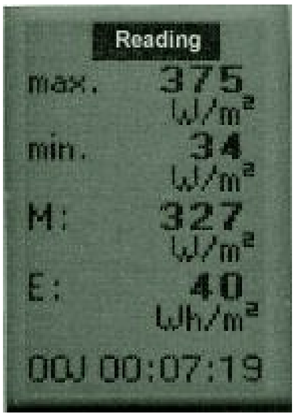

Global values

Time-recorded stored values

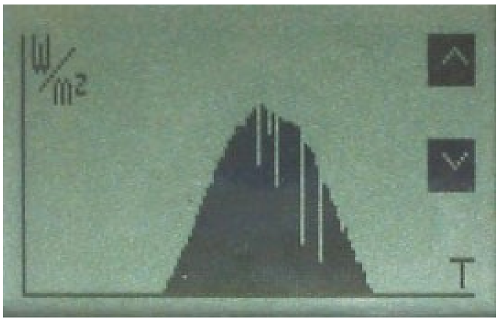

Graphic display 00H /24H

Scrolling of the successive graphs 00H-24H

3. Transfer

SUPPLIED WITH...

- Transport case with protective foam
- Mini-USB connection cable
- 3 LR3-AAA batteries
- CD-ROM with the Instructions for use, setup software for USB driver, datas transfer software.
- Calibration certificate

OPTIONAL

- Tripod
- Fixing kit for solar panels
- Extensions : (possibility to connect 2 extensions max)
- Power supply adapter

www.kimo.fr

Distributed by :

EXPORT DEPARTMENT
Tel : + 33. 1. 60. 06. 69. 25 - Fax : + 33. 1. 60. 06. 69. 29
e-mail : export@kimo.fr

KIMO®
INSTRUMENTS

CERTIFICAT D'ETALONNAGE

CALIBRATION CERTIFICATE

N°QER1800008

Délivré à : **KIMO INSTRUMENT SVERIGE AB**
Issued for : Stigbergsliden 5

41463 GOTEBORG - SWEDEN

INSTRUMENT ETALONNE
CALIBRATED INSTRUMENT

Désignation : *Designation :*	**Solarimètre SL200** **Solarimeter SL200**
Constructeur : *Manufacturer :*	**Kimo**
Type : *Type :*	**SL200**
N° de série : *Serial number :*	**18020489**
N° Inventaire : *Inventory number :*	

Ce certificat comprend 2 page(s)
The certificate includes

Date : **28 Février 2018**

La reproduction de ce certificat n'est autorisée que sous la forme de Fac Similé Photographique Integral.
This certificate may not be reproduced other than in full by photographic process.

Responsable Métrologie
Metrology Manager

Sébastien COUPEAU

P.O. Damien TRITTER
Service Laboratoire

Ce document est en tout point conforme à la norme FD X 07-012

This document is complying standard FD X 07-012

Kimo Instruments
ZA Bernard Moulinet - Bâtiments C et N - Rue Koufra
24700 Montpon-Ménestérol
Tél : 05 53 80 85 00 - Fax : 05 53 80 16 81
kimo@kimo.fr - www.kimo.fr

Bretagne 02 99 54 77 00
Centre 02 38 23 00 40
Est 03 88 48 16 90
Midi-Pyrénées 05 61 72 84 00

Nord 03 20 90 92 95
PACA 04 42 97 33 94
Paris Est 01 60 06 14 72
Paris Ouest 01 30 02 81 20

Rhône-Alpes 04 72 15 88 72
Sud-Ouest 05 53 81 44 44

SA au capital de 1 027 657 € - RCS Périgueux 349 282 095 - Siret 349 282 095 000 18 - APE 2651 B - TVA FR 14 349 282 095

KIMO - Société du Groupe Sauermann

Certificat d'étalonnage N°QER1800008

ETALONNAGE EN RADIOMETRIE

RADIOMETRY CALIBRATION

1- Caractéristiques de l'appareil :
Instrument features :

Désignation : Solarimètre SL200
Description : Solarimeter SL200
Avec cellule solaire

N° série sonde / *Probe S.N.* :9290 N° inventaire sonde / *Probe I.N.* :

Echelle : 0 à 1300 W/m2
Range :

Résolution : 1 W/m2
Resolution :

2- Méthode d'étalonnage :
Calibrating principles :

Les points d'étalonnage sont réalisés par comparaison avec les moyens suivants:
- MR001 Banc de radiométrie,
- ETR002 étalon n°:10080019 + 7552, certificat d'étalonnage n°EER1200000, contrôlé(s) avec la référence ETR001 type 7001, raccordement aux étalons nationaux et internationaux et à la Référence Radiométrique mondiale CRA1206017.

The points of calibration are realized with means of calibration according to:
- MR001 Bench of radiometry,
- ETR002 a standard sn°:10080019 + 7552, calibration certificate n°EER1200000, controlled with standard ETR001 type 7001, traceable by national and international standards and World Radiometric Reference CRA1206017.

3- Conditions d'environnement :
Environmental conditions :

Température ambiante : 21.6 °C
Ambient temperature:

Humidité relative : 11.5 %HR
Relative humidity :

Pression atmosphérique 1008 hPa
Atmospheric pressure :

4- Conditions d'étalonnage :
Calibrating conditions :

Tolérance appliquée à l'étalonnage : 5%mes+/-0 W/m2 de 0 à 1300 W/m2
Calibrating accuracy :

Remarque : Le coefficient d'étalonnage de la cellule solaire est de 98,56 µV/W/m².

5- Résultats des mesures :
Measurement results :

n°	Vref	Unit	Vref conv	Unit	Vi	Unit	Vi-Vref con	Unit	Incertitude
1	948	W/m2	948,000	W/m2	948	W/m2	0,000	W/m2	95

Vref: valeur lue sur l'appareil étalon, Vref conv: Vref convertie dans l'unité de l'appareil du client.
Vi: valeur lue sur l'appareil du client.
L'unité de l'incertitude de mesure est exprimée dans la même unité que Vref. Les incertitudes mentionnées prennent en compte les incertitudes de l'étalonnage (étalon de référence, moyen, condition d'environnement, résolution de l'appareil ...). Ces incertitudes sont élargies avec un coefficient k=2.
Vref: value displayed by our reference instrument, Vref conv : conversion of Vref in customer's unit instrument.
Vi: value displayed by customer's instrument.
For uncertainty, unit is the same as the one of Vref. Uncertainties above mentionned take into account calibration uncertainties (reference instrument, calibration mean, environment conditions, instrument resolution...). These uncertainties are extended with coefficient k=2.

Etalonnage effectué par Vergnaud Stéphane **le** 26/02/18
Calibration performed by

.5 Appendix 5 - Blower door tests

BUILDING LEAKAGE TEST

TEST HUT 1

Date of Test: 2018-03-01 Test File: Untitled

Technician: Ali Karim

Project Number:

Customer: Climate Curtains

Building Address:

Phone:

Fax:

Test Results at 50 Pascals:

q_{50} :	l/s (Airflow)	16 (+/- 1.3 %)
n_{50} :	1/h (Air Change Rate)	4.55
q_{F50} :	lps/m² (Floor Area)	2.40
q_{E50} :	lps/m² (Envelope Area)	0.48

Leakage Areas:

ELA $_{50}$:	m²	0.0017 (+/- 1.3 %)
ELA $_{F50}$:	m²/m²	0.0002637
ELA $_{E50}$:	m²/m²	0.0000529

Building Leakage Curve:

Air Flow Coefficient (C_{env}) = 1.1 l/s/Pa^n (+/- 8.8 %)

Air Leakage Coefficient (C_L) = 1.1 l/s/Pa^n (+/- 8.8 %)

Exponent (n) = 0.674 (+/- 0.024)

Coefficient of Determination (r^2) = 0.99839

Test Standard: ISO 9972

Test Mode: Pressurization

Type of Test Method:

Purpose of Test:

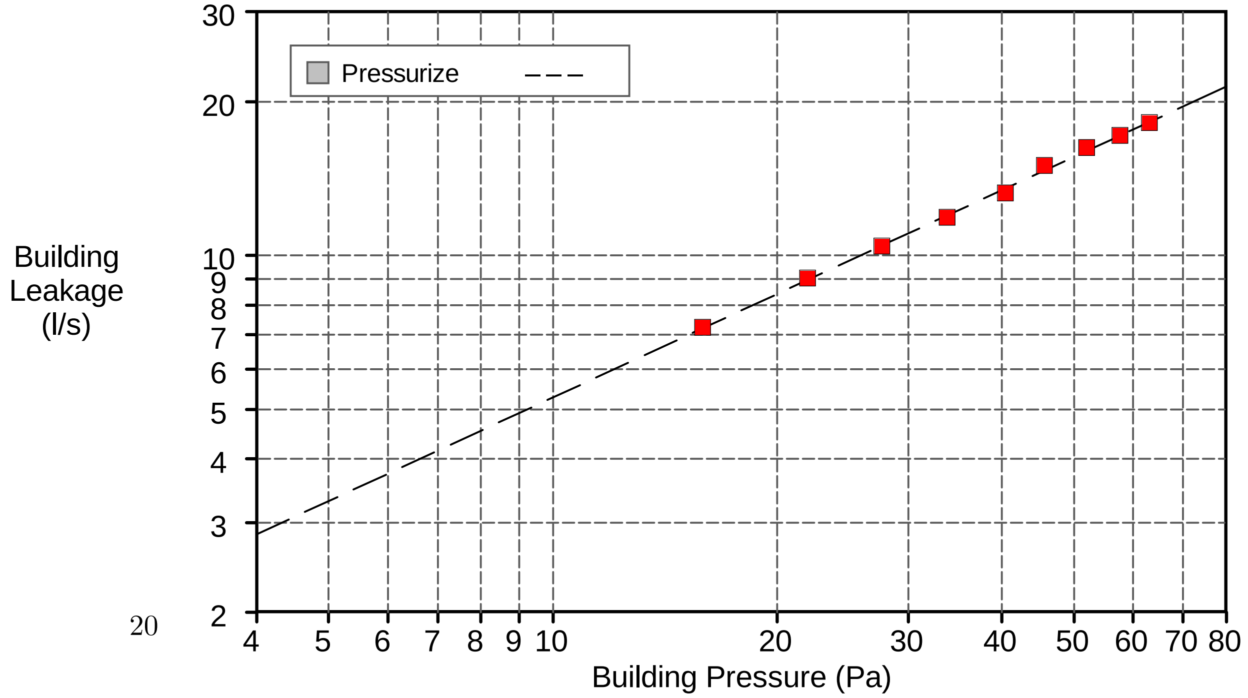

Date of Test: 2018-03-01 Test File: Untitled

Building Information

Internal Volume, V (m³) (according to ISO)	12.35
Net Floor Area, A_F (m²) (according to ISO)	6.5
Envelope Area, A_E (m²) (according to ISO)	32.38
Height (m)	1.9
Uncertainty of Dimensions (%)	1
Year of Construction	
Type of Heating	
Type of Air Conditioning	
Type of Ventilation	None
Building Wind Exposure	Partly Exposed Building
Wind Class	Moderate Breeze

Equipment Information

Type	Manufacturer	Model	Serial Number	Custom Calibration Date
Fan	Energy Conservatory	Model 3 (110V)		-
Micromanometer	Energy Conservatory	DG700	33973	2012-02-02

Date of Test: 2018-03-01 Test File: Untitled

Pressurization Test:

Environmental Data

Indoor Temperature (°C)	Outdoor Temperature (°C)	Barometric Pressure (Pa)
-4.0	-4.0	101325.0

Baseline Pressure Data

Pre-Test			Post-Test		
$\Delta p_{0,1}$-	$\Delta p_{0,1}$+	$\Delta p_{0,1}$	$\Delta p_{0,2}$-	$\Delta p_{0,2}$+	$\Delta p_{0,2}$
-0.1	0.0	-0.1	-0.1	0.3	-0.0

Data Points - Automated Test (TTE 5.0.7.3)

Nominal Building Pressure (Pa)	Baseline adjusted Building Pressure (Pa)	Fan Pressure (Pa)	Nominal Flow q_r (l/s)	Adjusted Flow q_{env} (l/s)	Adjusted Flow q_L (l/s)	% Error	Fan Configuration
-0.1	n/a	n/a					
63.2	63.2	30.8	18	18	18	-0.6	Ring D
57.7	57.7	27.4	17	17	17	-0.2	Ring D
51.9	52.0	24.5	16	16	16	1.3	Ring D
45.6	45.6	20.9	15	15	15	2.2	Ring D
40.4	40.5	86.3	13	13	13	-2.1	Ring E
33.8	33.8	70.0	12	12	12	-1.0	Ring E
27.6	27.7	54.7	11	10	10	-0.5	Ring E
21.9	22.0	41.7	9	9	9	0.6	Ring E
15.9	15.9	27.3	7	7	7	0.2	Ring E
-0.0	n/a	n/a					

Deviations from Standard ISO 9972 - Test Parameters

- The minimum pressure is not within +/- 3Pa of the greater of 10 Pa or (5 * zero-flow pressure Δp01).

Date of Test: 2018-03-01 Test File: Untitled

Comments

None

BUILDING LEAKAGE TEST

TEST HUT 2

Date of Test: 2018-03-01 Test File: Untitled

Technician: Ali Karim

Project Number:

Customer: Climate Curtains

Building Address:

Phone:

Fax:

Test Results at 50 Pascals:

q_{50} :	l/s (Airflow)	19 (+/- 1.5 %)
n_{50} :	1/h (Air Change Rate)	5.58
q_{F50} :	lps/m² (Floor Area)	2.94
q_{E50} :	lps/m² (Envelope Area)	0.59

Leakage Areas:

ELA_{50} :	m²	0.0021 (+/- 1.5 %)
ELA_{F50} :	m²/m²	0.0003231
ELA_{E50} :	m²/m²	0.0000649

Building Leakage Curve:

Air Flow Coefficient (C_{env}) = 1.2 l/s/Pa^n (+/- 7.4 %)

Air Leakage Coefficient (C_L) = 1.2 l/s/Pa^n (+/- 7.4 %)

Exponent (n) = 0.700 (+/- 0.021)

Coefficient of Determination (r^2) = 0.99864

Test Standard: ISO 9972

Test Mode: Pressurization

Type of Test Method:

Purpose of Test:

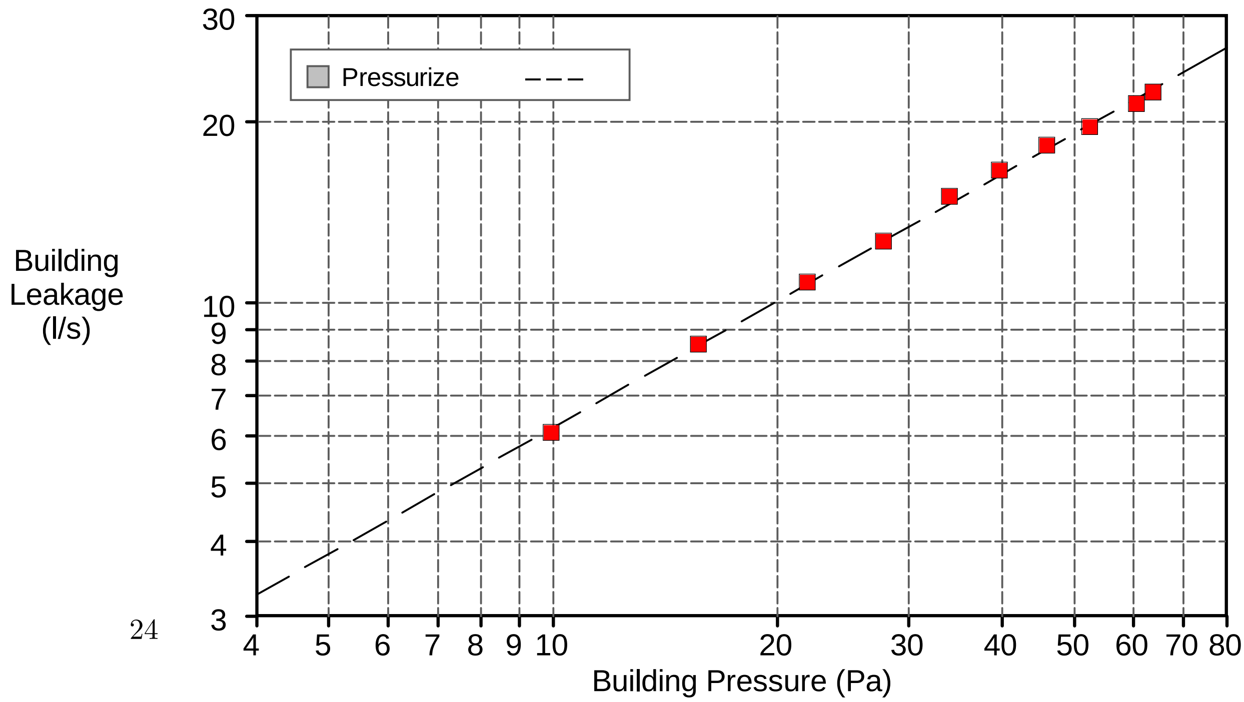

Date of Test: 2018-03-01 Test File: Untitled

Building Information

Internal Volume, V (m^3) (according to ISO)	12.35
Net Floor Area, A_F (m^2) (according to ISO)	6.5
Envelope Area, A_E (m^2) (according to ISO)	32.38
Height (m)	1.9
Uncertainty of Dimensions (%)	1
Year of Construction	
Type of Heating	
Type of Air Conditioning	
Type of Ventilation	None
Building Wind Exposure	Partly Exposed Building
Wind Class	Moderate Breeze

Equipment Information

Type	Manufacturer	Model	Serial Number	Custom Calibration Date
Fan	Energy Conservatory	Model 3 (110V)		-
Micromanometer	Energy Conservatory	DG700	33973	2012-02-02

Date of Test: 2018-03-01 Test File: Untitled

Pressurization Test:

Environmental Data

Indoor Temperature (°C)	Outdoor Temperature (°C)	Barometric Pressure (Pa)
-4.0	-4.0	101325.0

Baseline Pressure Data

Pre-Test

$\Delta p_{0,1-}$	$\Delta p_{0,1+}$	$\Delta p_{0,1}$
-0.1	0.0	-0.1

Post-Test

$\Delta p_{0,2-}$	$\Delta p_{0,2+}$	$\Delta p_{0,2}$
-0.2	0.0	-0.2

Data Points - Automated Test (TTE 5.0.7.3)

Nominal Building Pressure (Pa)	Baseline adjusted Building Pressure (Pa)	Fan Pressure (Pa)	Nominal Flow q_r (l/s)	Adjusted Flow q_{env} (l/s)	Adjusted Flow q_L (l/s)	% Error	Fan Configuration
-0.1	n/a	n/a					
63.7	63.8	47.0	23	22	22	-1.4	Ring D
60.4	60.6	43.0	22	21	21	-2.1	Ring D
52.3	52.4	36.0	20	19	20	-0.9	Ring D
45.9	46.0	31.2	19	18	18	1.2	Ring D
39.5	39.7	25.6	17	16	17	1.9	Ring D
33.9	34.0	20.9	15	15	15	2.6	Ring D
27.6	27.7	79.1	13	12	13	-0.3	Ring E
21.8	21.9	58.9	11	11	11	0.6	Ring E
15.6	15.7	37.3	9	8	9	0.1	Ring E
9.8	9.9	19.7	6	6	6	-1.7	Ring E
-0.2	n/a	n/a					

Deviations from Standard ISO 9972 - Test Parameters

None

Date of Test: 2018-03-01 Test File: Untitled

Comments

None

BUILDING LEAKAGE TEST

TEST HUT 3

Date of Test: 2018-03-01 Test File: Untitled

Technician: Ali Karim

Project Number:

Customer: Climate curtains

Building Address:

Phone:

Fax:

Test Results at 50 Pascals:

q_{50} :	l/s (Airflow)	13 (+/- 1.1 %)
n_{50} :	1/h (Air Change Rate)	3.90
q_{F50} :	lps/m² (Floor Area)	2.06
q_{E50} :	lps/m² (Envelope Area)	0.41

Leakage Areas:

ELA_{50} :	m²	0.0015 (+/- 1.1 %)
ELA_{F50} :	m²/m²	0.0002259
ELA_{E50} :	m²/m²	0.0000454

Building Leakage Curve:

Air Flow Coefficient (C_{env}) = 1.0 l/s/Paⁿ (+/- 7.0 %)

Air Leakage Coefficient (C_L) = 1.0 l/s/Paⁿ (+/- 7.0 %)

Exponent (n) = 0.664 (+/- 0.019)

Coefficient of Determination (r^2) = 0.99893

Test Standard: ISO 9972

Test Mode: Pressurization

Type of Test Method:

Purpose of Test:

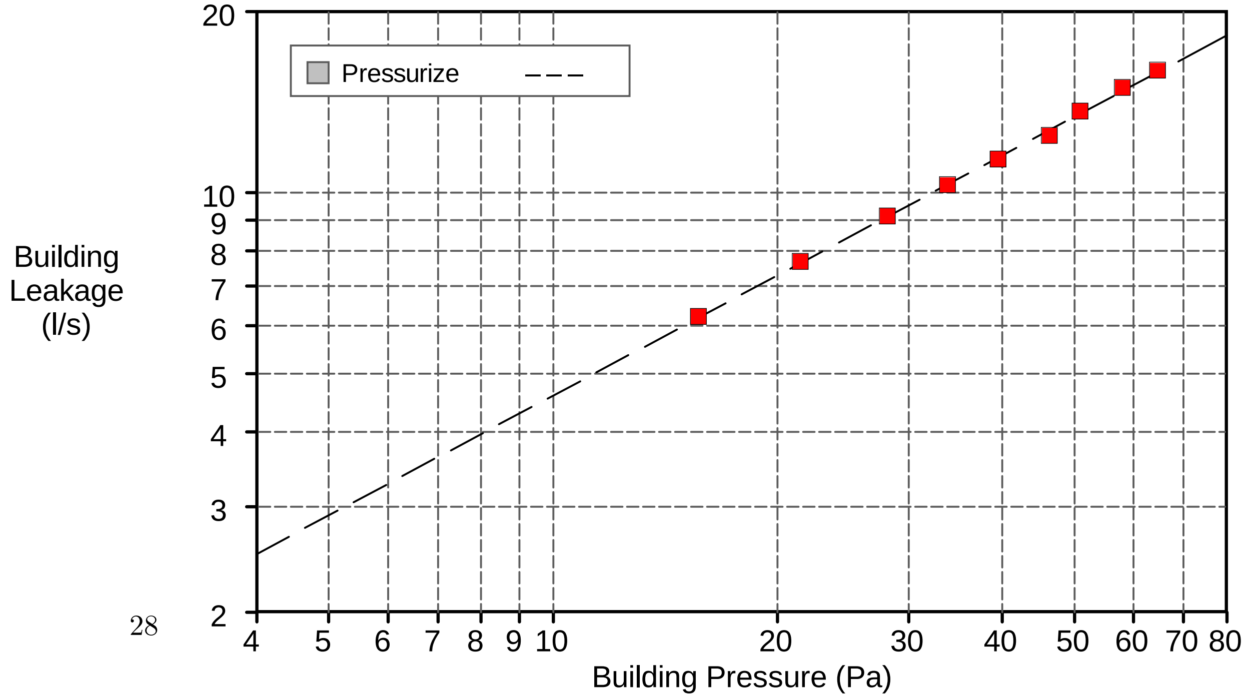

Date of Test: 2018-03-01 Test File: Untitled

Building Information

Internal Volume, V (m^3) (according to ISO)	12.35
Net Floor Area, A_F (m^2) (according to ISO)	6.5
Envelope Area, A_E (m^2) (according to ISO)	32.38
Height (m)	1.9
Uncertainty of Dimensions (%)	1
Year of Construction	
Type of Heating	
Type of Air Conditioning	
Type of Ventilation	None
Building Wind Exposure	Partly Exposed Building
Wind Class	Moderate Breeze

Equipment Information

Type	Manufacturer	Model	Serial Number	Custom Calibration Date
Fan	Energy Conservatory	Model 3 (110V)		-
Micromanometer	Energy Conservatory	DG700	33973	2012-02-02

Date of Test: 2018-03-01 Test File: Untitled

Pressurization Test:

Environmental Data

Indoor Temperature (°C)	Outdoor Temperature (°C)	Barometric Pressure (Pa)
-4.0	-4.0	101325.0

Baseline Pressure Data

Pre-Test

$\Delta p_{0,1-}$	$\Delta p_{0,1+}$	$\Delta p_{0,1}$
-0.1	0.0	-0.1

Post-Test

$\Delta p_{0,2-}$	$\Delta p_{0,2+}$	$\Delta p_{0,2}$
-0.0	0.1	0.0

Data Points - Automated Test (TTE 5.0.7.3)

Nominal Building Pressure (Pa)	Baseline adjusted Building Pressure (Pa)	Fan Pressure (Pa)	Nominal Flow q_r (l/s)	Adjusted Flow q_{env} (l/s)	Adjusted Flow q_L (l/s)	% Error	Fan Configuration
-0.1	n/a	n/a					
64.7	64.7	23.8	16	16	16	0.6	Ring D
58.0	58.1	20.8	15	15	15	1.1	Ring D
50.9	50.9	17.3	14	13	14	0.8	Ring D
46.3	46.3	76.3	13	12	12	-2.3	Ring E
39.5	39.5	64.2	12	11	11	-0.8	Ring E
33.8	33.8	53.4	10	10	10	-0.2	Ring E
28.1	28.1	42.5	9	9	9	0.1	Ring E
21.4	21.5	30.5	8	7	8	0.4	Ring E
15.6	15.7	20.5	6	6	6	0.4	Ring E
0.0	n/a	n/a					

Deviations from Standard ISO 9972 - Test Parameters

- The minimum pressure is not within +/- 3Pa of the greater of 10 Pa or (5 * zero-flow pressure Δp01).

Date of Test: 2018-03-01 Test File: Untitled

Comments

None

.6 Appendix 6 - Simulink model: Parameter study/ Air flow rate

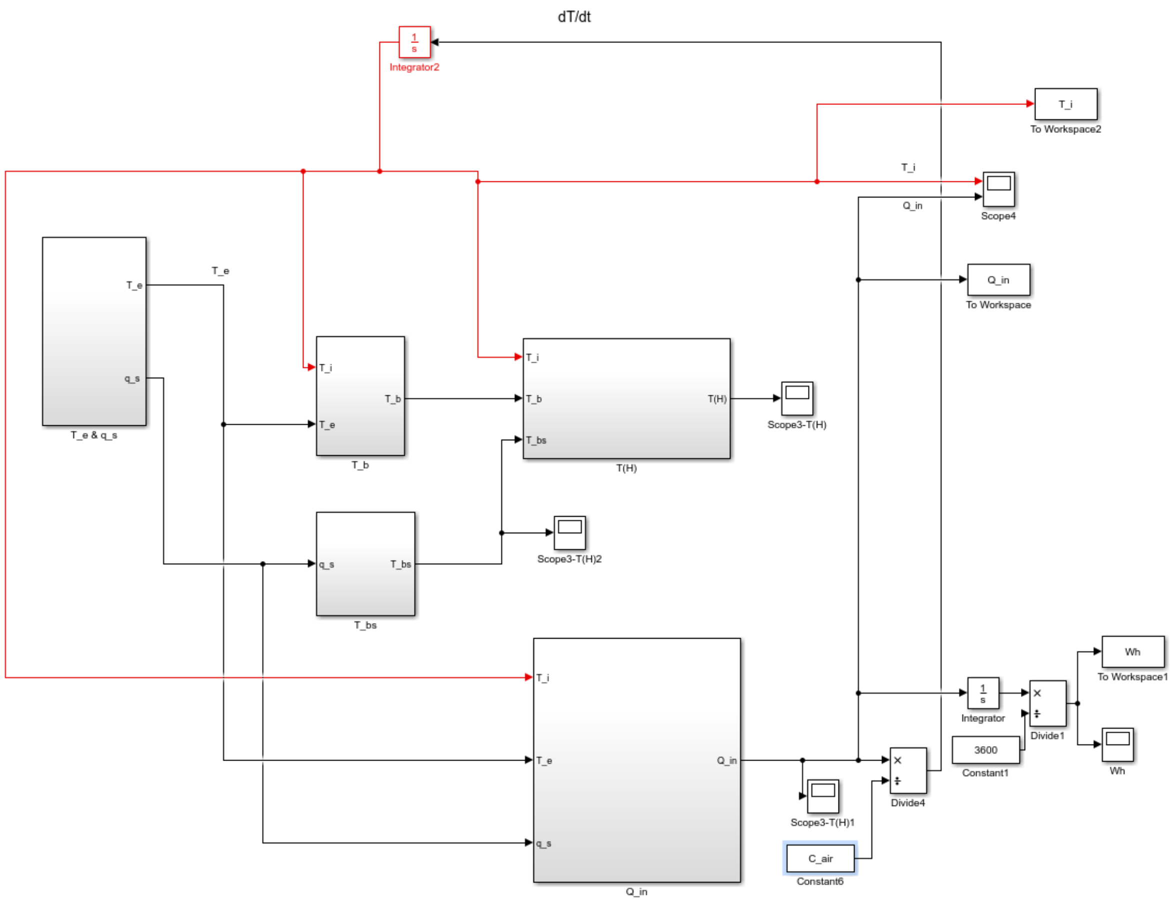
dT/dt
1/s
Integrator2
T_i
To Workspace2
T_i
Q_in
Scope4
Q_in
To Workspace
T_e
T_e
q_s
T_e & q_s
T_i
T_b
T_e
T_b
T_i
T_b
T_bs
T(H)
T(H)
Scope3-T(H)
q_s
T_bs
T_bs
Scope3-T(H)2
T_i
T_e
q_s
Q_in
Q_in
Scope3-T(H)1
C_air
Constant6
Divide4
1/s
Integrator
3600
Constant1
Divide1
Wh
To Workspace1
Wh

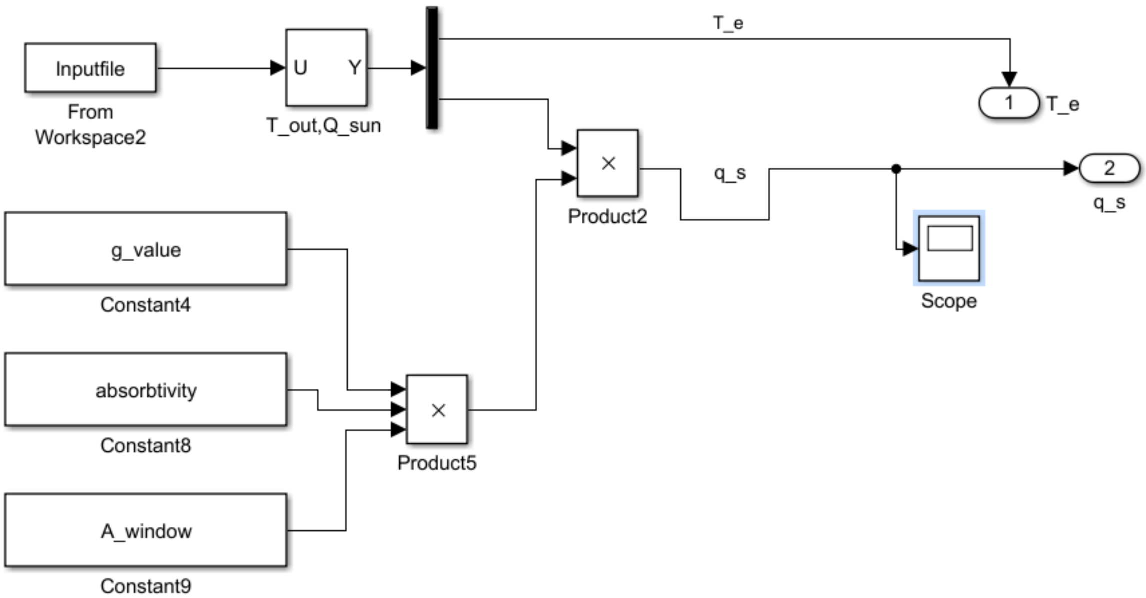
Inputfile
From Workspace2
U
Y
T_out,Q_sun
T_e
1
T_e
Product2
q_s
2
q_s
Scope
g_value
Constant4
absorbtivity
Constant8
A_window
Constant9
Product5

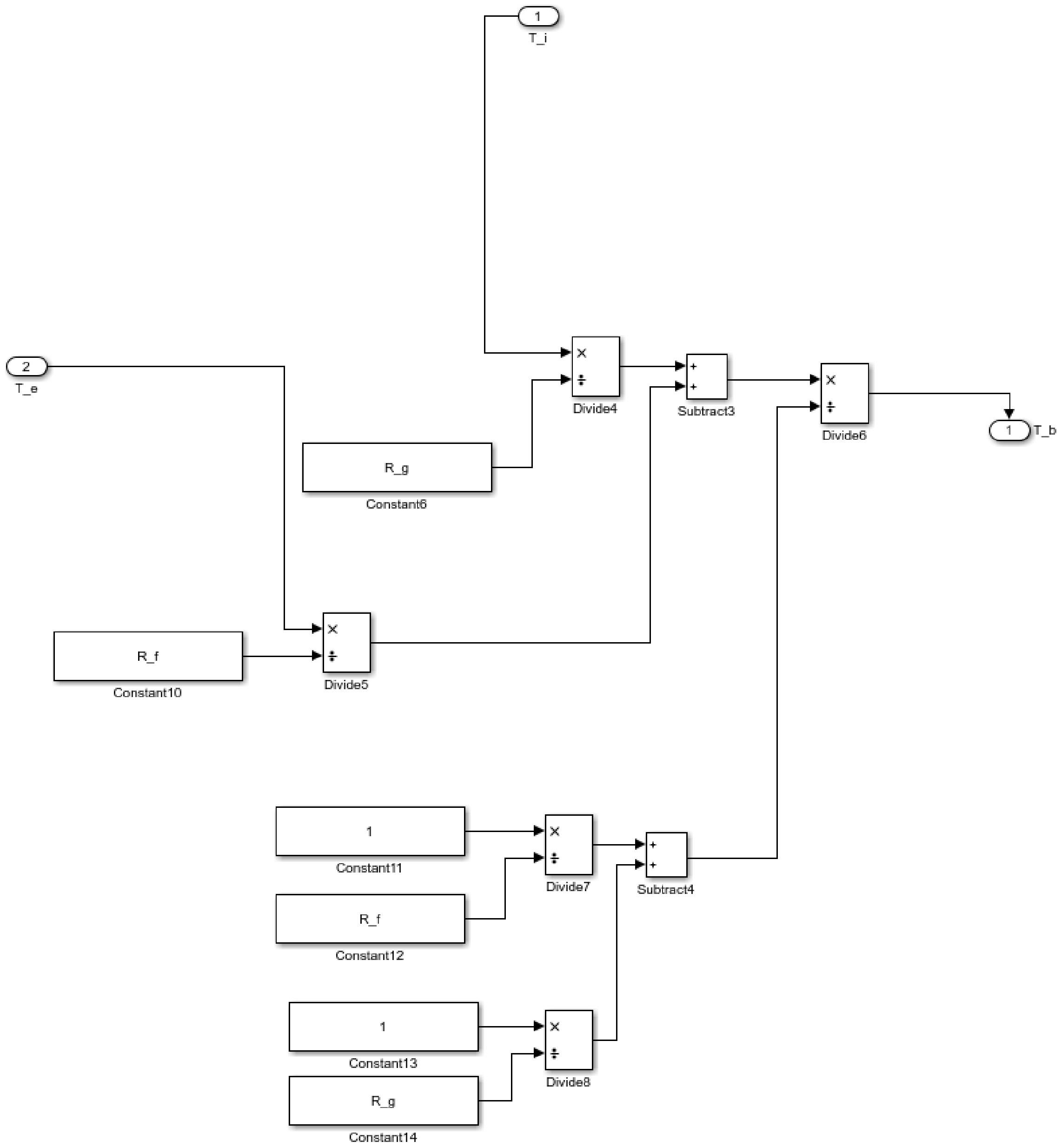
1
T_i
2
T_e
R_g
Constant6
Divide4
Subtract3
Divide6
1
T_b
R_f
Constant10
Divide5
1
Constant11
Divide7
Subtract4
R_f
Constant12
1
Constant13
Divide8
R_g
Constant14

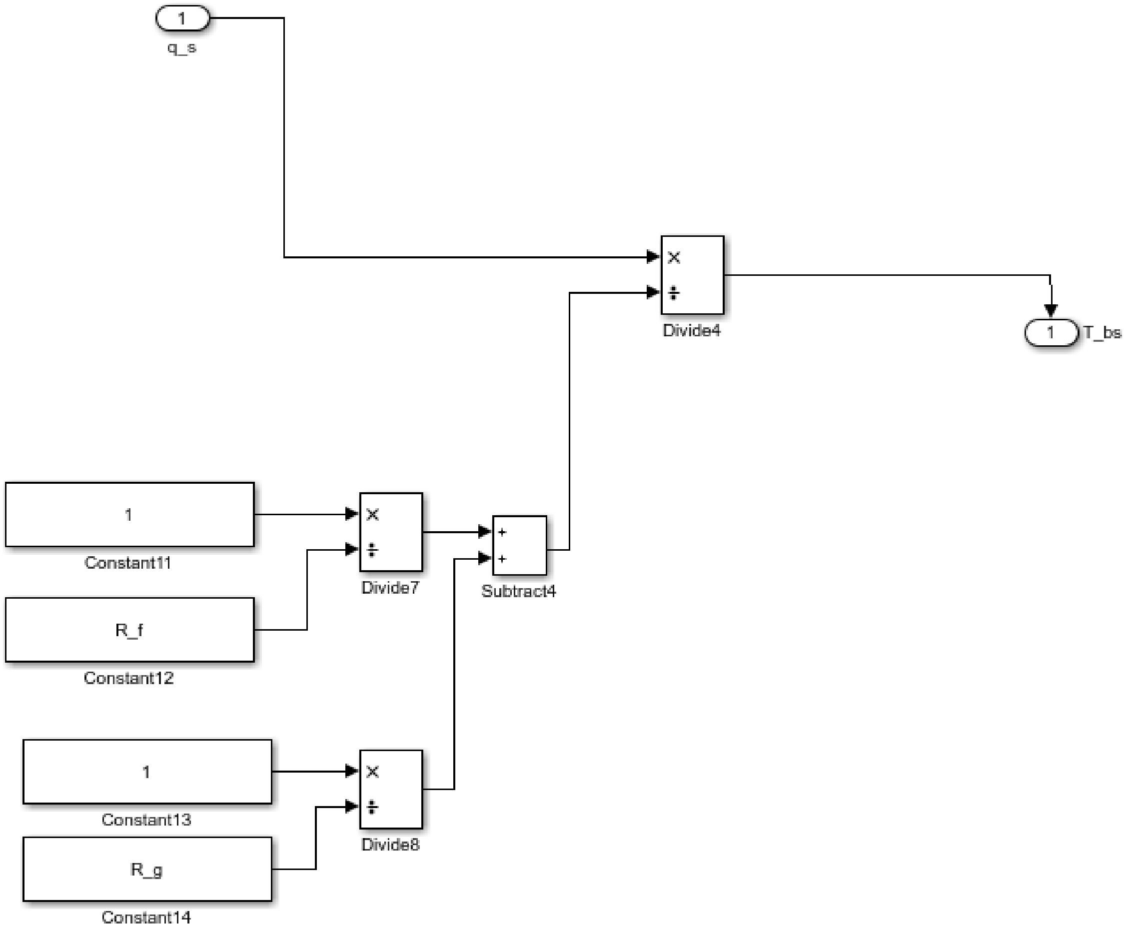
1
q_s
Divide4
1
T_bs
1
Constant11
Divide7
Subtract4
R_f
Constant12
1
Constant13
Divide8
R_g
Constant14

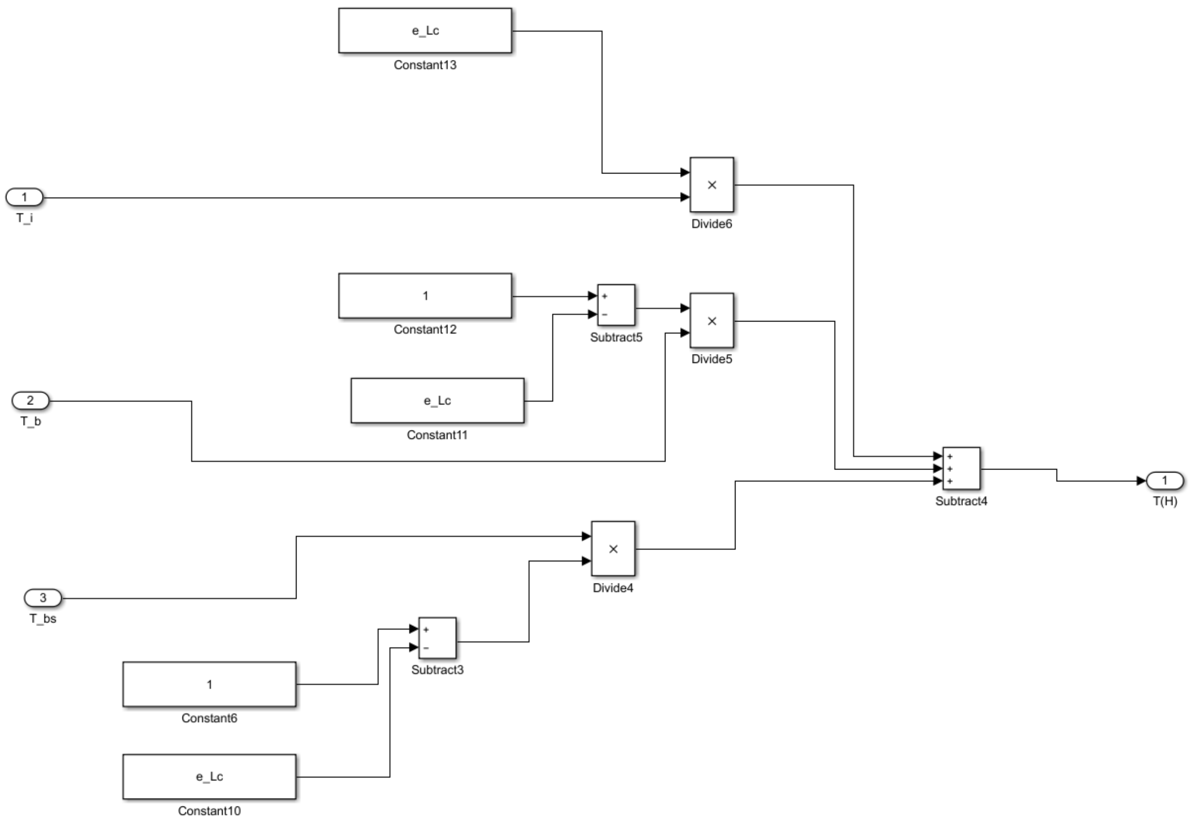
e_Lc
Constant13
1
T_i
Divide6
1
Constant12
Subtract5
Divide5
2
T_b
e_Lc
Constant11
Subtract4
1
T(H)
Divide4
3
T_bs
Subtract3
1
Constant6
e_Lc
Constant10

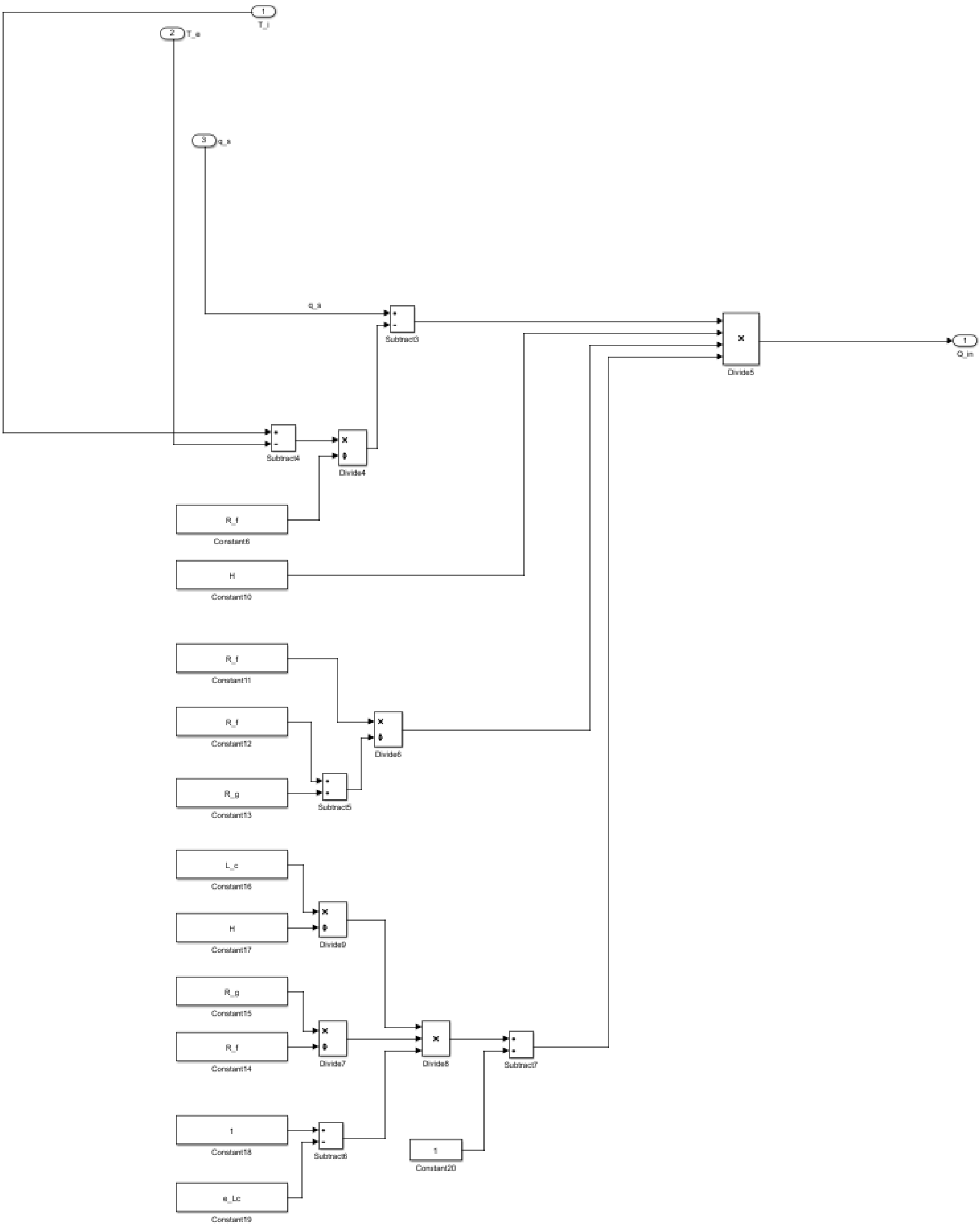
T_i
T_e
q_s
Subtract3
Divide5
Q_in
Subtract4
Divide4
R_f
H
Constant10
R_f
Constant11
R_f
Constant12
R_g
Constant13
Divide6
Subtract5
L_c
Constant16
H
Constant17
Divide9
R_g
Constant15
R_f
Constant14
Divide7
Divide8
Subtract7
1
Constant18
Subtract6
e_Lc
Constant19
1
Constant20

.7 Appendix 7 - Simulink model: Case study/ Energy consumption

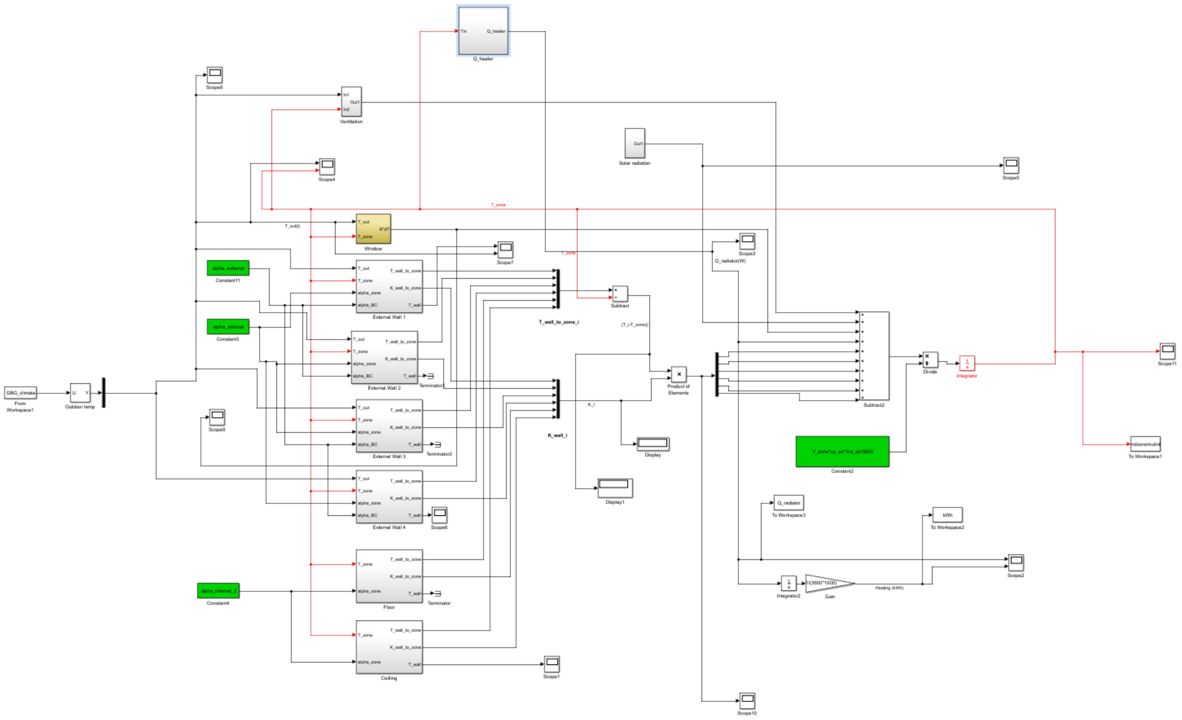

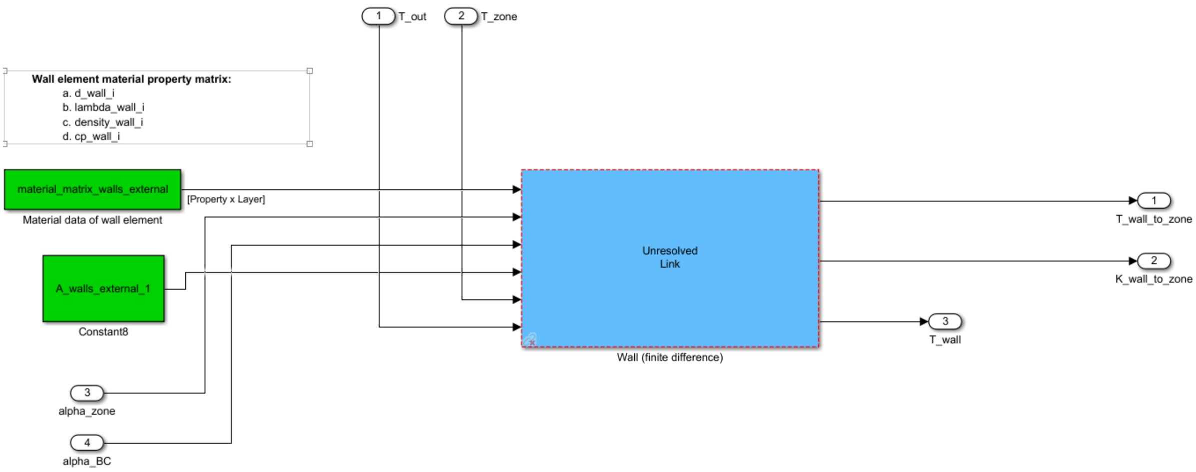
1
T_out
2
T_zone
Wall element material property matrix:
a. d_wall_i
b. lambda_wall_i
c. density_wall_i
d. cp_wall_i
material_matrix_walls_external
Material data of wall element
[Property x Layer]
A_walls_external_1
Constant8
3
alpha_zone
4
alpha_BC
Unresolved
Link
Wall (finite difference)
1
T_wall_to_zone
2
K_wall_to_zone
3
T_wall

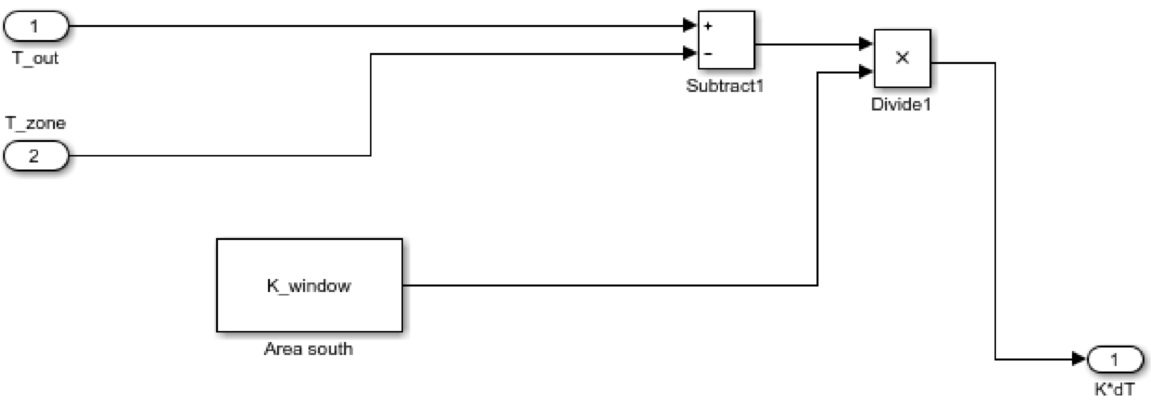
1
T_out
T_zone
2
Subtract1
Divide1
K_window
Area south
1
K*dT

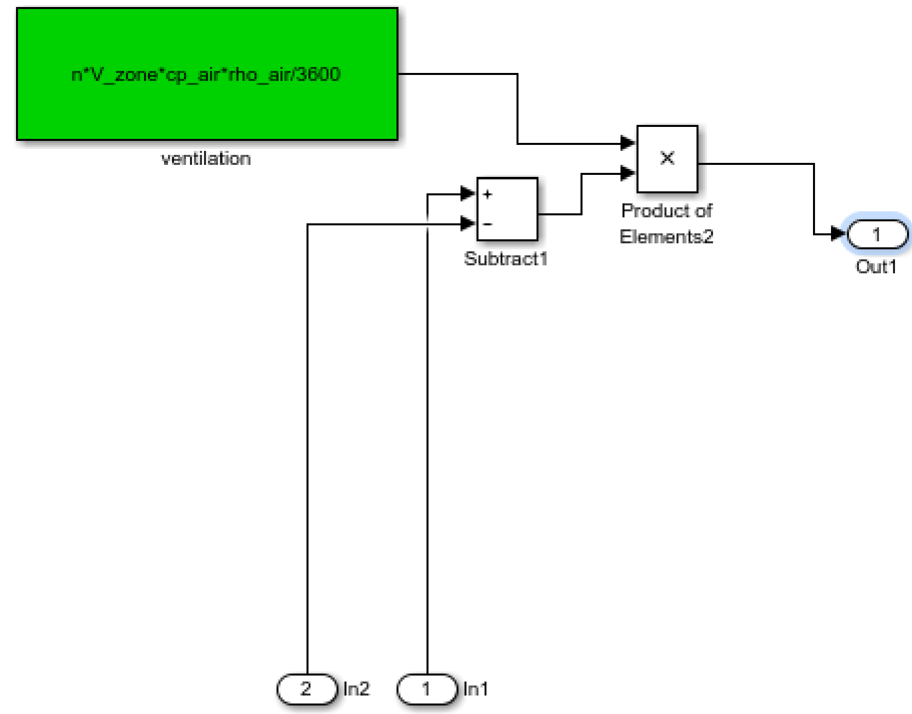
n*V_zone*cp_air*rho_air/3600
ventilation
Product of Elements2
Subtract1
Out1
In2
In1

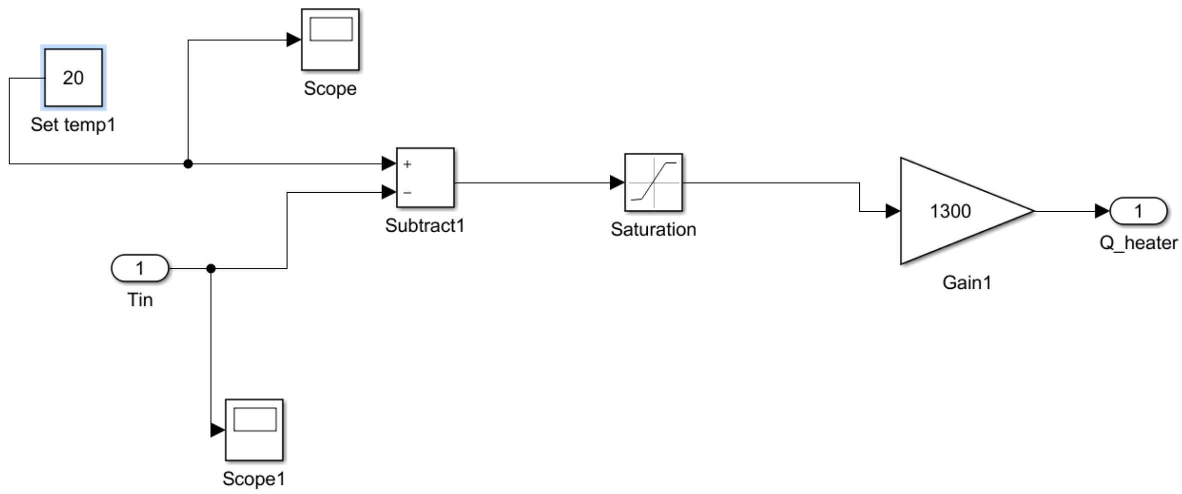
20
Set temp1
Scope
Subtract1
Saturation
1300
Gain1
Q_heater
Tin
Scope1

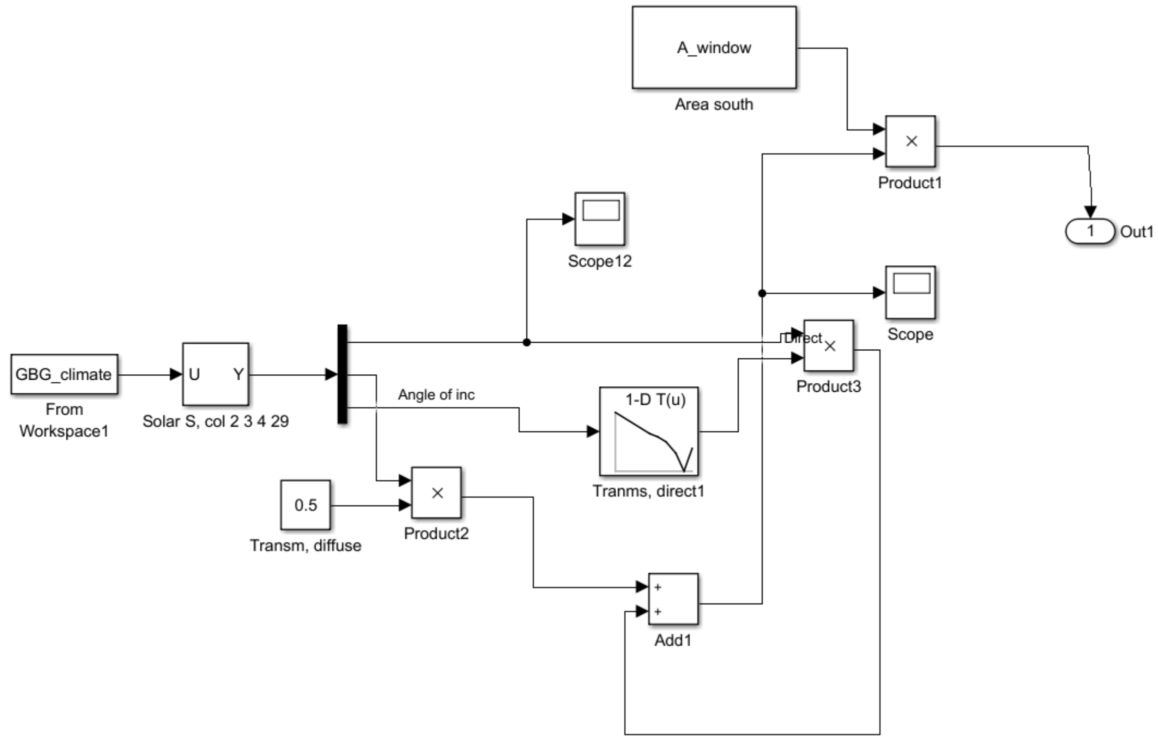
A_window
Area south
Product1
1
Out1
Scope12
Scope
Direct
Product3
GBG_climate
From
Workspace1
U
Y
Solar S, col 2 3 4 29
Angle of inc
1-D T(u)
Tranms, direct1
0.5
Transm, diffuse
Product2
Add1

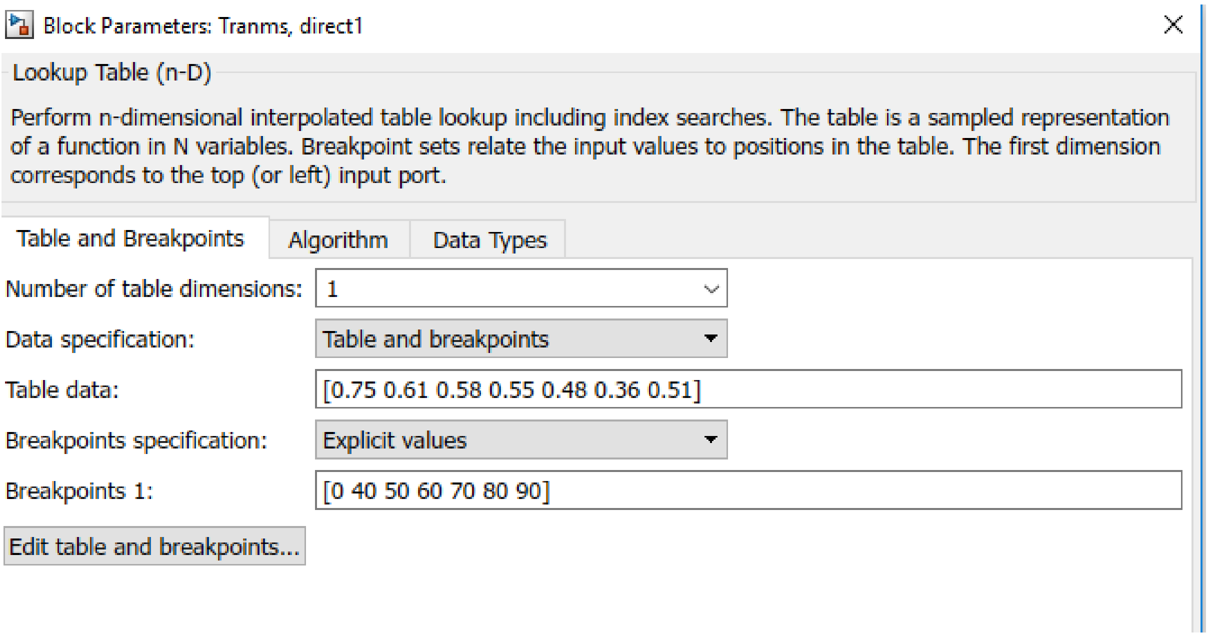
Block Parameters: Tranms, direct1
Lookup Table (n-D)
Perform n-dimensional interpolated table lookup including index searches. The table is a sampled representation of a function in N variables. Breakpoint sets relate the input values to positions in the table. The first dimension corresponds to the top (or left) input port.
Table and Breakpoints
Algorithm
Data Types
Number of table dimensions:
1
Data specification:
Table and breakpoints
Table data:
[0.75 0.61 0.58 0.55 0.48 0.36 0.51]
Breakpoints specification:
Explicit values
Breakpoints 1:
[0 40 50 60 70 80 90]
Edit table and breakpoints...

.8 Appendix 8 - Documentation of the test conducted by RISE

Contact person
Bertil Jonsson
Sustainable Built Environment
+46 10 516 51 60
bertil.jonsson@sp.se

Climate Curtains AB
Kyrkbyn 531
468 90 VÄNERSNÄS

Determination of thermal transmittance according to SS-EN ISO 12567-1

(4 appendices)

Test object

The test object was a curtain with outer dimensions of approximately 1.20 x 1.37 m. A detailed description of the tested object can be found in Appendix 4.

The tested was delivered to SP 2016-08-08 in good condition.

Test procedure

The curtain was built into a 150 mm thick partition wall and an auxiliary wall made of polystyrene (EPS). A single window pane was mounted on the cold side of the curtain. The flow of air to the hot and cold side was natural convection and forced convection by fans, see Appendix 1.

Results

The thermal transmittance (U-value) of the curtain in the opening were determined to

$U = 0.89$ W / (m^2 K) curtain including window pane

The thermal resistance for the curtain (from surface to surface) excluding the window pane 0.83 m^2 K / W

The measured results which concerns only tested product presented in detail in Appendix 2.

SP Technical Research Institute of Sweden
Sustainable Built Environment - Building Physics and Indoor Environment

Performed by

Bertil Jonsson

Appendices

1 Test procedure
2 Results
3 Test Set-up
4 Description of tested prototype curtain

Postal address
SP
Box 857
SE-501 15 BORÅS
Sweden

Office location
Brinellgatan 4
SE-504 62 BORÅS

Phone / Fax / E-mail
+46 10 516 50 00
+46 33 13 55 02
info@sp.se

Appendix 1

Test procedure

The thermal transmittance (U-value) was determined with the "Hot-box" method according to EN ISO 12567-1:2010. During the test the test sample was placed in a 15 cm thick foam surround wall, which separates the warm and cold side. The connection between the test sample and the surround wall were sealed with duct tape to prevent unwanted air leakage. The tested object was built into the surround wall, see Appendix 3

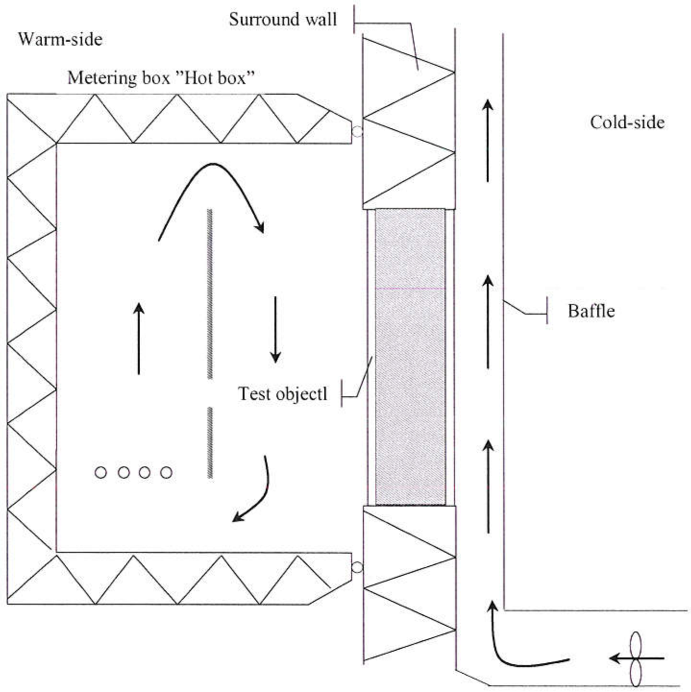

The sample was placed vertically in the surround wall and the direction of heat flow is therefore horizontal. Natural convection creates a downward heat flow along the warm side of the test object. The air speed of the upward air flow on the cold side is set by adjusting the fan in the calibration process. After calibration, the fan setting to remain constant but is checked during the test procedure.

Hot Box dimensions

Area, m^2:	4.12
Depth, m	0.45

Appendix 2

Results

Manufacturer	Climate Curtains AB
Test specimen	Prototype of curtain built into the surround panel, see Appendix 3 and 4.
Test equipment	Climate Chamber 1 Hot box 4,12 m² Agilent 34980A measure unit
Test date	2016-08-12—15

Results for prototype curtain

	Cold-side	**Warm-side**
Air, °C	0.0	20.9
Baffle, °C	0.0	20.1
Surround wall, °C	0.2	20.1
Air speed, m/s	2.0	<0.1

	Intermediate
Surface temperature, layer 3, °C	16.2
Surface temperature, layer 5, °C	14.4
Surface temperature, layer 7, °C	10.9

Calibration

The following regression curves were calculated using The method of least squares for calibrating measured values:

Thermal resistance surround panel (R_{sur}) $\quad R_{sur} = 4{,}802 - 0{,}0094 \cdot \theta_{me,sur}$

Convective part, warm side $\quad F_{c,i} = 0{,}3389 + 0{,}0033 \cdot q_{sp}$

cold side $\quad F_{c,e} = 0{,}7931 + 0{,}0011 \cdot q_{sp}$

Total heat resistance ($R_{s,tot}$) $\quad R_{s,tot} = 0{,}2653 \cdot q_{sp}^{-0{,}12}$

q_{sp} = heat flow density through test object, W/m²

$\theta_{me,sur}$ = average temperature for surround panel, °C

Appendix 2

Calculation of thermal transmittance (U-value)

Average temperature of partition wall, °C	9.9
Thermal resistance of surround panel, m²K/W	4.71
Area of surround panel, m²	2.48
Ψ_{edge}, W/(mK)	0.000
Heat input, Hot Box, W	35.0
Heat flow through partition wall, W	10.6
Heat flow rate, edge zone, W	0.0
Convective part – warm-side	0.39
Convective part – cold-side	0.81
Total heat resistance	0.192
Mean radiant temperature – warm-side, °C	20.1
Mean radiant temperature – cold-side, °C	-0.1
Mean environmental temperature – warm-side, °C	20.5
Mean environmental temperature – cold-side, °C	0.0
Mean environmental temperature difference, °C	20.5

Auxiliary wall

Temperature difference, °C	8.7
Thermal resistance, m²K/W	1.65
Area, m²	0.43
Heat flow rate, W	2.3

Metering area

Heat flow rate, W	22.2
Measured thermal transmittance, W/(m²K)	0.89
Thermal resistance air gap, m²K/W	0.16
Thermal resistance curtain (surface to surface), m²K/W	0.83

Appendix 3

Test set-up

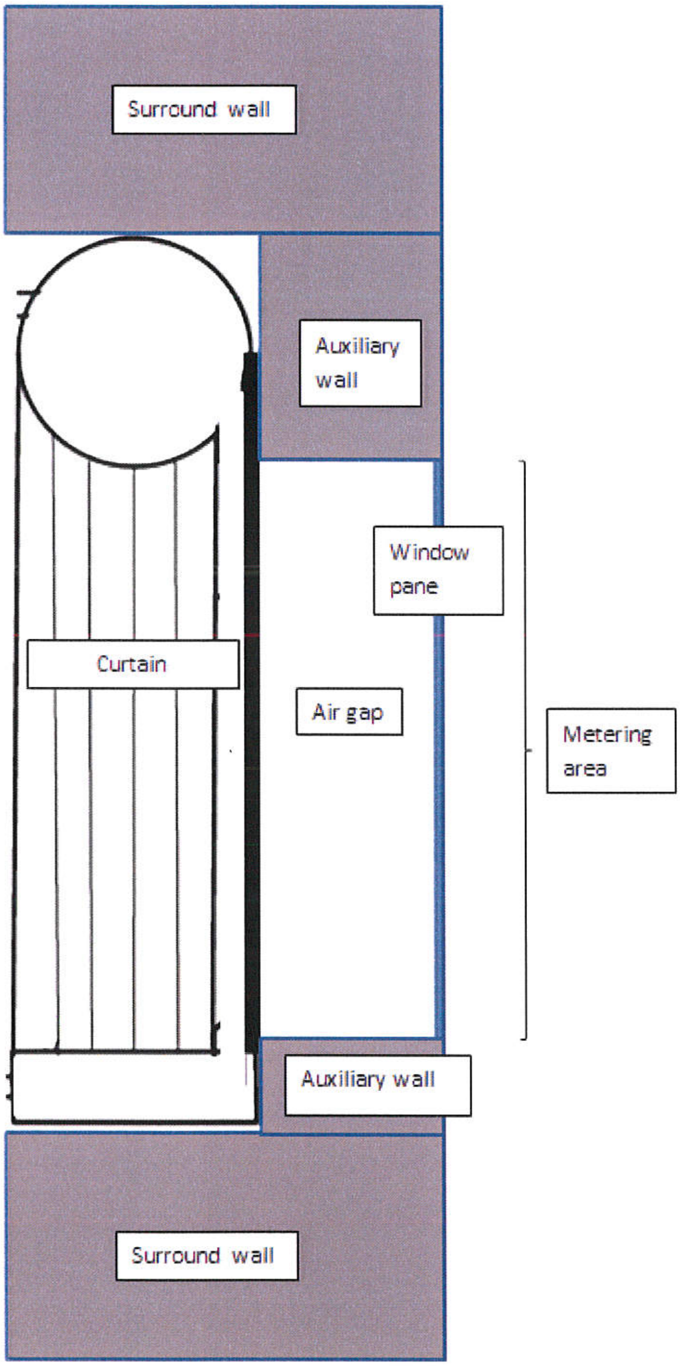

Appendix 4

Description of tested prototype curtain

The curtain consists of eleven sheets of paper fabric creating ten air-gaps.

Thickness of tested specimen/curtain: approximately 0.10 m

The innermost layer is made of plastic-coated fabric (d=0.30 mm). The outer layer, closest to the window, is made of black cardboard/paper (d=0.10 mm). The intermediate layers are made of thin brown grey paper (d=0.06 mm). The layers are forming ten air gaps of which the outermost is connected to a cylinder at the top edge of the curtain, and with a plastic profile in the lower edge of the curtain. There is created a through-gap between from the upper cylinder by the outer air gap, closest to the window, to the lower profile. In this test, the entrance aperture in the upper cylinder and the exhaust opening in the lower plastic profile are sealed with duct tape.